

A Magnetic Resonance Approach to Neurodegeneration

by

Yin-Ching Iris Chen

B.S. Electrical Engineering
National Taiwan University, Taipei, Taiwan (1989)

M.S. Biomedical Engineering
National Yang-Ming Medical College, Taipei, Taiwan (1991)

SUBMITTED TO THE HARVARD-MIT DIVISION OF HEALTH SCIENCES AND
TECHNOLOGY
AND THE DEPARTMENT OF NUCLEAR ENGINEERING
IN PARTIAL FULFILLMENT OF THE REQUIREMENTS FOR THE DEGREE OF

Doctor of Philosophy
i n
Radiological Sciences

at the
Massachusetts Institute of Technology
May, 1997

© 1996 Yin-Ching Iris Chen
All rights reserved

The author hereby grants to MIT permission to reproduce and to distribute publicly paper and electronic copies of this thesis document in whole or in part.

Signature of Author
Harvard-MIT Division of Health Sciences and Technology, and
Department of Nuclear Engineering, May, 1997

Certified by
Professor Bruce G. Jenkins
Thesis Supervisor

Approved by
Professor Bruce R. Rosen
Reader

.....
Professor David Cory
Reader

.....
Professor M. Flint Beal
Reader

Accepted by
Professor Jeffrey P. Friedberg
Chairman, Departmental Committee on Graduate Students

MASSACHUSETTS INSTITUTE
OF TECHNOLOGY

ABSTRACT

A Magnetic Resonance Approach to Neurodegeneration

by

Yin-Ching Iris Chen

Submitted to the Harvard-MIT division of Health Sciences and Technology
and MIT Department of Nuclear Engineering
on May, 1997 in partial fulfillment of the requirements for the
degree of Doctor of Philosophy in Radiological Sciences

The primary objectives of this thesis were to investigate and verify the utility of magnetic resonance techniques to probe neurodegenerative processes. We focused primarily on Parkinson's disease (PD). We demonstrated how various factors could alter the accuracy in estimating the absolute metabolite concentration by using computer simulation. We found that it would be difficult to obtain accurate relaxation times T_1 and T_2 due to the problems of spectral overlap, macromolecular contamination and J-coupling effects. In estimating the metabolite concentration, we found that the errors propagated from the T_2 errors are more critical than the T_1 errors. In human study, we found that PD patients' striatal lactate level was elevated 59% than the normal controls ($p < 0.004$). We also found a significant lactate asymmetry in the 2 striata, which is significant higher in the PD group (64.51% increase, $p < 0.05$) in the "big side". However, we did not have similar finding in the animals of PD model. However, the neuronal marker N-acetylaspartate (NAA) in these animals showed a significant decrease in the striatum ipsilateral to the lesioning (9.61%, $p < 0.0003$). To assess the neuronal activity by using pharmacological MRI (phMRI), we used D-amphetamine and CFT as our specific dopaminergic ligands. We have shown that 1) the BOLD signal change delineated to the blood pCO_2 and global blood pressure changes, 2) phMRI response is regionally specific to those brain areas with high dopaminergic innervation, 3) phMRI response correlates the ^{11}C -CFT binding via PET, 4) phMRI time course correlates the dopamine release assessed by microdialysis. We tested the phMRI technique on 3 groups of animals. We showed the phMRI responses were symmetric in the normal control rats, unilateral ablated in the unilateral dopaminergic denervated striatum, and restored right at the graft site in the dopaminergic cell transplanted rats. In conclusion, the data presented in this thesis demonstrate the ability of using MR technique to explore the neurodegenerative processes and could elucidate treatment strategies and benefit the patients suffering from neurodegenerative diseases.

Thesis Supervisor: Bruce Jenkins, Ph.D.; Department of Radiology, Massachusetts general Hospital, Harvard Medical School.

Acknowledgment

I would like to express my sincere gratitude to Dr. Bruce Jenkins. In the last five years, he has been a wise and inspirational mentor and has become a true friend. As been a foreign student in this country with both language and culture barrier, I thank his great patience and support to guide and assist me through the tough graduate school journey.

I would also like to deliver my hearty gratitude to many of the scientists for their assistance in my work in addition to many memorable experiences. I would like to thank Rick Matthews for providing knowledgeable neurosurgical and neurochemical information in animal model of rats. Without him, lots of the animal work involved in this thesis could not possibly be done. I also like to deliver my sincere appreciation to Dr. John Keltner. John has been a great friend who has been encouraging me to explore new scientific frontiers and sharing me the most up to date scientific information without a little bit of selfishness. I also like to deliver my thanks to Dr. Wendy Galpern and Dr. Anna-Liisa Brownell for their excellent expertise in animal neuro-transplantation and positron tomographic imaging. I am also grateful to Dr. Bruce Rosen for 6 years of excellent education and mentorship within the MGH NMR laboratory, Harvard-MIT Division of Health Sciences and Technology, as well as in the Nuclear Engineering Department.

I would like to express my great appreciation to my friends and family. My deepest gratitude goes to Dr. Beverly Yu. Without her, I won't be able to come to study at the great school MIT and won't be able to come to the dreamland laboratory in MGH. She was not only a great mentor for my master thesis, she also provides a family like hearty and dearing support.

I thank my parents, most of all, who have provides me with unfailing support through this entire experience.

Dedication

I dedicate this thesis to my loving parents

Chun-Yu Chen & Mei-Chun Lin

**for their encouragement and wisdom to guide me through
the travails of my young life.**

I also dedicate this thesis to my beloved husband

Wei-Chun Chang

**for his hearty support
in the past, now, and future.**

TABLE OF CONTENTS

CHAPTER 1 BACKGROUND -- WHY MR COULD BE USEFUL FOR STUDY OF NEURODEGENERATION11

REVIEW OF THE BASAL GANGLIA SYSTEM.....	12
<i>The neuronal network</i>	12
<i>The basal ganglial network</i>	13
POSSIBLE HYPOTHESES INVOLVED IN BASAL GANGLIA DEGENERATION.....	18
<i>Mitochondrial energy impairment</i>	18
<i>Free Radical</i>	20
<i>Iron accumulation</i>	21
WHAT MR CAN DO FOR THE STUDY OF NEURODEGENERATION.....	22
<i>Is ¹H Magnetic resonance spectroscopy (MRS) useful to investigate the mitochondrial energy stress theory?</i>	23
<i>What can functional MR technique do to investigate the neurotransmission system?</i>	25
REFERENCES.....	27

CHAPTER 2 ERROR ANALYSIS OF THE CEREBRAL METABOLITE CONCENTRATIONS IN ¹H MAGNETIC RESONANCE SPECTROSCOPY

.....	33
INTRODUCTION.....	33
METHOD TO ESTIMATE THE CEREBRAL METABOLITE CONCENTRATIONS FROM ¹ H MR SPECTROSCOPY...	35
SPECTRAL QUALITY.....	38
<i>Spectral Overlap</i>	38
<i>Signal to Noise Ratio (SNR)</i>	40
PROBLEMS WITH RELAXATION RATE MEASUREMENTS.....	41
<i>Methods to measure the relaxation times T1 and T2</i>	41
<i>Methods</i>	44
<i>Computer Simulation</i>	44
<i>Phantom and in vivo spectra</i>	48
RESULTS AND DISCUSSIONS.....	49
<i>Spectral simulation</i>	49
<i>T2 measurement errors</i>	58

<i>Absolute concentration measurement errors</i>	63
CONCLUSIONS	67
REFERENCES.....	69

**CHAPTER 3 ¹H MAGNETIC RESONANCE SPECTROSCOPIC STUDIES
IN PARKINSON'S DISEASE PATIENTS.....72**

INTRODUCTION AND BACKGROUND.....	72
METHODS.....	75
RESULTS.....	77
<i>Average result from the individual spectra</i>	78
<i>Asymmetric of the lactate levels in the two striata of the subject</i>	80
<i>Aspartate Elevation</i>	84
DISCUSSION.....	87
<i>Morphology and SNR considerations</i>	87
<i>Therapeutic Implication</i>	90
<i>Asymmetric Lactate levels</i>	91
CONCLUSIONS	92
REFERENCES.....	92

**CHAPTER 4 AN ANIMAL MODEL OF PARKINSON'S DISEASE USING
6-HYDROXYDOPAMINE LESIONS IN RATS --- ANATOMICAL
AND METABOLITE MAGNETIC RESONANCE IMAGING
STUDIES.....97**

INTRODUCTION AND BACKGROUND.....	97
METHODS.....	99
<i>Animals</i>	99
<i>MR Studies</i>	100
<i>Data Analysis</i>	103
RESULTS:.....	103
<i>Water images</i>	103
<i>Metabolite images</i>	106
DISCUSSION.....	108
CONCLUSIONS	111
APPENDIX—BEHAVIORAL TEST.....	112
REFERENCE.....	113

CHAPTER 5 PHARMACOLOGICAL MRI (<i>phMRI</i>).....	119
INTRODUCTION.....	119
METHODS.....	122
<i>Animal preparation</i>	122
<i>MR Measurements</i>	122
<i>PET Measurements</i>	124
<i>Microdialysis</i>	125
<i>Data Analysis</i>	125
RESULTS.....	127
DISCUSSION.....	144
CONCLUSIONS.....	148
REFERENCES.....	148
CHAPTER 6 THESIS SUMMARY AND FUTURE WORK.....	152
TECHNICAL CONCERNS IN USING ¹ H-MRS TO EXPLORE THE STRIATAL METABOLITES.....	154
¹ H-MRS IN PD PATIENTS AND ANIMAL MODEL OF PD.....	156
VALIDATION OF USING PHARMACOLOGICAL MRI (<i>phMRI</i>) TO ASSESS THE DOPAMINERGIC NEURONAL ACTIVITY.....	160
CONCLUSIONS.....	163
REFERENCES.....	164

LIST OF TABLES

Table 1-1	Common ¹ H-MRS detectable neurochemicals	24
Table 2-1	Common ¹ H-MRS detectable neurochemicals	37
Table 2-2	List of major spectral overlap groups in ¹ H-MRS	44
Table 2-3	Spectral elements used in Lorentzian line simulation	46
Table 3-1	Clinical characteristics of the PD patients in our study	77
Table 3-2	Cerebral metabolite levels measured from PD patients and controls ...	78
Table 3-3	Correlation of the PD lac/NAA ratio with clinical parameters	83
Table 3-4	Cerebral metabolite levels: big versus small groups	83

LIST OF FIGURES

Fig 1-1 Basal ganglia circuit I 15

Fig 1-2 Basal ganglia circuit II 18

Fig 2-1 Computer synthesized spectra, $\Delta R2^* = 10\text{Hz}$ 50

Fig 2-2 Computer synthesized spectra, $\Delta R2^* = 50\text{Hz}$ 53

Fig 2-3 NAA signal intensity as a function of echo time TE 60

Fig 2-4 Creatine and choline signal intensity as a function of echo time TE 61

Fig 2-5 Stack spectra with different TE: phantom study 62

Fig 2-6 Stack spectra with different TE: human study 62

Fig 2-7 NAA concentration error as function of errors in T1 and T2 65

Fig 2-8 NAA concentration error as function of TR 66

Fig 2-9 *In vivo* spectra from 1.5T and 4.7T 68

Fig 3-1 Striatal spectra from PD patients and normal controls 79

Fig 3-2 Distribution of the individual Lac/NAA in PD patients and controls 81

Fig 3-3 Asymmetric lactate spectra 82

Fig 3-4 Lac/NAA ratio: big versus small groups 84

Fig 3-5 Spectra with elevated aspartate peaks 86

Fig 3-6 Criterion to screen striatal spectra 90

Fig 4-1 T2 and diffusion weighted images in 6-OHDA lesioned rats 105

Fig 4-2 rCBV and rCBF maps in 6-OHDA lesioned rats 105

Fig 4-3 NAA image from 6-OHDA lesioned rats 107

Fig 5-1 pHMRI responses versus blood pressure and pCO2 changes 128

Fig 5-2 Regional specificity in pHMRI 129

Fig 5-3 Partial volume averaging in the parietal cortex 130

Fig 5-4 Blood pressure and pCO2 changes in all animals..... 132

Fig 5-5	phMRI time courses with microdialysis data	133
Fig 5-6	phMRI activity: good to bad activation maps	135
Fig 5-7	phMRI time courses in the unilaterally lesioned rats	136
Fig 5-8	rCBV and rCBF maps in the unilaterally lesioned rats	137
Fig 5-9	Behavior versus phMRI and dopamine release	138
Fig 5-10	phMRI and PET images	141
Fig 5-11	Asymmetry in lesioned only and neuron transplanted rats	142
Fig 5-12	Correlations: behavior versus PET and phMRI	143

Chapter 1 Background --- Why could MR be useful for study of neurodegeneration?

In this thesis, we demonstrate the use of magnetic resonance (MR) as a tool to investigate neurodegenerative diseases of the basal ganglia. In order to answer the question of whether or not magnetic resonance is a useful tool for the investigation of the neurodegenerative processes, we start by defining possible mechanisms of neurodegeneration and then explain MR techniques may be employed to verify the hypotheses. The overall outline is:

- review of the basal ganglia system,
- review of hypotheses concerning the mechanisms of basal ganglia degeneration,
- demonstrations of MR to investigate the neurodegenerative process.

Review of the basal ganglia system:

This section is a brief review of the basal ganglia, including the neuronal anatomy and the neural circuits involved in the basal ganglia function. In addition, this section will discuss the possible mechanisms involved in disorders of the basal ganglia such as Parkinson's disease (PD) and Huntington's disease (HD).

The neuronal network:

The question of how the brain works has never been fully answered. However, scientists have found their ways to explore the possible mechanisms of brain function. The brain is comprised of hundreds of billions of neurons. Groups of neurons compose suborgans of the brain. How the individual neurons talk to each other has never been easily answered. In short, neurons rely on stereotyped electrical signals and chemical signals to communicate. The interconnections of neurons integrate and play out the functions. Two types of membrane potential signals are used by neurons: localized potentials and action potentials. The localized potentials are only effective in a very short distance and the neurons have to rely on the action potentials to transmit signals over long distances (via axons). The bridge for individual neurons to talk to each other is primarily via neurotransmitters and their corresponding receptors. The arrival of the action potentials at the axonal terminals causes the release of neurotransmitters from the presynaptic neurons. The binding of the neurotransmitters to their corresponding receptors can modulate the electrical potentials on the postsynaptic neuronal membrane. Different types of neurons possess different kinds of neurotransmitters and receptors, which may potentiate or inhibit the

formation of the action potentials on the postsynaptic neurons (excitatory post synaptic potential (EPSP) or inhibitory post synaptic potential (IPSP)). Based on the precise balance between the excitatory and inhibitory interactions, the neuronal signals can be modulated and transmitted.

The basal ganglia network:

The basal ganglia is a submodule of this complicated neuronal network system. Although the complete mechanism of how the basal ganglia function is yet to be determined, scientists have successfully mapped out some neurotransmission routes. Based on these neurotransmission routes, numerous hypotheses have been proposed to reveal the role basal ganglia may be playing in brain function. The basal ganglia may act as a self-regulated current-regulation center to modulate the cortical activities. Further elaboration of this current regulation theory (described below) may be applied to help solve the etiologic mysteries of some of the basal ganglia relative disorders, such as Parkinson's disease (PD), Huntington's disease (HD), hemiballismus, athetosis, etc. Let's take a closer look of the basal ganglia.

Terminology of basal ganglia subunits:

The traditional term of "basal ganglia" refers to the deep gray matter buried inside the cerebrum: caudate nucleus (CA), putamen, (internal / external) globus pallidus (GPi/GPe), subthalamic nucleus (STN), and substantia nigra (SN). Because the caudate nucleus and putamen share the same embryological origin, these two organs are generally referred as the neostriatum or striatum. However, the nucleus accumbens, which is the fusion part between caudate nucleus and

putamen, is generally referred to as part of the limbic system but not striatum. The putamen and globus pallidus comprise the lenticular nucleus because of their lens like shapes. The combination of the lenticular nucleus and the neostriatum is called the corpus striatum.

Basal ganglia circuit theory:

The striata basically form C-shaped courses along the lateral ventricles and receive a broad range of signals from various cortical areas. Although the striatum is relatively small in volume compared to the cerebral cortex, the topographical innervation pattern from and to the cortical areas has been mapped out by immunohistologic techniques. Generally, the primary afferent neurotransmitter of the striatum is glutamate. The caudate nucleus receives glutamatergic input primarily from the prefrontal cortex and thus is thought to have its major role in cognitive functions; while the putamen primarily receives the glutamatergic input from the somatosensory and motor cortex and thus its involvement in motor functions. The excitatory cortico-striatal glutamatergic neurons set the basic tone of the striatal neuronal firing rate. The striatum then serves as a relay or modulation center which can integrate or modulate the glutamatergic input signal by interactions with other neurotransmitters, such as dopamine, serotonin, etc., through several suborgans of basal ganglia. The signals from basal ganglia finally reach thalamus and are relayed back to the cerebral cortex via glutamate.

In order to understand how the basal ganglia are involved in motor activity, we may simplify the complicated cortical-striatal-thalamic-cortical route as shown in figure 1-1. As shown in the figure, both

the striatum and STN receive excitatory glutamatergic input from cortex and they also share the GPi as the main output node to the thalamus (GABA, inhibitory) which then relays the signal back to cortex (glutamate, excitatory). The cortical-STN-GPi route is of short fast latency to inhibit unwanted motions and thus maintain the posture. The cortical-striatal-pallidal-thalamic route is of long latency with a tendency to inhibit the activity in GPi and thus to disinhibit the desired motor activity. [1]

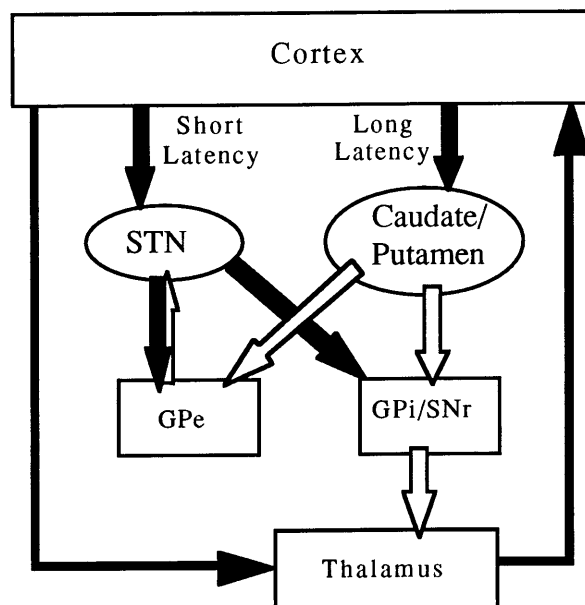


Figure 1-1 The two parallel disynaptic pathways from cortex to globus pallidus. The solid arrow indicates an excitatory pathway and the open arrow indicates an inhibitory pathway. GPe: globus pallidus external, GPi: globus pallidus internal, SNr: substantia nigra pars reticulata, STN: subthalamic nucleus.

The long latency circuit can be further divided into 2 parallel pathways: the direct versus the indirect pathway (figure 1-2). Each segment has its particular neurotransmitters such as GABA, substance P (SP), enkephalin, etc., as specified in figure 1-2 and they

are mainly inhibitory substances. According to this kind of neuropathway layout, the direct pathway is essentially the positive feedback route while the indirect pathway is the negative feedback route. Based on the basal ganglial circuit theory, hypokinetic disorders, such as Parkinsonism can be the result of an overactive 'indirect' pathway while hyperkinetic disorders, like Huntington's disease and hemiballismus, could be due to an underactive 'indirect' pathway. [2,3,4,5] This simplified circuit theory provides a plausible mechanism regarding movement disorders and also provides valuable therapeutic strategies. Subthalamotomy has been performed in PD patients to improve parkinsonism. [6,7] Pallidotomy and thalamotomy (VA/VL) have been performed in PD patients to reduce some of the side effects caused by the dopamine replacement therapy ("wearing-off" and "on-off" effects) and the occurrence of dyskinesias caused by levodopa.

However, some of the clinical findings from the stereotaxic surgery in Parkinson's disease have contradicted this theory. For example, a thalamotomy, which might be expected to increase motor disability according to the circuit theory, does not worsen movement in clinical trials. [8] This may only suggest that the basal ganglia function is far more complicated than the simple circuit theory presented and the etiology of the neuronal degeneration in the striatum is far from understood.

The nigro-striatal dopaminergic neurons seem to play an important role in modulation of the main afferent glutamatergic signal. Dopamine can either reduce the presynaptic neuronal activity (via D2 autoreceptors), enhance the postsynaptic neuronal activity (via D1

receptors, mainly on the direct pathway), or inhibit the postsynaptic neuronal activity (via D2 receptors, mainly on the indirect pathway). The pathologic finding in idiopathic Parkinsonism is that there is a tremendous amount of cell loss in the substantia nigra pars compacta. The evidence from the postmortem studies on the patients with idiopathic Parkinson's disease showed that the onset of the parkinsonism did not show up approximately to 80-90% neuronal loss in the SNc. [9,10,11] An animal model of parkinsonism which uses the selective dopaminergic neurotoxin 6-hydroxydopamine (6-OHDA) to interrupt the nigro-striatal dopaminergic pathway in rats also demonstrated similar results. [12] The reasons why the nigral cells die and how the insufficient dopamine concentration in the striatum causes the dysfunction of the striatum are still unclear. Several hypotheses have been proposed in an attempt to explain these neuronal degeneration processes. The next section will discuss some of the most popular hypotheses.

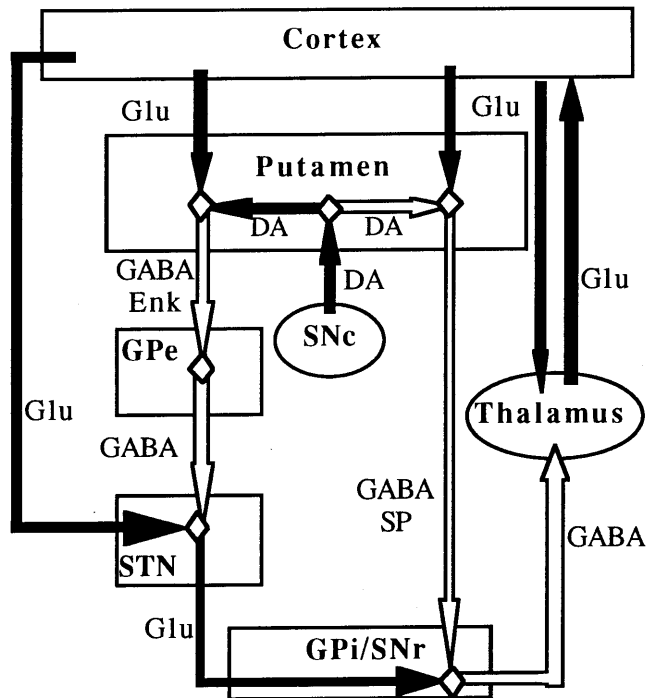


Figure 1-2 Basal ganglia motor circuit -- direct versus indirect pathways. Solid arrow indicates excitatory pathway and open arrow indicates inhibitory pathway. The direct pathway is a positive feedback loop and the indirect pathway is a negative feedback loop. DA: dopamine, Enk: enkephaline, Glu: glutamate, GPe: globus pallidus external, GPi: globus pallidus internal, SNc: substantia nigra pars compacta, SNr: substantia nigra pars reticulata, STN: subthalamus nucleus, SP: substance P.

Possible etiologic hypotheses of basal ganglia degeneration

Mitochondrial energy impairment;

This hypothesis postulates that impairment of the mitochondrial electron transport chain either directly or indirectly causes the cell death in the substantia nigra. The evidence for this was discovered accidentally in humans who had injected the street drug 1-methyl-4-phenyl-1,2,3,6-tetrahydropyridine (MPTP), which was a contaminant

of synthetic heroin analogue. The drug abusers who received MPTP developed symptoms resembling idiopathic Parkinson's disease. Further studies on MPTP discovered that this compound has the potential to destroy the dopaminergic neurons in the substantia nigra pars compacta (SNc) in human, primates, and some other animal species. Actually, MPTP is not neurotoxic but its metabolite 1-methyl-4-phenylpyridinium ion (MPP⁺) is. MPP⁺ can inhibit complex I (NADH dehydrogenase) in the mitochondrial electron transport chain. Consequently, a decrease in the NAD⁺/NADH ratio and an increase in the conversion rate of pyruvate to lactate are expected and were observed in cell culture studies by Vyas et al. [13]

The key enzyme required to oxidize MPTP is the monoamine oxidase subtype B (MAO-B), which is located on the astrocytes. MPTP is oxidized by MAO-B to the intermediate substance MPTP⁺, and then subsequently oxidized to MPP⁺. This metabolite MPP⁺ is then released from the glial cell and freely diffuses into the extracellular space. Since MPP⁺ is a substrate of the dopamine reuptake protein, it can be transferred to the substantia nigra through the dopamine reuptake pathway. MPP⁺ is finally accumulated inside the mitochondrial matrix to inhibit the action of complex I and thus causes the nigral cells to die. [14,15] Inspired by the MPTP/MPP⁺ findings, researchers have proposed that the neuronal degeneration in idiopathic parkinsonism may be caused by some environmental or endogenous toxins which may induce similar damage as MPP⁺ does in the mitochondrial electric transport chain in the SNc, possibly through the MAO-B/dopamine reuptake pathway. If MAO-B is really involved in idiopathic parkinsonism, using MAO-B inhibitors may be

able to postpone the neuronal degenerative process. Clinical trials to treat PD patients with L-dopa conjugating with deprenyl, the selective and long-lasting MAO-B inhibitor, showed up to 56% improvement in the disability score. [16,17] This clinical evidence supported the hypothesis that the etiology of the idiopathic parkinsonism may be related to mitochondrial energy stress. However, other studies showed little effect. The latter finding may be more consistent with the observation that by the time someone is diagnosed with PD, 80 - 90% of the nigral dopamine neurons are already dead.

Free Radicals:

As mentioned in the mitochondrial energy impairment section, MPP⁺ will interrupt the activity of NADH dehydrogenase in the electron transport chain. However, some of the researchers suggest that the mechanism of toxicity of MPP⁺ is not to cause the interruption of the electron transport but to generate oxygen radicals (superoxide) while the electron transport is blocked at the stage of complex I. This free radical theory is supported by the evidence of reduced levels of glutathione and other antioxidants in substantia nigra and other brain areas after the MPTP neurotoxicity. [18,19] Further evidence is provided by studies showing free radical scavengers and antioxidants can provide neuroprotection in animal model of MPTP / MPP⁺ toxicity. [20,21] However, further studies showed that there is no detectable increase in lipid peroxidation [22] and there is a mismatch between the degree of inhibition in the NADH

dehydrogenate and the rate of superoxide formation. [23] Nonetheless, all of the evidence suggests that free radical formation may not be the primary cause of neurotoxin of MPP⁺ but it may accelerate the damage done by the cessation of mitochondrial respiration.

Iron accumulation:

Several studies of post-mortem brains of the PD patients have reported an abnormal increase in iron concentration. Iron is an important trace element for electron transport, enzymatic catalysis and neuronal development [24] and the disturbance of the iron homeostasis may lead to neuronal dysfunction. Therefore, the finding of high nigral iron concentrations in PD patients may suggest that iron is involved in the pathogenesis of PD. Several groups have suggested that iron may prompt free radical formation and also catalyze lipid peroxidation, which may subsequently lead to neuronal death. However, from post-mortem studies with human brains, the abnormal nigral iron levels were only found in the severely affected PD patients but not in mildly affected PD patients. [25] And histochemical studies in rats with 6-OHDA lesions, a typical animal model of PD which is able to induce neuronal degeneration in SNc/VTA area, showed a substantial increase in Fe staining in the ipsilateral SNc/VTA areas. There were no changes in the contralateral side. [26] These data suggested that the high iron level in SNc may be a secondary effect of the neurodegenerative process. Although up to now how and why the iron accumulates in the SNc is still unclear, Oestreicher proposed 3 possible mechanisms: 1) iron may be associated with the infiltrating reactive glial cells; 2) loss of

the dopaminergic neurons in the SNc may cause dysregulation of the nigral iron homeostasis; 3) 6-OHDA lesions lead to the dysfunction of the blood-brain-barrier.

What MR can do for the study of neurodegeneration

As we discussed in the previous section, different hypotheses have been proposed in an attempt to explain the neuronal degeneration in PD. Among the 3 most popular hypotheses, we found that the energy impairment theory may be the most plausible one in that it has the most direct evidence. The first part of this thesis will search for appropriate evidence to support this hypothesis in PD patients by using magnetic resonance spectroscopy (MRS) to investigate cerebral metabolites such as the energy impairment marker of lactate and the neuronal marker of N-acetylaspartate. In addition to the patient group, a well characterized animal model for PD, the specific selective lesioning in the nigro-striatal dopaminergic neurons by the toxin 6-hydroxy-dopamine (6-OHDA), provides us a further opportunity to investigate the hypothesis that insufficient dopaminergic innervation in the striatum can induce striatal neuronal stress. The iron accumulation theory can also be investigated by monitoring ΔR_2^* changes. We therefore propose to use MR as a tool to investigate the question of whether or not in these 6-OHDA lesioned animals there is any disturbance of the striatal metabolite levels, or any change in the hemodynamic properties. Furthermore, we will test the possibility of using functional MRI (fMRI) to observe the coupling between the transmitter-receptor activity and the corresponding neuronal response. We will propose to use pharmacological stimulation to

make this neuronal coupling visible and thus we will propose to call this novel technique as pharmacological MRI (phMRI).

Before we can go further in to the experimental set up, we have to answer several questions:

Is ^1H Magnetic resonance spectroscopy (MRS) useful to investigate the mitochondrial energy stress theory?

The individual ^1H nucleus under a steady magnetic field will experience a slightly different magnetic field due to the shielding effect set up by the surrounding electrons. This perturbation of the magnetic momentum, called chemical shift, enables us to detect nuclei of different molecular structures via MR spectroscopy. There are a number of cerebral molecules which are ^1H magnetic resonance visible [27,28]. Table 1-1 shows a partial list and the properties of these molecules. Among these MR visible molecules, the most prominent one is N-Acetylaspartate (NAA), which is believed to be the marker of normal neurons because it is found almost exclusively in neurons but not glial cells [29,30]. The spectral peak labeled Cr at 3.03 ppm is composed of both Cr and PCr. When energy impairment occurs, one expects hydrolysis of PCr to Cr and the total resonance intensity would not change assuming the relaxation times are the same for both molecules. Creatine is thus usually taken as an internal standard when absolute or relative quantification of other molecules is necessary.

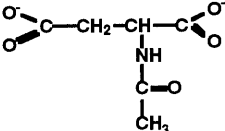
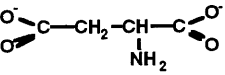
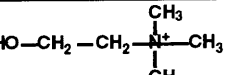
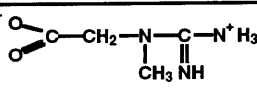
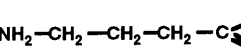
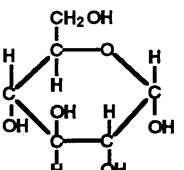
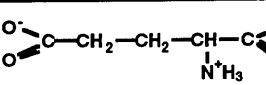
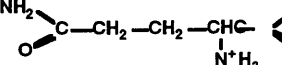
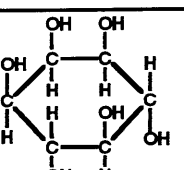
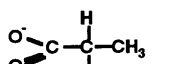
Compound (Chemical Shifts and Approximate Human Brain Concentration)	Structure	Relevance to Neurodegeneration
N-acetylaspartate (NAA) 2.023 ppm (CH ₃) 2.52 ppm (βCH) 2.70 ppm (β'CH) ≈ 8mM		Neuronal Marker Higher Concentration in Grey Matter Compared to White Matter
Aspartate (asp) 2.69 ppm (βCH) 2.82 ppm (β'CH) ≈ 2 mM		Excitatory neurotransmitter May possess excitotoxic potential
Choline / Phosphocholine (CHO) 3.23 ppm (CH ₃) ≈ 1.6 mM		Also composed of other trimethylamines May represent lipid breakdown products and/or gliosis
Creatine / Phosphocreatine (Cr/PCr) 3.03 ppm (CH ₂) 3.95 ppm (CH ₂) ≈ 7.6mM		Peak represents sum of total creatine. Supplies phosphate for conversion of ADP to ATP in creatine kinase reaction.
γ-aminobutyric acid (GABA) 1.91 ppm (βCH ₂) 2.31 ppm (αCH ₂) 3.02 ppm (γCH ₂) ≈ 3 mM		Inhibitory Neurotransmitter Large fraction of basal ganglia neurons are GABAergic
α-D-Glucose 3.2-4.1 ppm ([2-6]CH) 5.32 ppm ([1]CH) ≈ 0-3 mM		Fuel for the brain - most ND conditions show hypo-metabolism of glucose Detectable in 2D studies <i>in vivo</i> but quantitation at low field strengths nearly impossible except potentially peak at 5.32 ppm.
Glutamate (Glu) 2.06 ppm (βCH) 2.36 ppm (γCH ₂) 2.10 ppm (β'CH) 3.76 ppm (αCH) ≈ 6 - 10 mM		Major excitatory neurotransmitter in brain. Potential Excitotoxin. Quantifiable at high fields
Glutamine (Gln) 2.14 ppm (βCH ₂) 2.46 ppm (γCH ₂) 3.78 ppm (αCH) ≈ 3 mM		Source of glutamate for neurotransmission Quantitation problems as hard as for glutamate.
Myo-inositol (mI) 3.54 ppm ([1,3]CH) ≈ 5 mM		Possible osmoregulator. Precursor of inositol polyphosphate (IP ₃) intracellular messengers.
Lactate 1.33 ppm (βCH ₂) ≈ 0.5 mM		End product of anaerobic glycolysis Barely detectable in normal brain.

Table 1-1. Common neurochemicals observable in proton MRS

Table 1-1 indicates that MRS would allow us to evaluate many factors of the cerebral status during physiological challenge or following events relevant to neurodegeneration. By monitoring the amount of NAA (2.023ppm), one can determine the survivability of the neurons under neurotoxic challenge. By monitoring the lactic acid amount (1.33 ppm), one can investigate the degree of energy stress the neurons are experiencing. This lactate measurement can serve as an index to support the energy impairment theory in neuronal degeneration as we mention earlier. Furthermore, by monitoring the glutamate/glutamine (Glx) level, one can investigate the possibility that the vulnerability of the striatal neurons after dopaminergic stimulation may be caused by glutamate toxicity. Overall, although MRS possesses some technical difficulties related to the insensitivity of MR in general, such as the limitation in the spatial, temporal, and chemical resolutions, which are beyond the scope of this text to explain, it still provides us an excellent opportunity to investigate cerebral events at the molecular level. In this thesis, we will test the hypothesis that PD may be the result of energy impairment in the electron transport chain. And we would like to apply the MRS technique to PD patients to investigate whether there is any abnormality in the cerebral lactate levels. Furthermore, we would like to investigate any other abnormality of the ^1H spectra possibly found in this PD patient group.

What can functional MR technique do to investigate the neurotransmission system?

Neuronal activity is coupled with changes in regional cerebral blood flow (rCBF) [31], regional cerebral volume (rCBV) [32,33], blood

oxygenation [32,34], and metabolism [35,36]. Results of positron emission tomography (PET) studies indicate there is no or little change in oxygen consumption during neuronal activity [32,34,36]. Based on the rationale that changes in rCBF will be 2-4 times larger than changes in rCBV [37], the venous oxygenation will increase from base line level 30% to 75% due to neuronal activity with constant oxygen consumption [32,34,36]. Kwong et. al. demonstrated that these hemodynamic changes are detectable by using magnetic resonance techniques without exogenous contrast agents [38]. In the baseline condition, deoxyhemoglobin, which is paramagnetic, sets up a magnetic field gradient at the interface of the vessels and the surrounding tissues. This inhomogeneous field is manifested as a T_2^* effect and will decrease the magnetic resonance signal intensity. While in the activation state, the increase in the concentration of oxyhemoglobin and a decrease in the concentration of paramagnetic deoxyhemoglobin causes an increase in the MR signal intensity due to a reduction in T_2^* effect. The concept of detecting the oxygenation changes by using MR is also known as the BOLD effect (Blood Oxygenation Level Dependent) [39] has been widely applied to investigate the brain functions and is thus called functional MRI (fMRI). Although fMRI has been proved to be powerful to map out neuronal systems, such as language[40,41], the visual system [42,43], auditory system [44], etc., the question of whether fMRI has the ability to observe the *in vivo* neuronal activity at the neurotransmitter level is yet to be determined. Spatial, temporal resolution and the signal to noise ratio (SNR) are the main issue for MR to go down to the *in vivo* molecular level to follow the neuronal activation. However, since neuronal activity is coupled with rCBF and

rCBV, there is a possibility of investigating the neurotransmitter activity by following the corresponding hemodynamic responses. In this thesis, we propose to investigate the hemodynamic properties of the dopaminergic neurotransmission system in response to pharmacological stimulation. We propose to name this new application of functional MRI as pharmacological MRI or phMRI. With the aid of phMRI technique, we may monitor the remaining of the dopaminergic innervation in the elderly brain to evaluate the possibility of progressive PD before any symptom shows up.

Based on the background regarding basal ganglia degeneration and the ability to use MR to study Parkinsonism, in the following chapters this thesis will discuss:

- Development of appropriate MR techniques to study neurodegeneration
- Human studies of PD using MRS
- Animal studies of PD models using MRS and hemodynamics measurements.

References

- 1 JW Mink and WT Thach, basal ganglia intrinsic circuits and their role in behavior, *Current opinion in neurobiology*, **3**:950-97, (1993)
- 2 RL Albin, AB Young, JB Penney, The functional anatomy of basal ganglia disorders, *Trends Neurosci*, **12 (10)**: 366-75 (1989)
- 3 GE Alexander, MD Crutcher, MR DeLong, Basal ganglia-thalamocortical circuits: parallel substrates for motor, oculomotor,

-
- "prefrontal and limbic functions, *Prog Brain Res* ,**85**:119-46 (1990)
- 4 AM Graybiel et al. Chemical neuroanatomy, pp427-504 Raven Press, (1983)
 - 5 DeLong MR, Primate models of movement disorders of basal ganglia origin, *TINS*,**13(7)**:281-285 (1990)
 - 6 N. Diederich, CG Goetz, GT Stebbins, HL Klawans, K Nittner, A Koulosakis, P Sanker, V Sturm, Blinded evaluation confirms long-term asymmetric effect of unilateral thalamotomy or subthalamotomy on tremor in Parkinson's disease, *Neurology*, **42(7)** : 1311-4 (1992)
 - 7 J. Guridi, MR Luquin, MR Herrero, JA Obeso, The subthalamic nucleus: a possible target for stereotaxic surgery in Parkinson's disease, *Mov. Disord.*, **8(4)**: 421-9(1993)
 - 8 C.D. Marsden and J.A.Obeso, The functions of the basal ganglia and the paradox of stereotaxic surgery in Parkinson's disease, *Brain*,**117**: 877-897(1994)
 - 9 Bernheimer et al., 1973, *J. Neurol Sci*20, 415-455;
 - 10 Lloyed et al., 1975, *Exp. Ther.* 195; 453-464
 - 11 TE Robinson, E Castaneda, IQ Whishaw, Compensatory changes in striatal dopamine neurons following recovery from injury induced by 6-OHDA or methamphetamine: a review of evidence from microdialysis studies,*Can J Psychol*, **44(2)**: 253-75(1990)
 - 12 Ungerstedt, 1971, *Acta physiol, Scand.* 83 (S367) 95-122; Zigmond and Stricker, 1973, *Science* 182, 717-720
 - 13 Vyas et al, study of the neurotoxicity of MPTP: inhibition of NADH-linked substrate oxidation by its metabolite MPP+, *J. Neurochem*, **46**:1501-1507(1986)

-
- 14 KF Tipton and TP Singer, Advances in our understanding of the mechanisms of the neurotoxicity of MPTP and related compounds, *J Neurochemistry*, **61(4)**:1191-1206(1993)
 - 15 I Kanazawa, Short review on monoamine oxidase and its inhibitors, *Eur Neurol*, **34(suppl 3)**:36-39(1994)
 - 16 W Birkmayer, et al., the potentiation of the anti aknetic effect after L-dopa treatment by an inhibitor of MAO-B, deprenyl. *J. Neural Transm*, **36**:303-326(1975)
 - 17 W Birkmayer, et al, Implications of combined treatment with 'Madopar' and L-deprenyl in Parkinson's disease. *Lancet I*:439-443(1977)
 - 18 TL Perry et. al., Partial protection from the dopaminergic neurotoxin N-methyl-4-phenyl-1,2,3,6-tetrahydropyridine by four different antioxidants in the mouse. *Neurosci. lett.* **60**:109-114(1985)
 - 19 JD Adams and IN Odunze, Biochemical mechanisms of 1-methyl-4-phenyl-1,2,3,6-tetrahydropyridine toxicity: could oxidative stress be involved in the brain? *Biochem. Pharmacol.* **41**:1099-1105(1991)
 - 20 Y Haskel, R Udassin, MChevion, MPP+ toxicity in E. coli under aerobic and anaerobic conditions, *Free Radic Res Commun*, **12-13(2)**: 697-702, (1991)
 - 21 RM Wu, KP Mohanakumar, DL Murphy, CC Chiueh, Antioxidant mechanism and protection of nigral neurons against MPP+ toxicity by deprenyl (selegiline), *Ann N Y Acad Sci*, **738**: 214-21 (1994)
 - 22 FP Corongiu et. al., MPTP fails to induce lipid peroxidation in vivo. *Bioehm. Pharmacal*, **36**:2251-2253(1987)
 - 23 E Hasegawa el. al, 1-methyl-4-phenylpyridinium (MPP+) induces NADH-dependent superoxide formation and enhaces NADH-depent lipid peroxidation in bovine heart submitochondrial particles. *Biochem. Biophys. Res. Commun*, **170**: 1049-1055, (1990)

-
- 24 M Youdim, et al, The possible role of iron in etiopathology of Parkinson's disease, *mov. disord.*, **8**:1-14(1993)
 - 25 P Riederer, M Youdim et al., Transition metals, ferritin, glutathione and ascorbic acid in parkinsonian brains, *J Neurochem*, **52**:515-520(1989)
 - 26 Oestreicher E, Sengstock GJ, et al, Degeneration of nigrostriatal dopaminergic neurons increases iron within the substantia nigra: a histochemical and neurochemical study, *Brain Research*, **660**:8-18 (1994)
 - 27 T. Jue, F. Arias-Mendoza, NC Gonnella, GI Shulman, RG Shulman, A ¹H NMR technique for observing metabolite signals in the spectrum of perfused liver, *Proc. Natl. Acad. Sci.*, **82(16)** : 5246-9 (1985)
 - 28 BGJenkins and YI Chen, book chapter; to be published. Editor MF Beal et. al. (1998)
 - 29 DL Birken, WH Oldendorf, N-acetyl-L-aspartic acid: a literature review of a compound prominent in ¹H-NMR spectroscopic studies of brain, *Neurosci Biobehav Rev*, **13**:23-31 (1989)
 - 30 ML Simmons, CG Frandoza, JT Coyle, Immunocytochemical localization of N-acetyl-aspartate with monoclonal antibodies, *Neurosci*, **45**:37-45 (1991)
 - 31 PT Fox, MA Mintun, ME Raichle, FM Miezin, JM Allman, DC Van Essen, Mapping human visual cortex with positron emission tomography, *Nature*, **323(6091)**: 806-809(1986)
 - 32 Fox PT & Raichle ME, Focal physiological uncoupling of cerebral blood flow and oxidative metabolism during somatosensory stimulation in human subjects, *Proc. Natl. Acad. Sci. USA* **83**:1140-1144(1986)
 - 33 JW Belliveau, DN Jr Kennedy, RC McKinstry, BR Buchbinder, RM Weisskoff, MS Cohen, JM Vevea, TJ Brady, BR Rosen, Functional

-
- mapping of the human visual cortex by magnetic resonance imaging, *Science*, **254**:716-719(1991)
- 34 PT Fox, ME Raichle, MA Mintun, Dence C Nonoxidative glucose consumption during focal physiologic neural activity, *Science*, **241**:462-464(1988)
- 35 Phelps ME et. al., *Science*, 1981, 211:1445-1448
- 36 J Prichard; D Rothman; E Novotny; O Petroff; T Kuwabara; M Avison; A Howseman; C Hanstock; R Shulman, Lactate rise detected by ¹H NMR in human visual cortex during physiologic stimulation, *Proc. Natl. Acad. Sci. USA*, **88(13)**:5829-5831(1991)
- 37 RL Grubb et al., *Stroke*, 1974, 5: 630-639
- 38 K. K. Kwong, J. W. Belliveau, D. A. Chester, I. E. Coldberg, R. M. Weisskoff, B. P. Poncelet, D. N. Kennedy, B. E. Hoppel, M. S. Cohen, R. Turner, H. M. Cheng, T. J. Brady, B. R. Rosen, Dynamic magnetic resonance imaging of human brain activity during primary sensory stimulation. *Proc. Natl. Acad. Sci.*, **89**:5675-5679 (1992).
- 39 S. Ogawa, D. W. Tank, R. Menon, J. M. Ellermann, S-G. Kim, H. Merkle, K. Ugurbil, Intrinsic signal changes accompanying sensory stimulation: functional brain mapping with magnetic resonance imaging, *Proc. Natl. Acad. Sci.*, **89**: 5951-5955 (1992)
- 40 LG 3rd Morris, WM Mueller, FZ Yetkin, VM Haughton, TA Hammeke, S Swanson, SM Rao, A Jesmanowicz, LD Estkowski, PA Bandettini, et al., Functional magnetic resonance imaging in partial epilepsy, *Epilepsia*, **35 (6)**: 1194-8(1994)
- 41 RR Benson , WJ Logan, GR Cosgrove, AJ Cole, H Jiang, LL LeSueur, BR Buchbinder, BR Rosen, VS Jr Caviness, Functional MRI localization of language in a 9-year-old child, *Can J Neurol Sci*, **23 (3)**: 213-9 (1996)

-
- 42 RB Tootell, JB Reppas, KK Kwong, R Malach, RT Born, TJ Brady, BR Rosen, JW Belliveau, Functional analysis of human MT and related visual cortical areas using magnetic resonance imaging. *J Neurosci*, **15 (4)**: 3215-30 (1995)
- 43 RB Tootell, JB Reppas, AM Dale, RB Look, MI Sereno, R Malach, TJ Brady, BR Rosen, Visual motion aftereffect in human cortical area MT revealed by functional magnetic resonance imaging, *Nature*, **375 (6527)**: 139-41 (1995)
- 44 D Le Bihan, P Jezzard, J Haxby, N Sadato, L Rueckert, V Mattay, Functional magnetic resonance imaging of the brain., *Ann Intern Med*, **122 (4)**: 296-303 (1995)

Chapter 2 Error Analysis of the Cerebral Metabolite Concentrations in ^1H Magnetic Resonance Spectroscopy

Introduction

Over the past decade, ^1H Magnetic Resonance spectroscopy (^1H MRS) has developed into a powerful tool for investigation of cerebral metabolites *in vivo* and *in vitro*. Comparisons using both relative amplitudes among the metabolite peaks [1,2] as well as the absolute metabolite concentrations [3,4,5] have been proposed to monitor the neurochemical changes during cerebral pathologies or physiological challenges. However, the absolute metabolite concentrations reported from different groups are not always consistent. For instance, the NAA concentration could be as low as $4 \mu\text{mol/g}$ [6] or

as high as 17 μ mol/g [8] and the creatine values have been reported between 7.7 μ mol/g [6] and 10 μ mol/g [8]. One criterion for measurement of an accurate metabolite comparison, whether it is relative or absolute metabolite concentration estimate, is the existence of an internal reference metabolite peak whose amount should remain constant during various physiological and pathophysiological conditions. Creatine [7,8] and unsuppressed water signals are two of the most popular spectral peaks used as the internal standards. However, uncertainty in the invariance of the internal standard makes the relative concentration comparison less reliable. Several investigators have proposed using external standards such as MnCl_2 -doped [9] water or trimethylsilylethanol (TSE) [10,11] with known T_1 and T_2 values and concentrations. This approach also has some difficulties, such as the distortion of the signal amplitude due to the possible field inhomogeneity (B_1 field and static field B_0) when the external standard sample is placed beside the head. Nonetheless, if the accurate absolute metabolite concentration is achievable, it is highly desirable because it would allow one to:

- 1) make inter-subject comparisons,
- 2) make physiologic parameter estimations, such as $\text{CMR}_{\text{glucose}}$ calculations.

In this chapter, we will discuss the possible factors which may alter the accuracy of the metabolite amounts estimated from ^1H MR spectroscopy.

Method to Estimate the Cerebral Metabolite Concentrations
from ^1H MR Spectroscopy:

In principle, different chemical groups may experience slightly different magnetic fields due to shielding by electrons and thus express themselves at different MR spectral positions called chemical shifts. The chemical shift is invariant as expressed in ppm but is proportional to the magnetic field strength as expressed in Hz. Like fingerprints, most of the chemical groups have their own chemical shift values and are represented as resonances centered at the specific chemical shift locations (ppm or Hz). Depending upon the scalar coupling effects among different chemical groups of the same molecule, the lines may be split into doublet, triplet, or even higher order multiplicities. Over the past several decades, most of the observable cerebral spectral peaks from ^1H MRS have been identified and assigned to their corresponding chemical groups. Table 2-1 is a list of most of the major cerebral metabolites which are ^1H MRS detectable. From basic magnetic resonance spectroscopy theory, the signal intensity of a singlet spectral peak from a spin-echo experiment should follow the expression shown in equation 2-1:

$$SI_{Aa} = M_{oA} \left(1 - \exp\left(-\frac{TR}{T1_{Aa}}\right) \right) \exp\left(-\frac{TE}{T2_{Aa}}\right) \quad (2-1)$$

where

SI_{Aa} = signal intensity from the spectral peak 'a' of molecule A

M_{oA} = proton density of molecule A

$$\propto N_{Aa} X [A] \quad (2-2)$$

N_{Aa} = number of protons in this spectral group 'a' of molecule

A,

$[A]$ = concentration of molecule A.

And

$$\frac{SI_{Aa}}{SI_{Bb}} = \frac{M_{oA} (1 - \exp(-\frac{TR}{T1_{Aa}})) \exp(-\frac{TE}{T2_{Aa}})}{M_{oB} (1 - \exp(-\frac{TR}{T1_{Bb}})) \exp(-\frac{TE}{T2_{Bb}})} \quad (2-3)$$

$$= \frac{N_{oA}[A](1 - \exp(-\frac{TR}{T1_{Aa}})) \exp(-\frac{TE}{T2_{Aa}})}{N_{oB}[B](1 - \exp(-\frac{TR}{T1_{Bb}})) \exp(-\frac{TE}{T2_{Bb}})} \quad (2-4)$$

where, a and b are the 2 spectral peaks from the 2 different molecules A and B.

Compound (Chemical Shifts and Approximate Human Brain Concentration)	Structure	Relevance to Neurodegeneration
N-acetylaspartate (NAA) 2.023 ppm (CH ₃) 2.52 ppm (β CH) 2.70 ppm (β' CH) ≈ 8mM		Neuronal Marker Higher Concentration in Grey Matter Compared to White Matter
Aspartate (asp) 2.69 ppm (β CH) 2.82 ppm (β' CH) ≈ 2 mM		Excitatory neurotransmitter May possess excitotoxic potential
Choline / Phosphocholine (CHO) 3.23 ppm (CH ₃) ≈ 1.6 mM		Also composed of other trimethylamines May represent lipid breakdown products and/or gliosis
Creatine / Phosphocreatine (Cr/PCr) 3.03 ppm (CH ₃) 3.95 ppm (CH ₂) ≈ 7.6mM		Peak represents sum of total creatine. Supplies phosphate for conversion of ADP to ATP in creatine kinase reaction.
γ-aminobutyric acid (GABA) 1.91 ppm (β CH ₂) 2.31 ppm (α CH ₂) 3.02 ppm (γ CH ₂) ≈ 3 mM		Inhibitory Neurotransmitter Large fraction of basal ganglia neurons are GABAergic
α-D-Glucose 3.2-4.1 ppm ([2-6]CH) 5.32 ppm ([1] CH) ≈ 0-3 mM		Fuel for the brain - most ND conditions show hypo-metabolism of glucose Detectable in 2D studies <i>in vivo</i> but quantitation at low field strengths nearly impossible except potentially peak at 5.32 ppm.
Glutamate (Glu) 2.06 ppm (β CH) 2.36 ppm (γ CH ₂) 2.10 ppm (β' CH) 3.76 ppm (α CH) ≈ 6 - 10 mM		Major excitatory neurotransmitter in brain. Potential Excitotoxin. Quantifiable at high fields
Glutamine (Gln) 2.14 ppm (β CH ₂) 2.46 ppm (γ CH ₂) 3.78 ppm (α CH) ≈ 3 mM		Source of glutamate for neurotransmission Quantitation problems as hard as for glutamate.
Myo-inositol (mI) 3.54 ppm ([1,3]CH) ≈ 5 mM		Possible osmoregulator. Precursor of inositol polyphosphate (IP ₃) intracellular messengers.
Lactate 1.33 ppm (β CH ₃) ≈ 0.5 mM		End product of anaerobic glycolysis Barely detectable in normal brain.

Table 2-1 Common neurochemicals observable in proton MRS

In theory, if the molar concentration of chemical A is known, then the absolute concentration of chemical B can be estimated with the knowledge of T_1 and T_2 values of both of the spectral groups a and b:

$$[B] = \frac{SI_{Bb}}{SI_{Aa}} [A] \frac{N_{Aa}}{N_{Bb}} \frac{(1 - \exp(-\frac{TR}{T1_{Aa}})) \exp(-\frac{TE}{T2_{Aa}})}{(1 - \exp(-\frac{TR}{T1_{Bb}})) \exp(-\frac{TE}{T2_{Bb}})} \quad (2-5)$$

For *in vivo* cerebral spectral studies, the molar levels of cellular water and creatine are relatively stable and are usually taken as the internal spectral standards, to map out the amounts of other cerebral metabolites. However, according to equation (2-5), the measurements of absolute metabolite concentrations are only feasible when the measurements of the spectral signal intensities and T_1/T_2 values are accurate. In the following sections, we will discuss the possible errors which may propagate into the absolute concentration measurements.

Spectral quality:

Spectral Overlap

The spectral peaks can be expressed as Lorentzian lines centered at their corresponding chemical shifts (ppm or Hz). The line width of the Lorentzian line is proportional to the relaxation rate R_2^* ($R_2^* = 1/T_2^*$, $\Delta\nu_{1/2} = 1/\pi T_2^*$) which is composed of several factors:

$$R_2^* = R_2 + \sum_n R_{2n}' \quad (2-6)$$

where R_2 is the intrinsic spin-spin relaxation rate of this particular molecule in the magnetic field and R_{2n} s are some external factors which can accelerate the relaxation rate, such as the inhomogeneity of the magnetic field, flow rate, etc. In the practical world, there are several factors which may lead to magnetic field inhomogeneity, such as an imperfect shim of the magnetic field caused by sudden changes of the magnetic susceptibility χ_m close to the interface of two different tissue compartments (e.g., grey-white matter boundary, brain-CSF or brain-air sinus interface, etc.). The bigger the relaxation rate is, the broader the Lorentzian line width will be. The typical line width of ^1H MR cerebral spectra can as low as 2 Hz in small single voxel experiments. However, since the chemical shift distance (Hz) between 2 chemical groups is proportional to the strength of magnetic field, the ^1H spectra from a low field clinical magnet (0.5 ~ 1.5 T) may not allow one to resolve one individual spectral peak from the adjacent ones at a given broad spectral line width. Prior work using 2D COSY experiments has demonstrated that there are many overlapping ^1H chemical shifts which cannot be resolved without the use of the 2D technique [12]. The spectral composition may be even more complicated if some of the spectral peaks are J-coupled and split to various multiplicities which can undergo phase modulation as a function of echo time (TE). We will discuss this phenomenon later. General speaking, one can reduce the spectral line width with a better shim of the magnetic field, and with care to the choice of the imaging voxel cover as few heterogeneous tissues as possible, and to keep the voxel as far away

from interfaces such as sinuses with huge magnetic susceptibility differences as is possible .

Signal to Noise Ratio (SNR)

The concentrations of cerebral metabolites are generally in the millimolar range while the cellular water/lipid contents are in the molar range. To detect these concentration differences in the ^1H MRS measurement, the signal from water or lipid will be thousands of times bigger than the signal from the cerebral metabolites. Therefore, water/lipid suppression has to be applied to make the cerebral metabolite signals visible. However, imperfect water/lipid suppression can still lead to some problems. As water and lipid are present in such huge quantities compared to the cerebral metabolites, reduction of the signal intensity to only one tenth of the original water/lipid amount still leaves the water or lipid signal much bigger than the metabolite signal. As most of the receiver bits would be used to digitize the massive water/lipid signals, there would not be enough dynamic range to digitize the tiny spectral signals of cerebral metabolites. In other words, the signal to noise ratio (SNR) of the metabolites will be too small to detect the metabolite signals. Furthermore, as the shoulders of the water/lipid peaks may extend over quite a wide range of chemical shift with non-negligible amplitude, this may lead to problems like baseline shift and phase distortion of the metabolite peaks. So, the lower the SNR the ^1H MR spectrum has, the more complicated the spectral analysis will be and the more questionable the accuracy of the metabolite concentration measurements is.

Problems with relaxation rate measurements:

Methods to measure the relaxation times T_1 and T_2 ---

The longitudinal relaxation time (T_1) describes how fast the disturbed magnetization will return to thermal equilibrium. The T_1 value is traditionally measured by a series of inversion recovery experiments stepping through variable inversion recovery waiting times (TI). The spin-spin relaxation time (T_2) is a function of echo time TE and can be measured by series of spin-echo experiments stepping through several TE values. Equations (2-7) and (2-8) describe the mathematical expressions of these measurements:

$$SI = M_0(1 - 2\exp(-\frac{TR}{T_1}))(1 - \exp(-\frac{TR}{T_1}))\exp(-\frac{TE}{T_2}) \quad (2-7)$$

$$T_2 = \frac{(TE_2 - TE_1)}{\ln(SI_1 - SI_2)} \quad (2-8)$$

However, there are a number of possible problems involved in the relaxation time measurements:

Partial volume averages and heterogeneous environments:

Due to the limitation of spatial resolution, for both in plane and through plane resolutions, the spectral voxel may cover heterogeneous structures and may be contaminated by structures adjacent to but outside the voxel. Different types of tissues (e.g., gray matter(GM), white matter(WM), and cerebrospinal fluid (CSF)) have different metabolite compositions and the same metabolites in different types of tissues may possess different relaxation times (e.g., brain tissue H₂O with $T_2 \approx 70\text{ms}$ and CSF with $T_2 \approx 2\text{s}$). Kreis et. al. [11] has showed a large scatter in the *in vivo* relaxation time

measurements partially due to the contamination of CSF, arterial and venous blood, as well as other small sources. For a spectral voxel which contains or is contaminated by multiple tissue structures, the spectral signal will be just the sum of signals from all of the structures:

$$\begin{aligned}
 SI_A &= \sum_n SI_{An} \\
 &= \sum_n f_{An} \left(1 - \exp\left(-\frac{TR}{T1_{An}}\right)\right) \exp\left(-\frac{TE}{T2_{An}}\right) \quad (2-9)
 \end{aligned}$$

where,

SI_A = signal intensity of metabolite A,

SI_{An} = signal intensity of metabolite A from structure n,

f_{An} = fraction of total proton intensity contributed from structure n,

$T1_{An}, T2_{An} = T_1$ and T_2 of metabolite A from structure n.

As one can expect, the signal intensity will no longer follow a simple mono-exponential decay and the T_1 and T_2 relaxation time measurements will be unreliable.

Spectral overlap and J-coupling effects:

As mentioned earlier in this chapter, the conditions to resolve two spectral peaks are determined by their chemical shifts and line widths. Some of the cerebral metabolites have very close chemical shifts and it becomes difficult to resolve them from each other. This situation is especially severe at lower field strengths like 1.5T. For example, the spectral peak of the methyl group of NAA (2.023 ppm) overlaps with the peaks of GABA (1.91 ppm), NAAG (2.05 ppm), and glutamate (2.06 ppm). Other than the simple singlet spectral

overlaps, some of the overlapping peaks are J-coupled and their spectral phases are modulated by the echo time TE. This kind of complexity makes the spectral quantification difficult. Considering both the spectral overlap and the J-coupling effects, equation (2-9) can be rewritten as:

$$\begin{aligned}
 SI &= \sum_n SI_n \\
 &= \sum_n M_{on} \left(1 - \exp\left(-\frac{TR}{T1_n}\right)\right) \exp\left(-\frac{TE}{T2_n}\right) \times J_n
 \end{aligned}
 \tag{2-10}$$

where,

SI_n = signal intensity from metabolite N,

M_{on} = proton density of metabolite N

$T1_n, T2_n$ = T_1 and T_2 of metabolite N,

J = J-coupling effect

= 1 for singlet peak

= $1/2 \cos(2\pi J/2 TE)$ for each doublet peak

= $1/4 \cos(2\pi J TE)$ for the 2 side peaks of triplet

= $1/2$ for the middle peak of triplet

= others for higher multiplicity

Table 2-2 is a list of some of the spectral groups with possible spectral overlap.

	Metabolite	ppm	multiplicity	Mo (mM)
Group I	NAA (CH ₃)	2.023	s	8
	NAAG	2.05	s	0.79
	Glutamine (β-CH ₂)	2.1	m	6.8
	Glutamate (β -CH ₂)	2.14	m	6.8
	GABA (β -CH ₂)	1.91	qu	3.61
Group II	PCr/Cr (CH ₃)	3.05	s	7.6
	GABA (γ-CH ₂)	3.02	t	3.61
Group II	Choline (CH ₃)	3.25	s	1.6
	myo-Inositol	3.2	dd	5
	Taurine	2.3	t	2.3

Table 2-2. List of major spectral overlap groups in ¹H-MRS.

Here in this chapter, we will demonstrate how the spectral overlap and the J-multiplicity may degrade the spectral quality and thus reduce the accuracy in T₂ relaxation time measurements. Furthermore, we will describe how the errors in relaxation time measurements lead to errors in absolute metabolite concentration estimates.

Methods:

Computer Simulation

All of the computer simulations were performed with MATLAB (the Math Works, Inc.) programs.

Spectral simulation :

Human cerebral ^1H MR spectra were computer simulated with preassigned values of molar concentrations and relaxation rates (R1 and R2) with most of the major cerebral metabolites detectable from ^1H MRS as indicated in table 2-1. The absolute metabolite amounts were set to physiological levels [13]. Chemical shifts (ppm), multiplicities, and coupling constants of those spectral peaks were obtained from the literature [14]. The MATLAB program assumes a spin-echo experiment is performed and allows one to specify the magnetic field strength, spectral resolution (via spectral sweep and number of data points), and echo time (TE). The field inhomogeneity is reflected as an extra factor in $R2^*$ (Hz) as expressed in equation (2-6). This program assumes perfect water and lipid suppression (zero signal contamination from water or lipid) and weak J-coupling only. Macromolecular contamination was not included in this simulation [15,16]. For the spectral peaks with higher order J coupling, this MATLAB program simplified the complex spectral formation by using double doublet peaks (i.e., split a single spectral peak to be doublet peaks with $J1$ spectral distance (ppm); then split each peak to be doublet again by $J2$ spectral distance (ppm)). Table 2-3 illustrates the spectral elements used in this simulation. Amplitude spectra of both multi-metabolite (sum of all of the metabolite spectral lines) and individual metabolite spectra were plotted separately and coded with different colors.

metabolite	Mo (mM)	ppm	multiplicity	J	# of protons
NAA	11	2.01	1	N/A	3
		2.7	c	3.7, 15.9	1
		2.52	c	9.8, 15.9	1
		4.4	c	3.9, 9.8	1
creatine	7.6	3.05	1	N/A	2
choline	1.6	3.25	1	N/A	9
taurine	2.3	3.44	3	6.7	2
		3.27	3	6.7	2
myo-inositol	5	3.55	c	2.7, 9.9	2
		3.65	2	9.8	2
		3.77	2	9.8	1
		3.28	3	9.2	1
glutamate	6.8	3.80 α -CH ₂	3	7.3	1
		2.10 β -CH ₂	c	7.3, 7.3	1
		2.35 γ -CH	c	7.3, 7.3	1
glutamine	6.8	3.78 α -CH ₂	t	7.3	1
		2.14 β -CH ₂	c	7.3, 7.3	1
		2.46 γ -CH	c	3.6, 7.3	1
lactate	0.7	4.12	4	7.3	1
		1.33	2	7.3	3

Table 2-3 Spectral elements used in Lorentzian line simulation.

T₂ measurement errors:

For a simple singlet spectral peak without any overlapping peaks, the signal intensities from spin-echo experiments should follow mono-exponential decays as a function of echo time (TE) (equation (2-1)). However, due to the spectral overlap and J-coupling effects, the total signal intensity is not only likely to be a multi-exponential decay but also to oscillate in a sinusoidal-like form along TE axis [17]. We used MATLAB to simulate this multi-exponential decay and sinusoidal oscillation phenomenon. We paid particular attention to three prominent metabolite spectral groups in the typical ¹H MR cerebral spectrum: NAA(methyl group, 2.023 ppm), creatine(3.05 ppm), and choline(3.25 ppm). Metabolites with chemical shifts less than 0.1 ppm away from any of the 3 major spectral locations were classified

to be the same spectral group as the major metabolite (Table 2-2). The MATLAB programs ignore any chemical shift differences between the major and the minor metabolites (e.g. major = NAA and minors = NAAG, GABA, Glx) in the same spectral group and the total spectral signal intensity of the spectral group was calculated simply by summing up all of the metabolite signals in the same spectral group. The pure T_2 decay curves (as a function of TE) of the major metabolite as well as the composite T_2 decay curve from all of the metabolites are synthesized separately according to equation (2-10). The T_2 decay curves were then presented in a semi-logarithm fashion ($\log(SI)$ versus TE) and a least-squares fitting program was applied to the composite data set to estimate the “measured T_2 ” value of the major metabolite. The T_2 error was then computed as a percent deviation of the “measured T_2 ” from the “pure T_2 ” of the major metabolite.

Absolute concentration measurement errors:

The absolute concentration of the cerebral metabolite can be estimated according to equation (2-5). However, this measurement involves a lot of other measurements such as T_2 measurements of the internal standard metabolite and the one to be quantified. Statistically, the propagation of errors of the measured absolute concentration σ_b can be expressed as equation (2-11):

$$\left(\frac{\sigma_{[A]}}{[A]}\right)^2 = \left(\frac{\sigma_{M_o}}{M_o}\right)_s^2 + \left(\frac{\sigma_{M_o}}{M_o}\right)_A^2 \quad (2-11)$$

where,

$$\left(\frac{\sigma_{M_0}}{M_0}\right)^2 = \left(\frac{\sigma_{SI}}{SI}\right)^2 + \left(\frac{TE}{T_2}\right)^2 \left(\frac{\sigma_{T_2}}{T_2}\right)^2 + \left(\frac{TR}{T_1}\right)^2 \left(\frac{1}{1 - \exp\left(-\frac{TR}{T_1}\right)}\right)^2 \left(\frac{\sigma_{T_1}}{T_1}\right)^2 \quad (2-12)$$

We, again, utilized MATLAB to simulate the error properties of this absolute concentration estimation. In this case, water was used as the standard metabolite to measure the NAA concentration. The percent error of the NAA concentration was estimated according to equation (2-11) with the four variables : errors of T_1 of water (σ_{t1w}), T_2 of water (σ_{t2w}), T_1 of NAA (σ_{t1NAA}), T_2 of NAA (σ_{t2NAA}). The simulation fixed 3 of those 4 variables and varied the 4th variable in the range of error between -100% and 100% with an increment step of 10% error in the relaxation time. In this fashion, one is able to study the property of the concentration error caused by this particular relaxation time error.

Phantom and *in vivo* spectra

In order to verify the computer simulation results, especially for the T_2 measurement errors, phantom spectra as well as *in vivo* human cerebral spectra were obtained with the same parameter settings as used in computer simulations. All of the spectroscopy experiments were conducted on a 1.5 T imager (Signa, GE). In order to get single voxel spectra, a PRESS sequence was used to acquire data instead of using spin-echo sequence as was used in computer simulation. Two second repetition times (TR) were used in both human and phantom studies and the echo time was stepped from 51 to 304 ms with approximately 10 to 17 ms increments for total of 18 points. Shorter

echo times ($TE < 40$ ms) were desirable but were not possible using the GE PRESS sequence at the time. For the phantom study, a bottle of agar gel mixed with NAA (10mM), glutamate (9.7mM), glutamine (3.7mM), and GABA (3.29 mM) was used to simulate the cerebral metabolite contents. For the *in vivo* study, spectra were taken from occipital cortex of healthy human volunteers.

Results and Discussions:

Spectral simulation:

The spectra were computer simulated specifically for the magnetic field strengths of 1.5, 4.7, and 9.4T (the major magnets used at NMR center, Massachusetts General Hospital, MA). To simplify the complicated metabolite compositions, we assumed the T_2 of NAA to be 450 ms and the other metabolites to be 400 ms. The spectra were synthesized either with short echo times ($TE = 68$ ms), intermediate echo times ($TE = 136$ ms) or long echo times ($TE = 272$ ms). To set the echo times to be multiple of 68 ms is essential to refocus those magnetizations with J-modulation of 7.3 Hz. Figure 2-1 shows typical spectra with reasonable magnetic field homogeneity ($\delta R2 = 10$ Hz) under the three main magnetic field settings. Figure 2-2 shows spectra with relatively bad shims ($\delta R2 = 50$ Hz). In each diagram, the top box shows the mixing spectrum (the summation of the individual spectra) with different color codes to highlight the 'presumable' major metabolite peaks (NAA, Cr, and Cho) and the bottom box shows the 'real' spectra from the individual metabolites.

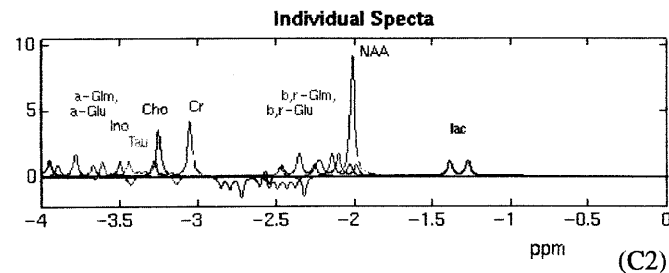
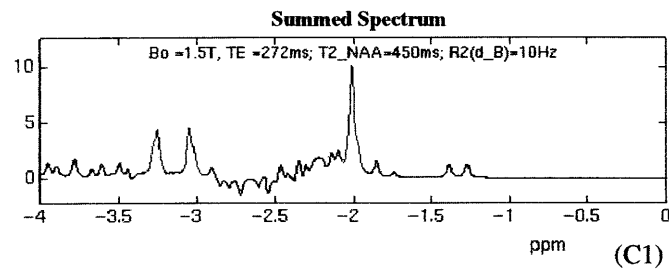
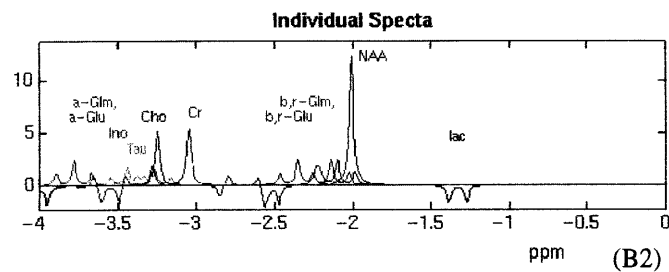
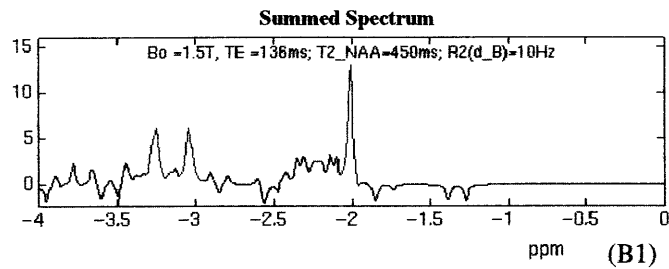
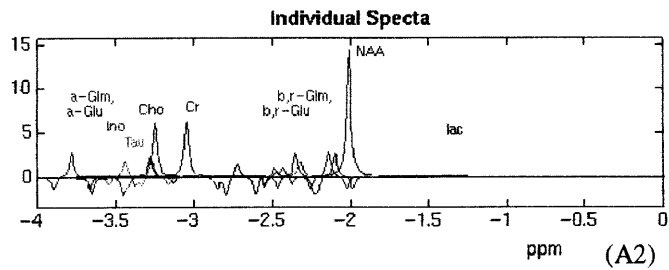
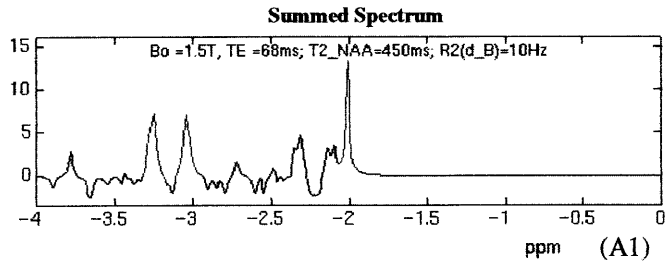


Figure 2-1(a) Spectra simulation: B0 = 1.5T, TE = 68,136, and 272ms (A,B,C respectively), $\Delta R2 = 10\text{Hz}$ (relatively good shim).

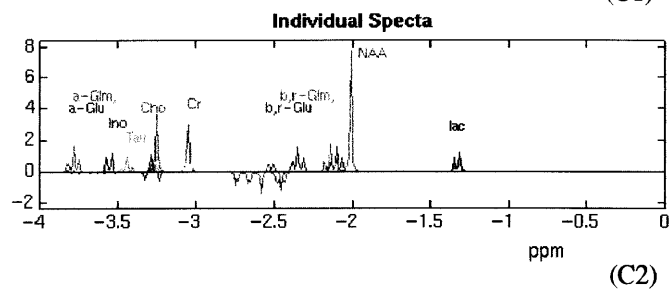
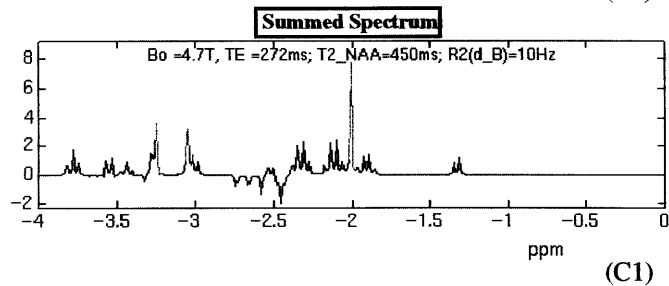
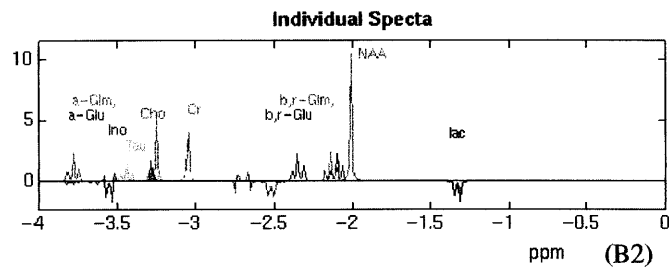
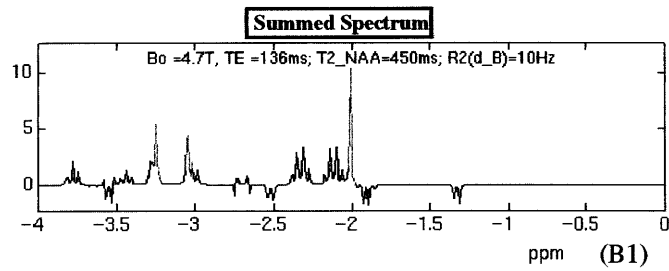
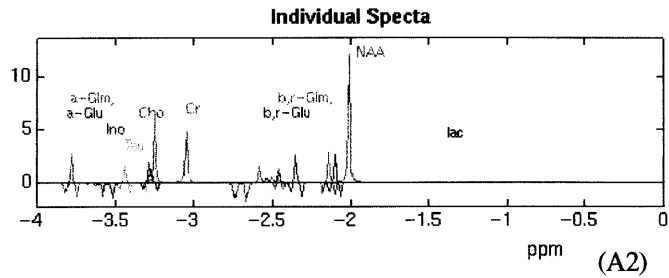
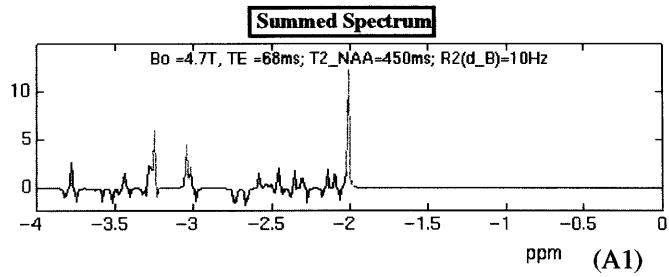


Figure 2-1(b) Spectra simulation: B0 = 4.7T, TE = 68,136,and 272ms (A,B,C respectively), $\Delta R2 = 10\text{Hz}$ (relatively good shim).

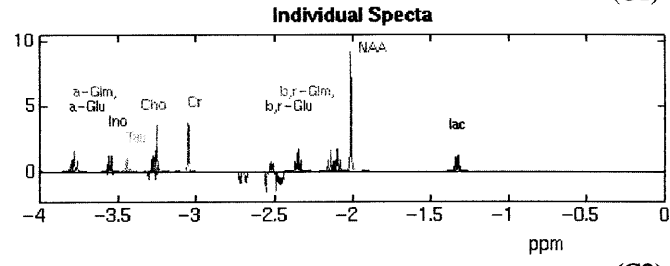
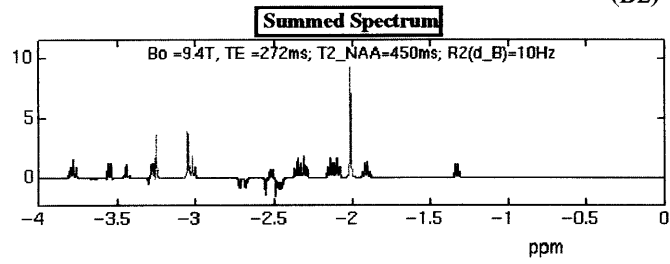
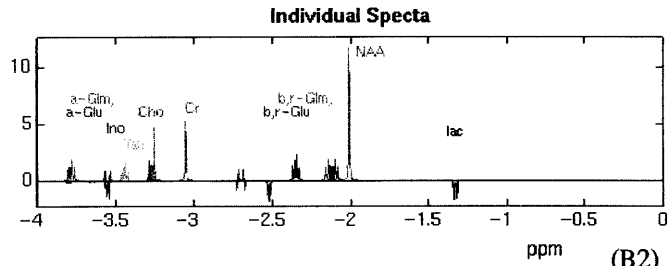
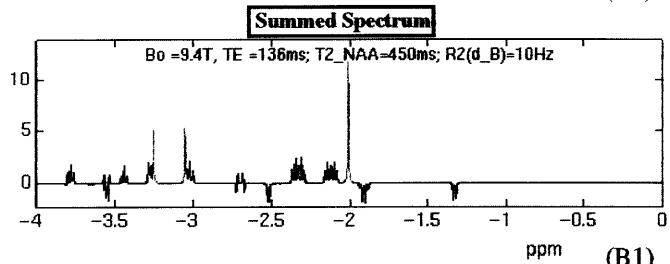
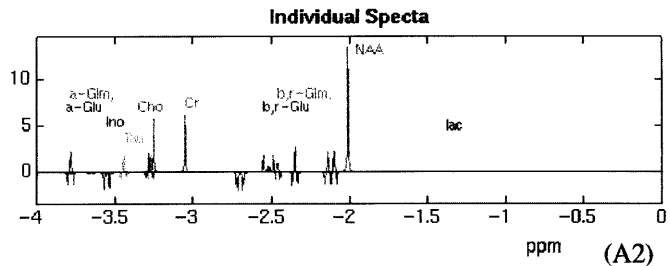
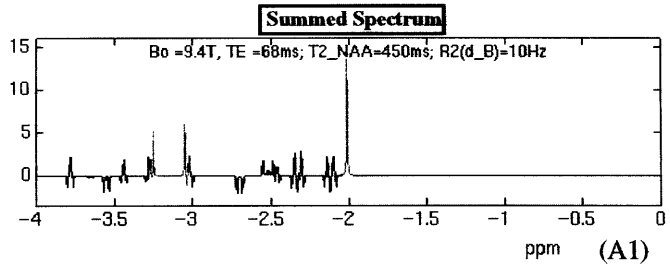


Figure 2-1(c) Spectra simulation: B0 = 9.4T, TE = 68,136, and 272ms (A,B,C respectively), ΔR2 = 10Hz (relatively good shim).

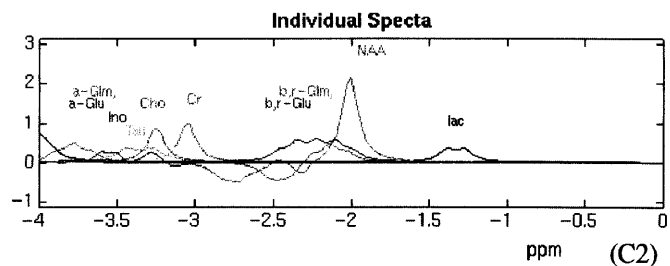
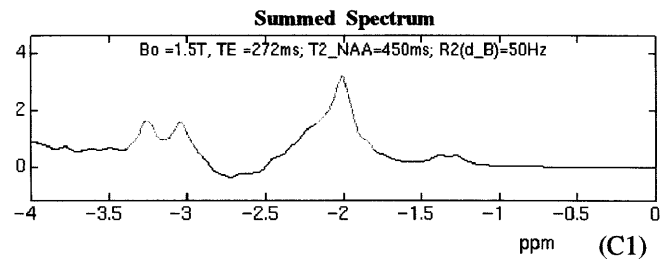
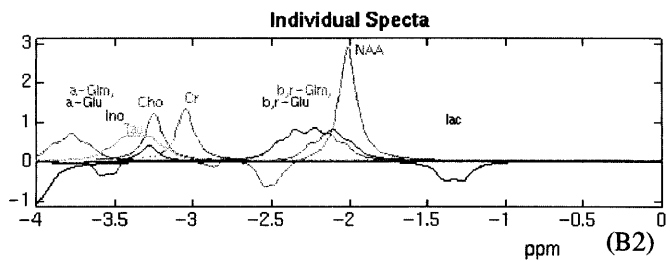
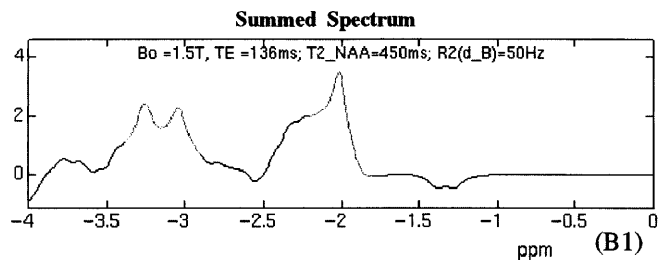
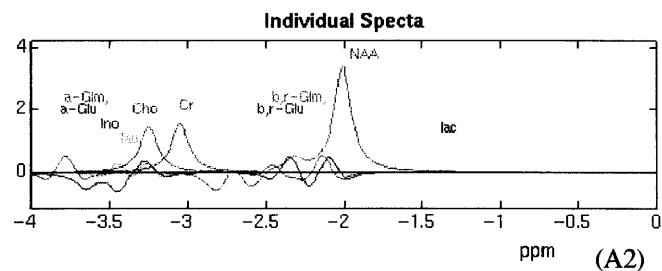
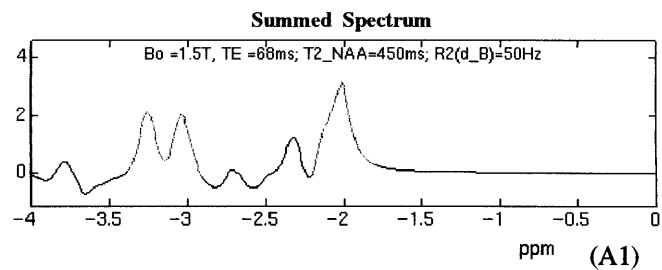


Figure 2-2(a) Spectra simulation: B0 = 1.5T, TE = 68,136, and 272ms (A,B,C respectively), $\Delta R2 = 50\text{Hz}$ (relatively bad shim).

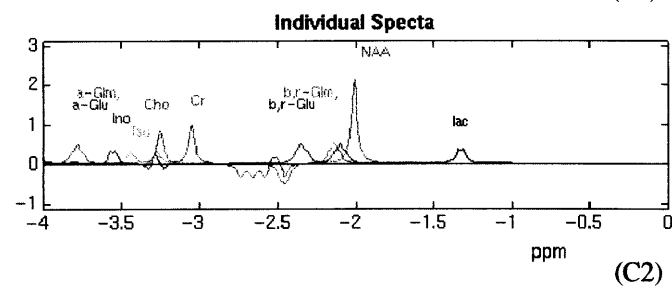
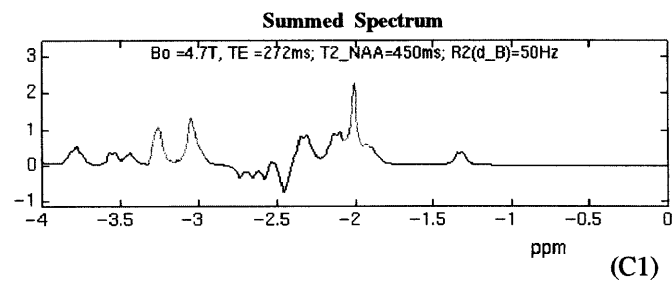
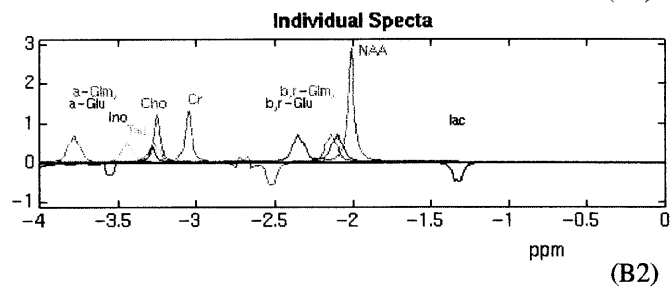
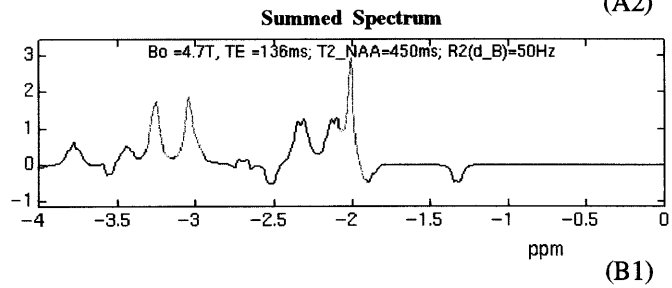
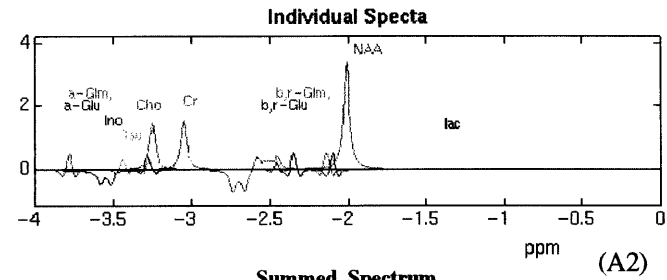
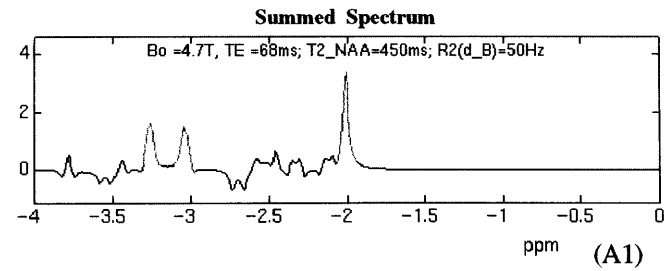


Figure 2-2(b) Spectra simulation: B0 = 4.7T, TE = 68,136, and 272ms (A,B,C respectively), $\Delta R2 = 50\text{Hz}$ (relatively bad shim).

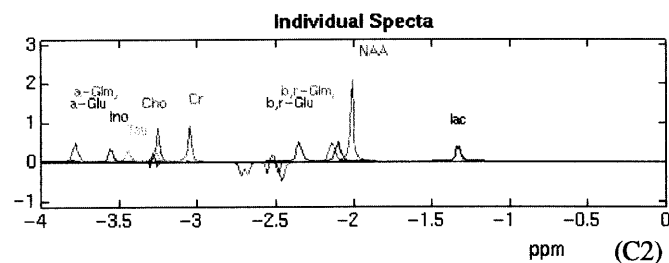
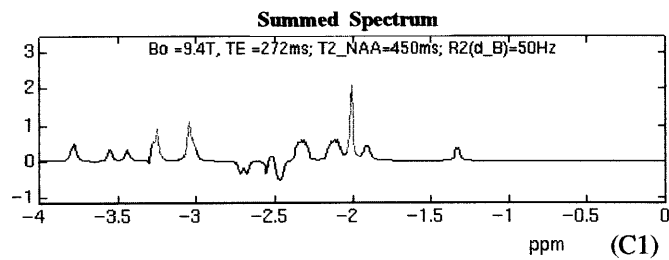
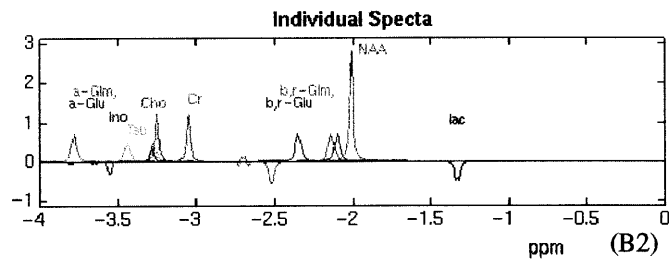
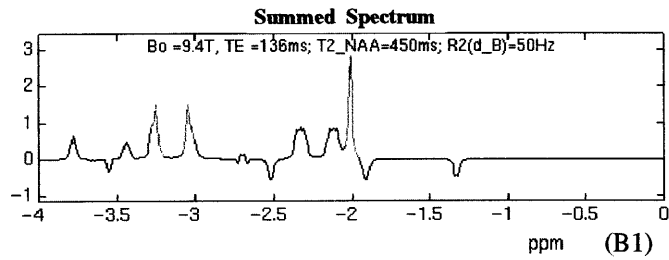
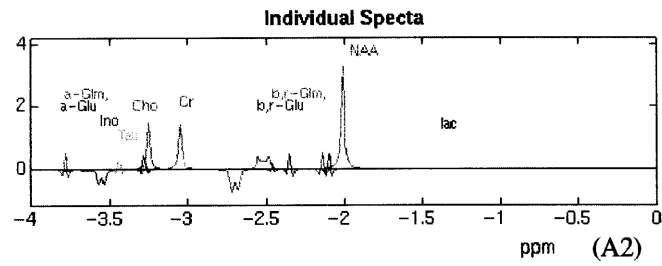
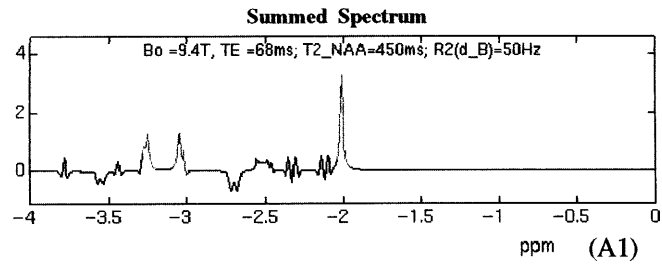


Figure 2-2(c) Spectra simulation: $B_0 = 9.4T$, $TE = 68, 136, \text{ and } 272ms$ (A,B,C respectively), $\Delta R_2 = 50Hz$ (relatively bad shim).

a.) Spectra with reasonable shim ($\delta R2 \approx 10$ Hz) -- For field inhomogeneities less than $\delta R2$ of 10 Hz, the NAA methyl group at 2.023 ppm is not severely contaminated by other metabolites at higher field strengths ($B_0 \geq 4.7$ T). However, at the low field strengths ($B_0 = 1.5$ T), this peak is heavily contaminated by glutamate, glutamine, NAAG, and GABA. At an echo time of 68 ms, those doublet and quadruplet peaks with J equal to 7.3 Hz, such as the quadruplet peaks of GABA at 1.91 ppm, will be out of phase and contribute no signal to the "observed NAA" peak. In other words, the NAA peak at 2.023 ppm is less contaminated by GABA at echo time of 68ms than echo times of 136 or 272ms. On the other hand, the doublet peaks of lactate at 1.33 ppm will be out of phase, too, and it would be a big loss to underestimate this important cerebral metabolite, which is of particular interest to cerebral physiology and studies of energy impairment. Since the linewidth is so narrow with $\delta R2 \approx 10$ Hz and the spectral amplitude of the pure NAA peak is usually much higher than the amplitudes of the overlapped metabolites, the pure NAA peak can thus be fit relatively accurately when one has a good baseline. However, for longer echo times such as 136 ms and 272 ms, this NAA peak is heavily distorted by glutamate, glutamine, and GABA. Under this condition, it becomes difficult to fit the pure NAA peak because the non-negligible amounts of glutamate, glutamine and GABA will modulate the baseline level and spectral phase. The same chemical contamination phenomena were observed for the creatine and choline peaks in low field cases. Comparing those spectra simulated at 1.5T with the 3 echo time settings, it is clear that the lower the echo time is, the

more spectral information is presented in the spectra. This is because SNR is degraded at the longer echo times, especially for those metabolites with low proton densities and high relaxation rates (R_2). Nevertheless, an echo time of 68 ms is generally not desirable because the loss of lactate information and the possible contamination of macromolecules. For other shorter echo times that people routinely use such as $TE = 20\text{ms}$, our computer simulation did not show great difference in the degree of spectral overlap in NAA, Cr, and Cho as in $TE = 272\text{ms}$ cases. However, this simulation with short echo time may not reflect the real spectra because our simulation did not take the consideration of macromolecules which have relatively short T_2 relaxation times. Also, lipid which is at around 1.33ppm is generally overlapped with lactate signal. Since lipid has relatively short T_2 relaxation time ($\approx 50\text{ms}$), the lipid contamination may only be problematic in shorter echo time instead of longer echo time experiments.

b.) Spectra with bad shim ($\delta R_2 > 50\text{Hz}$)-- The situation for the spectra with bad shim is much worse. For a field inhomogeneity of $\delta R_2 = 50\text{ Hz}$, it is almost impossible to separate the major metabolite peaks (NAA, Cr, Cho) from the minor metabolites (GABA, Glutamate, Glutamine, taurine, etc), especially at low magnetic fields. As indicated in figure 2-2a, the fusion of the minor metabolites disturbs the baseline level and makes the spectral phase adjustment difficult. Moreover, it becomes hard to determine the real spectral linewidth. Taking the methyl NAA peak as an example, it is difficult to determine how wide the Lorentzian line should be to match the true

NAA peak in the top spectrum of figure 2-2a. Even for higher magnetic field strengths, there is still certain degree of chemical shift overlap. For example, it is tricky to isolate out the pure creatine signal from the baseline due to the overlap of other chemicals. This is a particularly important issue because creatine is often used as the internal metabolite standard to measure the absolute or relative concentrations of the other cerebral metabolites.

T₂ measurement errors:

Figure 2-3 shows the semi-log plots of the synthesized 'NAA' signal intensity versus echo time (TE). The contents of this 'NAA' group include NAA with minor contributions from NAAG, glutamate, glutamine, and GABA. The solid red lines represent the "pure" NAA signal and the other color coded lines represent the "observed" NAA signals which are contaminated by the overlapping metabolites with different T₂ values. In this simulation, the T₂ value of one of the minor metabolites is fixed (e.g., glutamate = 300ms in figure 2-3a) while the T₂s of the other 2 minor metabolites (e.g., GABA and NAAG) were stepped between 100 to 500 ms in 100ms increments. The lines are coded to different saturation levels to represent the specific T₂ values over the T₂ span. The darker the line is, the smaller the T₂ value is. Because all of the minor metabolites in this 'NAA' group are J-coupled, each single minor metabolite will have its signal decay in a sinusoidal oscillation. Depending upon the ratio of the preassigned molar concentrations among these minor metabolites, the summed signal will cross the 'pure' NAA line at different TE points. In other words, not knowing the relative amount of those other metabolites, it

is impossible to find the optimized TE values to ensure that the ‘observed’ NAA signal deviates the least from the ‘pure’ NAA decay line. Similar phenomena were found for ‘creatine’ and ‘choline’ as shown in figure 2-4. If we try to fit this oscillating decay curve to get the “measured T_2 ” value, T_2 errors can be expected. The estimated T_2 error of NAA can be as big as 50% with reasonable T_2 settings of the minor metabolites (≈ 360 ms).

Our experiments of both phantoms and *in vivo* occipital cortex spectra showed similar oscillatory phenomena. The phantom and *in vivo* spectra turned out to match the computer synthesized spectra quite well even though the simulation assumed weak J-coupling only and a single spin-echo rather than PRESS (which has two 180 degree pulses). Figure 2-5 shows a stack plot of phantom spectra and figure 2-6 shows a stack plot of *in vivo* spectra. In the human spectra, several subsets from the 18 TE data sets were used to estimate the T_2 value of NAA. The results ranged between 400 ms to 1200 ms depending upon which TE points were included in the subsets. This confirms the observation from the computer simulation and leaves the accuracy of cerebral metabolite T_2 measurements to be suspect.

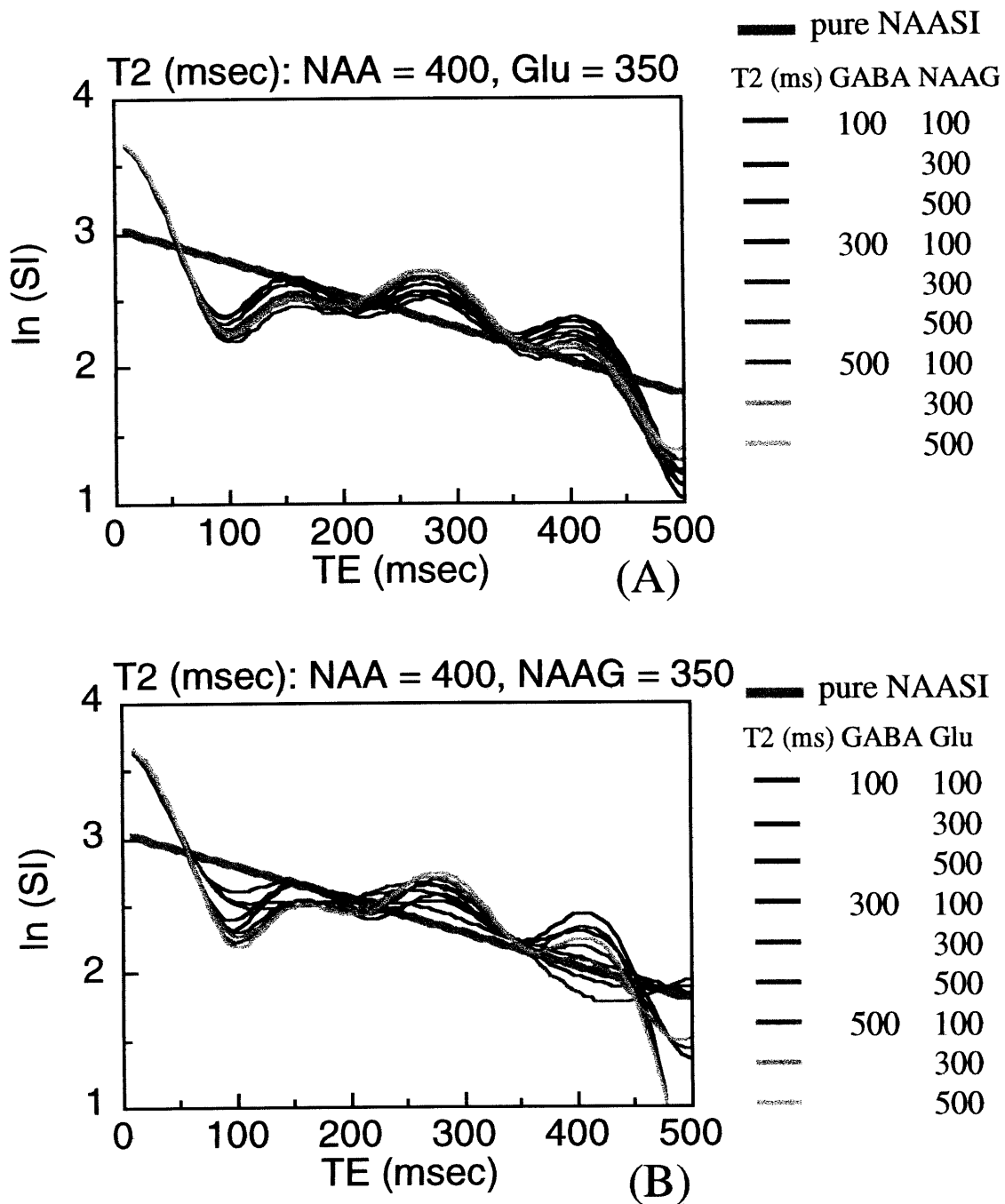


Figure 2-3 Signal intensity as a function of TE at around 2.023 ppm which is dominated by NAA. The pure signal intensity of NAA is presented as thick solid red line. The color curves represented the “measured” signal intensity with contamination of other overlapping compounds with different T2 value combination. (A) The “observed” signal of NAA with fixed T2 of glutamate. (B) The “observed” signal of NAA with fixed T2 of NAAG.

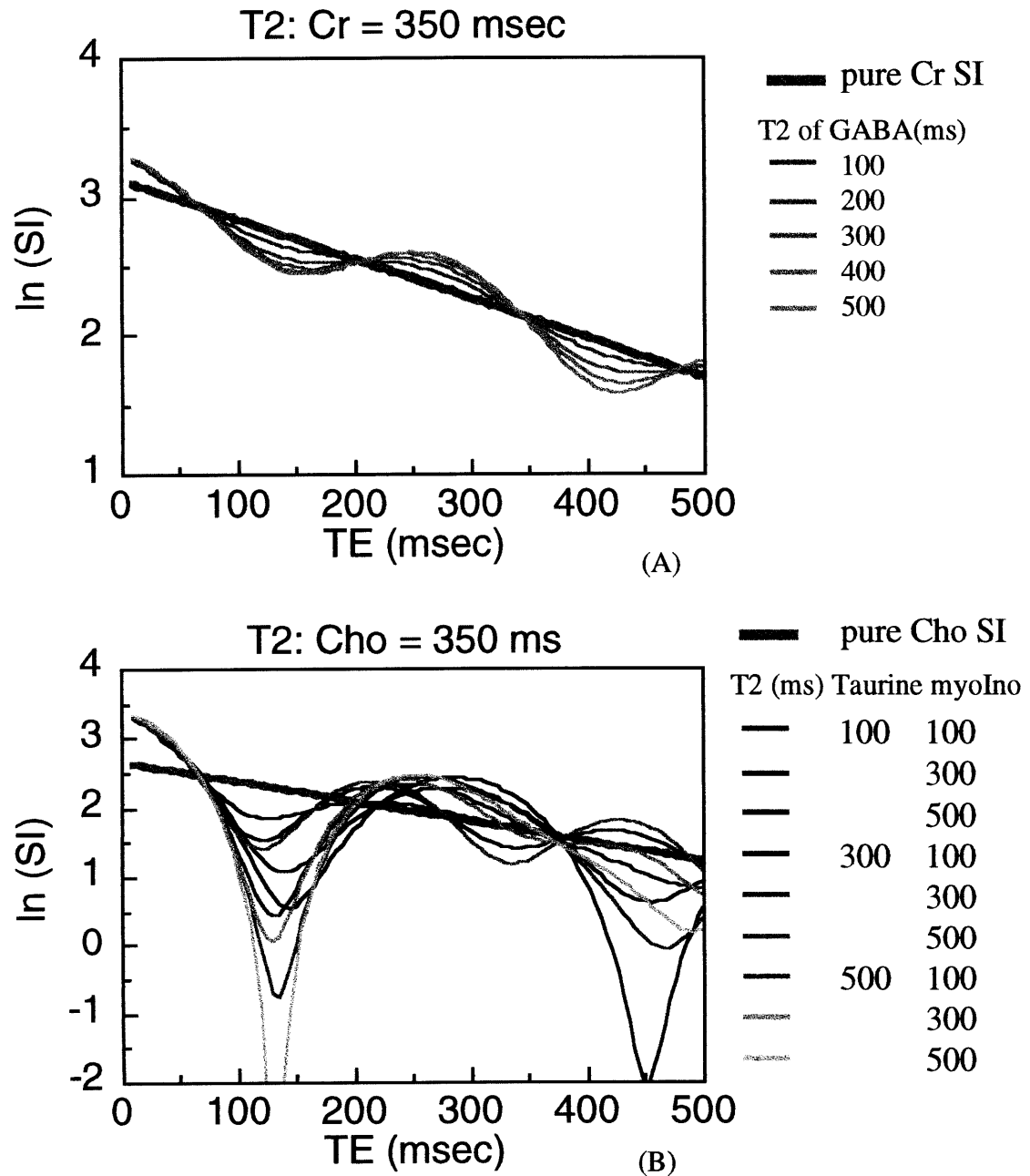
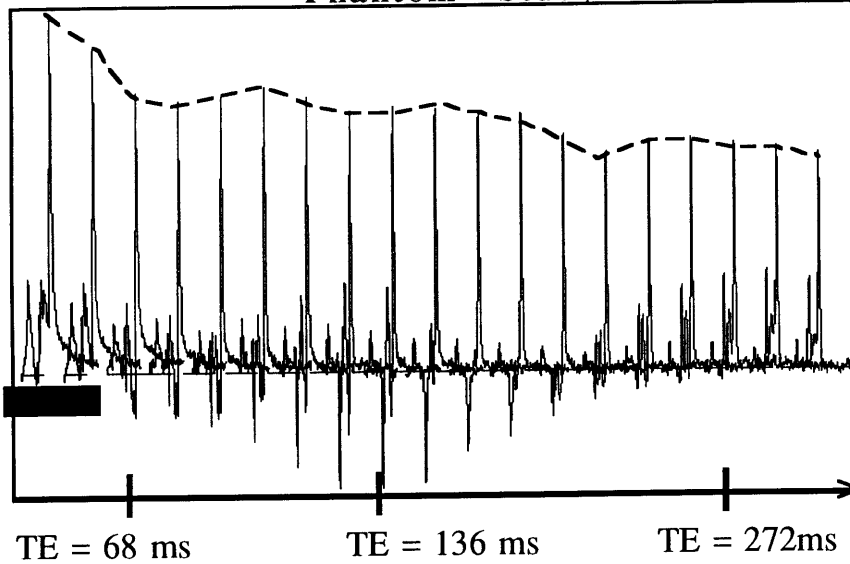


Figure 2-4 Signal intensity as a function of TE at around 3.03 ppm (A) and 3.23 ppm (B) which are dominated by creatine and choline, respectively. The pure signals for Cr and Cho are presented as thick solid red lines. The color curves represented the “measured” signal intensity with contamination of other overlapping compounds.

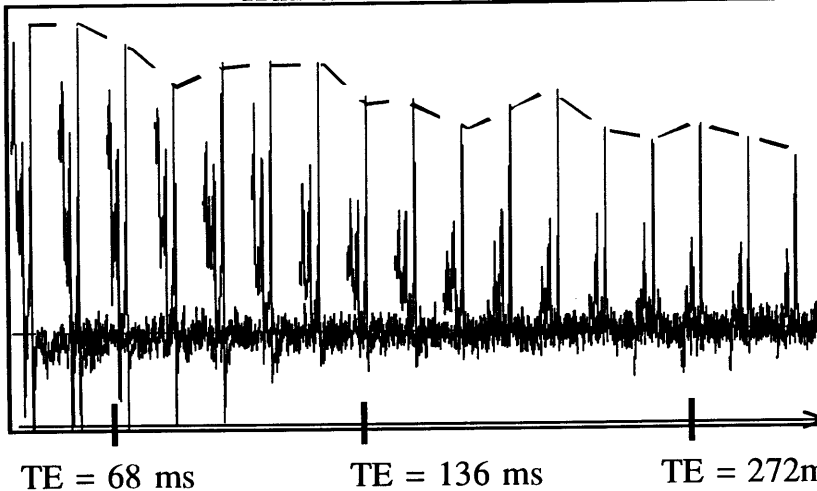
Phantom Study



NAA 10.0 mM
 Glutamate 9.7 mM
 Glutamine 3.5 mM
 GABA 3.29 mM

TE = 68 ms TE = 136 ms TE = 272ms
 Figure 2-5: phantom spectra

Human Study: Occipital Cortex



# of TE points	Measured T2 (ms)
4 (longest)	1150
4 (better)	441
4 (shortest)	365
18	476

TE = 68 ms TE = 136 ms TE = 272ms
 Figure 2-6: occipital cortex spectra.

Absolute concentration measurement errors:

Correlations between errors of the NAA concentration and relaxation time measurements were performed. Water was assumed to be the internal standard due to its relative invariance in molar concentration in the brain. Out of the 4 relaxation error variables ($[E_{t1w}, E_{t2w}, E_{t1NAA}, E_{t2NAA}] = [\sigma_{t1w}/T_{1w}, \sigma_{t2w}/T_{2w}, \sigma_{t1NAA}/T_{1NAA}, \sigma_{t2NAA}/T_{2NAA}]$), we assumed 3 of them with 10% errors from the principle values of relaxation times while the 4th variable was stepped between 0 and 100% error to build the error correlation curves. Figure 2-7 shows the simulation results. For a given repetition time (TR) of 2 s, which is the TR used for the phantom and *in vivo* studies, the water magnetizations will have enough time to be close to fully recovered between excitations (T_1 water \approx 950 ms) and thus the T_1 errors of water won't play an important role in the concentration error of NAA (figure 2-7 a). On the other hand, since the T_1 of NAA (\approx 1600 ms) is much longer, a two sec TR is not long enough to allow the full recovery of the magnetization of NAA and thus the T_1 error of NAA will not be negligible in the concentration estimate (figure 2-7 b). Figure 2-8 shows how TR effects NAA concentration estimate—the curves are steeper as TR goes shorter. For a TR value bigger than 2s, the concentration error induced by T_1 NAA will become tolerable (the amount of concentration error caused by every 1% increase in NAA T_1 error is smaller than 0.2%). Kreis et. al. [10] has reported that the longitudinal relaxation times (T_1) of the major peaks in an *in vivo* proton spectrum are close to each other

and the relative peak intensities are less sensitive to the repetition times (TR). In other words, if an appropriate saturation factor is used for corrections, the absolute concentration is less dependent on repetition times greater than about 1.5 second. The concentration error caused by T_2 errors of water or NAA, in the other hand, are not negligible no matter what TR and TE values have been chosen (figure 2-7 c,d). The error could be as high as over 100% in NAA concentration estimates. Therefore, the accuracy of T_2 measurements are much more important than the accuracy of T_1 measurements. This is bad because the T_2 s are harder to measure than the T_1 s due to J-modulation. For all of the cases we represent in figure 2-7, the error curves from shorter echo times are in the lower part of the plot than those with higher echo times. However, this does not imply that the smaller the echo time is, the more accurate the concentration estimate is. The spectra with shorter echo times are frequently further contaminated by macromolecules[15], which will complicate the spectral composition and decrease the accuracy of T_2 measurements, and will move the errors toward the lateral upper corners along the concentration- T_2 error curves(figure 2-7 c and d). The concentration error is especially notable in the T_2 water case due to the steeper slope as shown in figure 2-7c. Because the slope of this error curve is so steep, a small increase in the water T_2 error might triple the NAA concentration error.

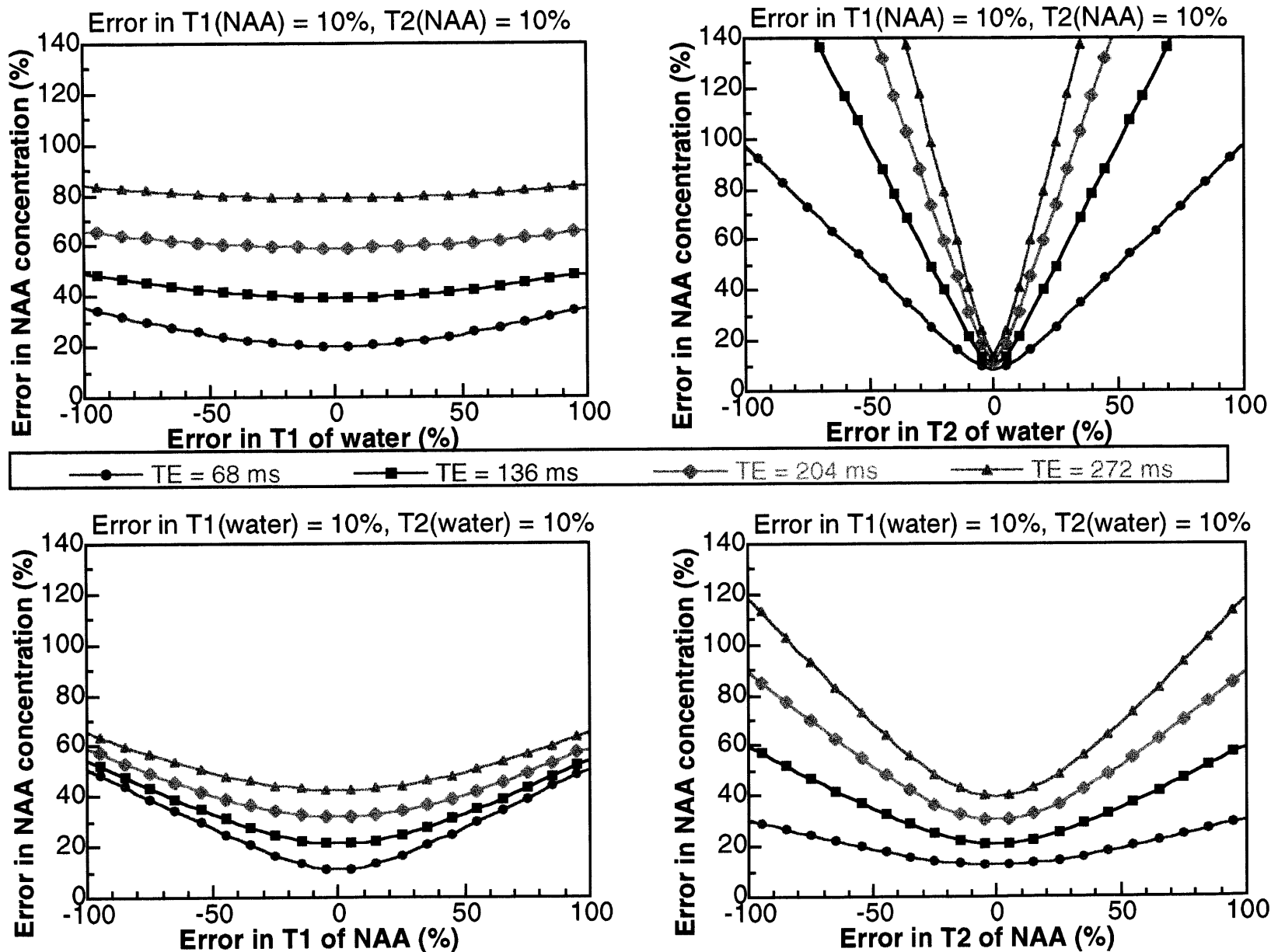


Figure 2-7 Error in NAA concentration due to T1 and T2 values of NAA and water.

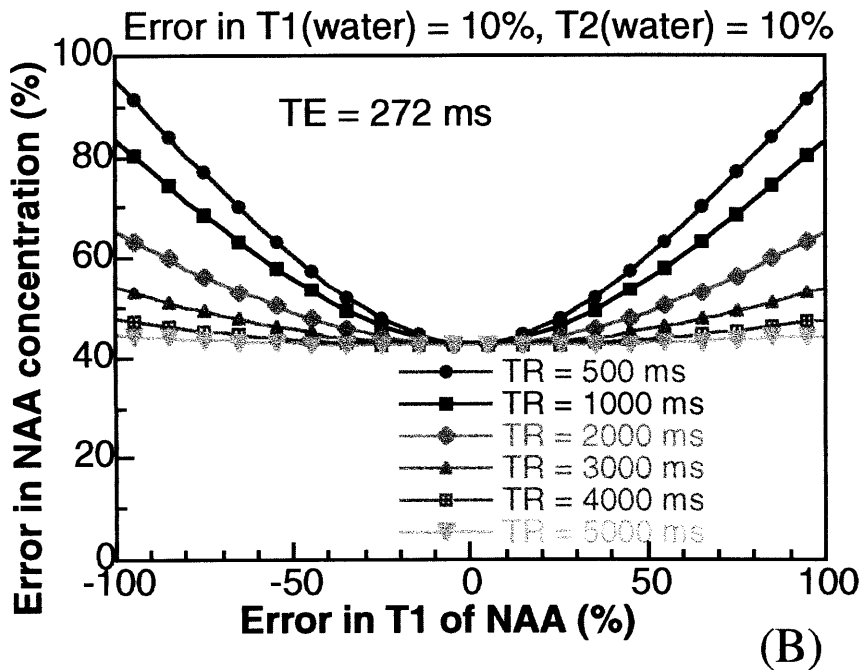
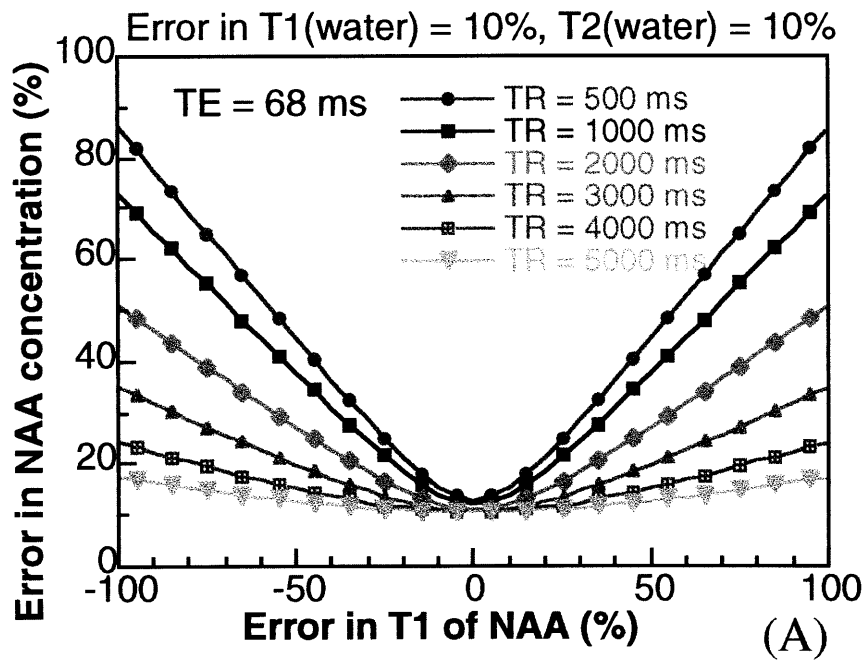


Figure 2-8 NAA concentration error due to different TR settings. (A) TE = 68 ms, (B), TE = 272 ms.

Conclusions:

By using computer simulations, we have synthesized ^1H spectra similar to real spectra from 1.5T and 4.7T (figure 2-9). This emphasizes the importance of the accuracy of relaxation time measurements in the metabolite concentration estimates. It also points out how problematic it is to obtain accurate “absolute” concentrations. Unless one knows: a) the behavior of the strongly coupled metabolites under the influence of the particular pulse sequence used, b) all the chemicals contributing to the overlap, and c) the macromolecular concentrations and chemical shifts, measurement of absolute concentration will remain elusive. An alternative solution is to use signal from proton density weighted experiments as an internal standard to obtain a metabolite index ($M_{\text{index}} = SI_{\text{metabolite}} / SI_{\text{proton density}}$). This metabolite index method will minimize the concentration error from the relaxation time measurements and allow relatively accurate inter-subject comparisons[18]. Although the absolute metabolite concentration measurements has been a great desire and the ‘holy grail’ of ^1H MRS over decades, relative concentration measurements may prove to be more useful and reasonable for quantitative analysis.

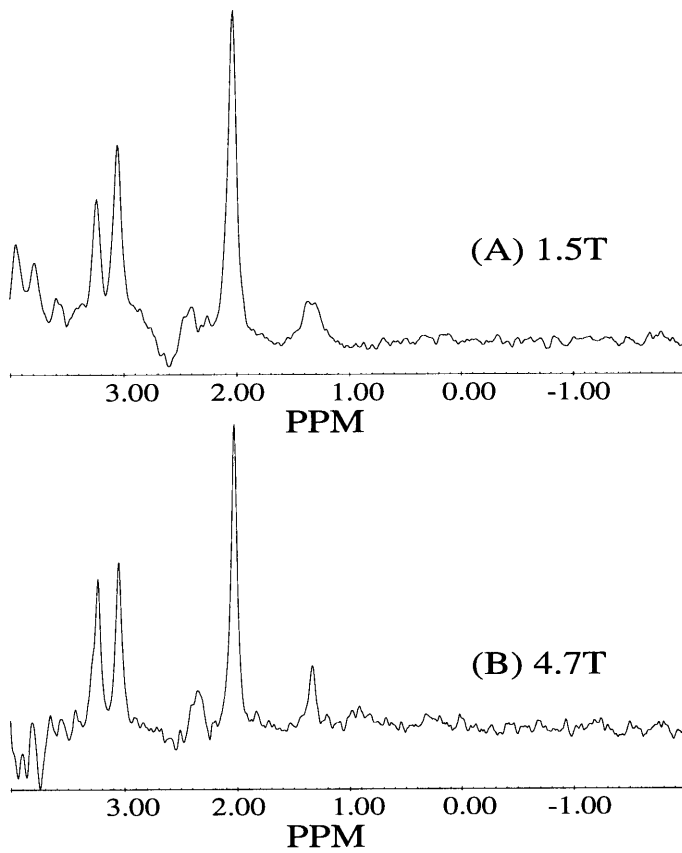


Figure 2-9. In vivo spectra from 1.5T (A) and 4.7T(B). (A) is from the occipital cortex of a HD patient and (B) is from the striatum of a rat with intrastriatal injection of MPP+.

References:

- 1 K. L. Behar, J. A. den Hollander, M. E. Stromski, T. Ogino, R. G. Shulman, O. A. C. Petroff, J. W. Prichard, High-resolution ^1H nuclear magnetic resonance study of cerebral hypoxia *in vivo*, *Proc. Natl. Acad. Sci. (USA)*, **80**:4945 (1983)
- 2 T. Michaelis, K. D. Merboldt, W. Hanicke, M. L. Gyngell, H. Bruhn, J. Frahm, On the identification of cerebral metabolites in localized ^1H NMR spectra of human brain *in vivo*, *NMR Biomed.*, **4**(2):90-98 (1991)
- 3 K. R. Thulborn, J. J. H. Ackerman, Absolute molar concentrations by NMR in inhomogeneous B_1 , A Scheme for analysis of *in vivo* metabolites, *J. Magn. Reson.* **55**:357-371 (1983)
- 4 P. S. Tofts, S. Wray, A critical assessment of methods of measuring metabolite concentrations by NMR spectroscopy, *NMR Biomed.*, **1**:1-10 (1988)
- 5 S. Wray, P. S. Tofts, Direct *in vivo* measurement of absolute metabolite concentrations using ^{31}P nuclear magnetic resonance spectroscopy, *Biochem. Biophys. Acta*, **886**:399-405 (1986)
- 6 O. A. C. Petroff, D. D. Spencer, J. R. Alger, J. W. Prichard, High-field proton magnetic resonance spectroscopy of human cerebrum obtained during surgery for epilepsy, *Neurology*, **39**: 1197-1202 (1989)
- 7 J. Frahm, H. Bruhn, M. L. Gyngell, K. D. Merboldt, W. Hanicke, R. Wauter, Localized high-resolution proton NMR spectroscopy using stimulated echoes; initial application to human brain *in vivo*, *Magn. Reson. Med.*, **9**:79-93 (1989)

-
- 8 J. Frahm, H. Bruhn, L. Gyngell, K. D. Merboldt, W. Hanicke, R. Sauter, Localized proton NMR spectroscopy in different regions of the human brain in vivo. Relaxation times and concentration of cerebral metabolites, *Magn. Reson. Med.*, **11**:47-63 (1989)
 - 9 P. A. Narayana, L. K. Fotedar, E. F. Jackson, T. P. Bohan, I. J. Butler, K. S. Wolinsky, Regional in vivo proton magnetic resonance spectroscopy of brain, *J. Magn. Reson.*, **83**:44-52 (1989)
 - 10 T. Ernst, R. Kreis, B. D. Ross, Absolute quantitation of water and metabolites in the human brain. I. Compartments and water, *J. Magn. Reson.*, **102**:1-8 (1993)
 - 11 R. Kreis, T. Ernst, B. D. Ross, Development of the human brain: in vivo quantification of metabolite and water content with proton magnetic resonance spectroscopy, *MRM* **30**:424-437 (1993)
 - 12 K. L. Behar, T. Ogino, Assignment of resonance in the ^1H spectrum of rat brain by two-dimensional shift correlated and J-resolved NMR spectroscopy, *Magn. Reson. Med.*, **17**:285-303 (1991)
 - 13 P. L. McGeer, J. C. Eccles, E. G. McGeer, *Molecular Neurobiology of the Mammalian Brain*, Plenum Press, New York (1987)
 - 14 T. Ernst, J. Henning, Coupling effects in volume selective ^1H spectroscopy of major brain metabolites, *Magn. Reson. Med.*, **21**(1):82-96 (1991)
 - 15 K.L. Behar D.L. Rothman, D. D. Spencer, O.A. Petroff, Analysis of macromolecule resonances in ^1H NMR spectra of human brain, *Magn. Reson. Med.*, **32**(3): 294-302 (1994)
 - 16 K.L. Behar and T. Ogino, Characterization of macromolecule resonances in the ^1H NMR spectrum of rat brain, *Magn. Reson., Med.*, **30**(1): 38-44 (1993)

-
- 17 R. Kreis, T. Ernst, B. D. Ross, Absolute quantitation of water and metabolites in the human brain. II. Metabolite concentrations, *J. Magn. Reson.*, **102**:9 (1993)
- 18 B.G. Jenkins, E. Brouillet, Y.I. Chen, E. Storey, J.B. Schulz, P. Kirschner, M.F. Beal, B.R. Rosen, Non-invasive neurochemical analysis of focal excitotoxic lesions in models of neurodegenerative illness using spectroscopic imaging, *J Cereb. Blood Flow Metab.*, **16**:450-461 (1996)

Chapter 3 ^1H Magnetic Resonance Spectroscopic Studies in Parkinson's Disease Patients

Introduction and background

Parkinson's disease (PD) is one of the most common neurological diseases in North America with an average onset age of 58 years. Statistically, the annual incidence rate of PD is 20.5/100,000 population and the prevalence rate is 300/100,000 population in North America as in 1991 [1]. The symptoms of PD usually starts asymmetrically on one side of the body. Although James Parkinson [2] described the motor disorders associated with PD in 1817 and since then the PD symptoms have been well documented, the etiology of this disease, however, is still unclear. One popular hypothesis of the etiology of PD was inspired by human evidence: seven street drug abusers received an intravenous injection of 1 -

methyl-4-phenyl-1,2,3,6-tetra-hydropyridine (MPTP) and developed symptoms resembling idiopathic Parkinson's disease[3]. The metabolite of MPTP, 1-methyl-4-phenylpyridinium ion (MPP⁺), is taken up by dopaminergic reuptake system and is transported to the substantia nigra pars compacta (SNc) where it accumulates in the matrix of mitochondria. MPP⁺ is a potent inhibitor of complex I in the electron transport chain. The accumulation of MPP⁺ in the mitochondrial matrix may lead to a reduction in ATP production [4] which may subsequently cause the death of the SNc neurons.

Several biochemical observations have shown a 30%-35% reduction in complex I activity in post-mortem substantia nigra[5,6,7] in PD patients but with no abnormal enzymatic activity for complex III and IV in immunohistochemical staining [3,8]. In contrast to this finding, multiple system atrophy (MSA), a similar neurological disorder associated with dopaminergic cell loss, appeared to have normal enzymatic activity in complex I [9]. The etiology of PD thus has been hypothesized to have a special association with a dysfunction of energy respiration. Since the cessation of oxidative phosphorylation may force pyruvate, the final product of glycolysis and the key element to enter TCA cycle, to be shunted to lactic acid instead of acetyl-CoA [10], a dysfunction in the enzymatic activity of complex I may lead to extra accumulation of lactic acid.

Localized ¹H MR spectroscopy has recently become a powerful technique to investigate cerebral metabolites. N-acetyl-aspartate (NAA), which is a neuron-specific brain metabolite [11,12,13,14], has been used as neuronal marker in ¹H MRS and has been widely used to verify the viability of the cerebral neurons. Detection of lactic

acid has been studied in ^1H MRS for many years [15,16] and has been used as an energy impairment marker to test the mitochondrial function [17,18]. Other ^1H MRS detectable metabolites have been proposed as useful markers for other cerebral conditions. Creatine can serve as an internal standard to estimate the relative ratio of all other cerebral metabolites due to its relative invariance in concentration in different disease states [see chapter 2]. The ^1H -MRS technique has been successfully applied to examine the clinical aspects and the possible etiologies of several neurological diseases. Huntington's disease (HD) is a genetic inherited movement disorder which has been hypothesized as a neurological disorder associated with energy impairment (complex II ~ IV) in the basal ganglia. Jenkins et. al. [17] applied localized ^1H -MRS to HD patients and observed significant lactate elevation in the striatum and occipital cortex. The elevated lactate level in the HD brain suggests an abnormality in oxidative phosphorylation and ^1H MRS has shown a promising ability to detect the possible energy impairment in human brain. We thus proposed use of ^1H MRS to investigate the energy metabolite condition in PD brains. Although one would like to examine metabolites in the substantia nigra (SNc) where histochemical studies in postmortem PD brains have found abnormal dopaminergic neuronal loss [19,20,21,22], it is difficult to acquire spectra with reasonable quality from this area because of the low signal to noise ratio (due to the very small structure size) and the possible signal distortion caused by magnetic susceptibility perturbations due to the high iron content in this organ. Since the SNc is the primary dopaminergic source for the central nervous system, degeneration of the SNc cells may lead to insufficient

dopamine innervation in the downstream structures of the meso-telencephalic dopaminergic pathway, such as striatum and frontal cortex. The deficit in the dopamine innervation of these downstream cerebral structures is the cause of the motor and/or mental disorder in Parkinson's disease. Although there is no evidence in PD patients of massive neuronal loss other than the dopaminergic terminals in the neostriatum, striatal tissue does show decreased staining of complex I proteins in a Western blot and decreased complex III activity [23,24]. Genetic studies have found mutations in mitochondrial DNA that may be associated with PD and the basal ganglia may be vulnerable to defects in oxidative phosphorylation [25,26]. We hence propose to examine the energy respiration status of basal ganglia instead of the tiny SNc to verify the energy impairment hypothesis. We propose to use localized *in vivo* ¹H MR spectroscopy to examine the striatal metabolites in PD brains, particularly the resonances of the methyl group of NAA at 2.023 ppm and lactate at 1.33 ppm. This ¹H-MRS metabolite study should provide further information to help understand the biochemical etiology of Parkinson's disease.

Methods

Idiopathic Parkinson's disease patients and age-matched normal volunteers were included in this study. The range of the disease severity of this patient group is listed in Table 3-1 . Most of the normal volunteers were the spouses or close relatives of the PD patients. MR studies were performed on a 1.5T whole body magnet (Signa, General Electric Co.) with a quadrature head coil as RF transmitter and receiver. The subjects' heads were packed tightly

inside the head coil to prevent head motion during the scan as the position and the grey/white-matter ratio inside the spectral voxel may change critically with only a slight shift in position. Coronal images with good grey/white matter contrast from a fast spin-echo (TR/TE = 287 / 3.4 ms, 16 echo trains) were used to locate the spectral voxel in the striatal areas. A point resolved spectroscopy sequence (PRESS) with water suppression was used to acquire the striatal spectra (TR/TE = 2 s/272 ms, number of averages > 400). Spectra of the PD patients were either taken unilaterally (n = 23) or from both of the striata (n=20). Twelve out of 19 normal controls also had the spectra obtained from both striata rather than a single striatum. Since the PRESS sequence can only excite a rectangular voxel, the spectral voxel was positioned to cover most of the caudate nucleus, putamen, globus pallidus. However, it is almost impossible to exclude part of the ventricle and white matter (internal capsule) from this spectral voxel and thus a certain degree of signal contamination from the heterogeneous structures is impossible to avoid. The spectral compositions for white matter and grey matter are different. Therefore, one has to pay particular attention to the amount of spectral contamination from white matter. A small voxel size ($= 4.0 \pm 0.6$ cc) thus becomes critical and necessary to estimate the striatal metabolite levels accurately to avoid the possible spectral distortion by the white matter. In contrast, cerebrospinal fluid (CSF) creates few problems and can plausibly be ignored in the striatal spectra. Previous studies [27] have shown that CSF does not contribute much of spectral signals in ^1H MRS due to the pulsation of the CSF. The striatal spectra acquired from the imager were then transferred to a SUN UNIX workstation and were analyzed by using

commercial spectroscopy analysis software NMR1 (New Methods Research Inc., Syracuse, NY). Data were processed using zero fill, baseline correction, exponential filtering and Fourier transformation. Each spectral peak was then fit to a Lorentzian line and the integral value of the peak was used as the index of the striatal metabolite level.

Age	onset age	Duration of illness	Hoehn-Yahr stage			DOPA dose
			I	II	III	
61±10	55±1	8±1 (3~17)	3	19	2	504±54

Table 3-1 *Clinical characteristics of the PD patients participating the ¹H MRS studies. Total number of PD patients is 22.*

Results

Among the spectra of 23 PD patients and 20 age-matched normal volunteers, we found that the metabolite ratio of creatine (3.02 ppm) to NAA (2.023 ppm) was quite consistent (42±0.5% of NAA, 2 tailed T test: P > 0.95). Since the spectral peak at around 2.02 ppm (dominated by the methyl group of NAA) has higher signal intensity and less baseline distortion than the spectral signal at around 3.02ppm (dominated by creatine), we chose to use NAA instead of creatine as the internal standard to yield higher precision in the relative metabolite measurements. The use of NAA as the internal standard is legitimate since there is no observable striatal or global brain atrophy in the PD patients. A two tailed student t statistic test was used to examine the significance of differences in the metabolites between the PD and the control groups.

Average result from the individual spectra—

When the lactate to NAA ratios from individual spectra were averaged together (Table 3-2), the average lactate level was significantly elevated in the PD group compared to the control group (59% higher; p value < 0.0004). This measurement treated each single spectrum as an individual entity regardless of which hemisphere the spectrum came from (the first affected striatum or not) and whether or not more than one spectrum was taken from the subjects. No other ¹H-MRS detectable metabolites were found with a significant difference in the PD group compared to the control group. Figure 3-1 shows pairs of spectra from PD patients and normal controls.

	PD	Control	
# of subjects	23	20	P value
# of spectra	43	30	
age (yrs)	62 ± 10	58 ± 12	> 0.3
Lac/NAA (%)	12.33 ± 0.59	7.77 ± 0.34	< 0.004
Cr/NAA (%)	42.86 ± 0.46	42.92 ± 0.66	> 0.95
Cho/NAA (%)	51.95 ± 1.03	47.86 ± 0.99	> 0.15
Glx/NAA (%)	13.58 ± 0.69	15.45 ± 0.98	> 0.4
Asp/NAA(%)	10.16 ± 0.50	10.31 ± 0.78	> 0.9

Table 3-2 Cerebral metabolite levels measured from PD patients and age-matched normal control volunteers. *Lac: lactate, Cr: Creatine, Cho: choline, Glx: glutamate and glutamine, Asp: aspartate.* (metabolite ratio: mean ± standard error; age: mean ± standard deviation)

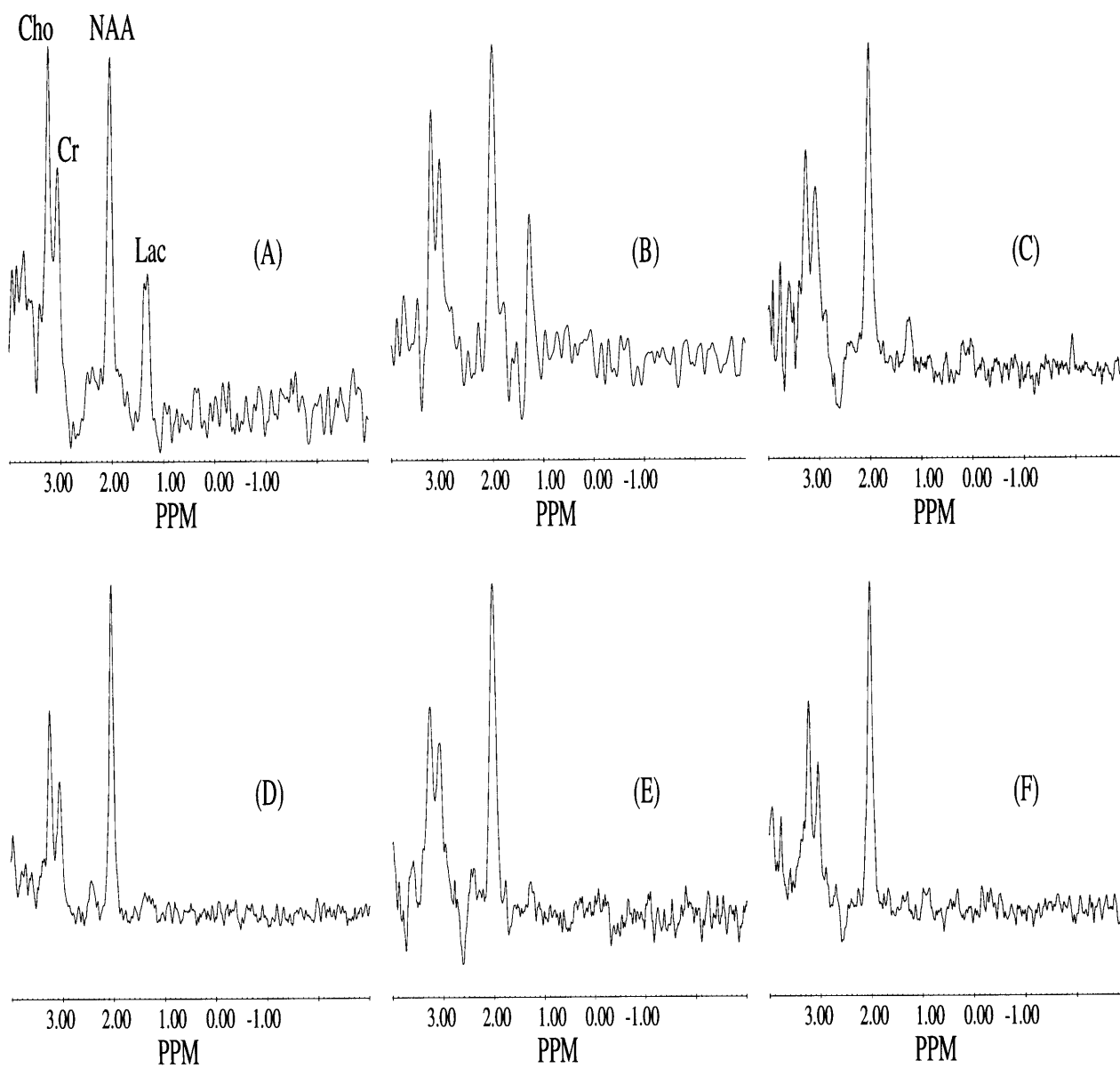


Figure 3-1. Striatal spectra from PD patients (A)(B)(C) and age matched normal controls (D)(E)(F).

Asymmetric of the lactate levels in the two striata of the subject—

Although the averaged data showed significant differences in the lactate to NAA ratio between the PD and control groups, the distribution of the individual ratios, however, fell into 2 categories — high versus low lactate groups (Figure 3-2). If a Lactate/NAA ratio of 10% (one standard deviation above the mean of the lactate level in the normal control group) is taken as a cutoff between low and high values, 21 out of 41 PD spectra belong to the high lactate level group while only 5 out of 29 normal control spectra are in this high lactate group. The lactate levels do not correlate with age, disease severity, DOPA dose administered, nor the duration of PD (Table 3-3). Upon closer examination of the double spectra taken from the same subjects (20 out of 23 PD patients and 9 out of 20 normal controls), we found significantly asymmetric lactate levels in the two striata for both PD and control groups. Figure 3-3 shows 2 sets of the asymmetric spectra from the PD patients and Table 3-4 shows the statistical results of the double spectra sorted according to ‘**big**’ versus ‘**small**’ lac/NAA sides of the same subject. Figure 3-4 shows the statistical results as a bar graph. Only the ‘**Big**’ side showed a significant elevation in lactate ($p < 0.045$). Interestingly, the “**big**” side seems to be mainly the left striatum (8 out of 9 in control group and 17 out of 18 in PD patients).

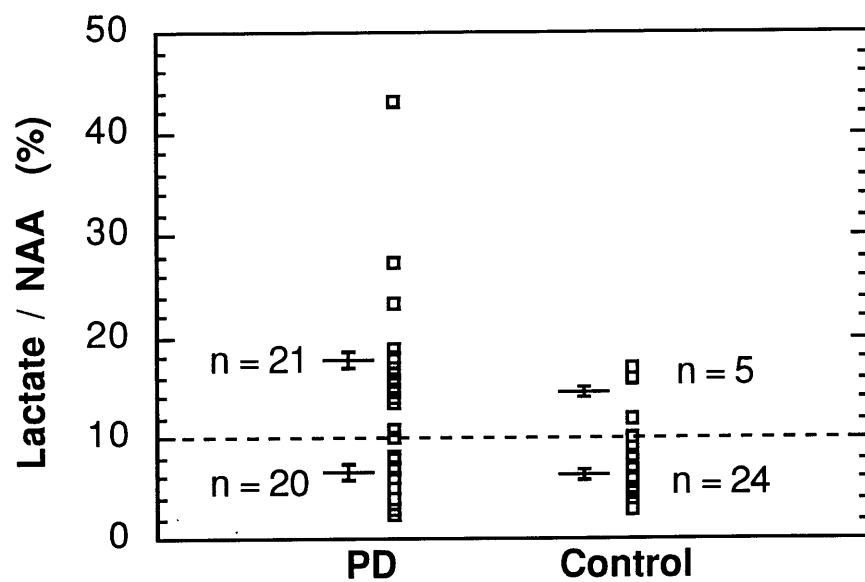


Figure 3-2 Distribution of the individual lactate to NAA ratios in the 42 PD and 33 control spectra from 24 PD patients and 22 normal control subjects.

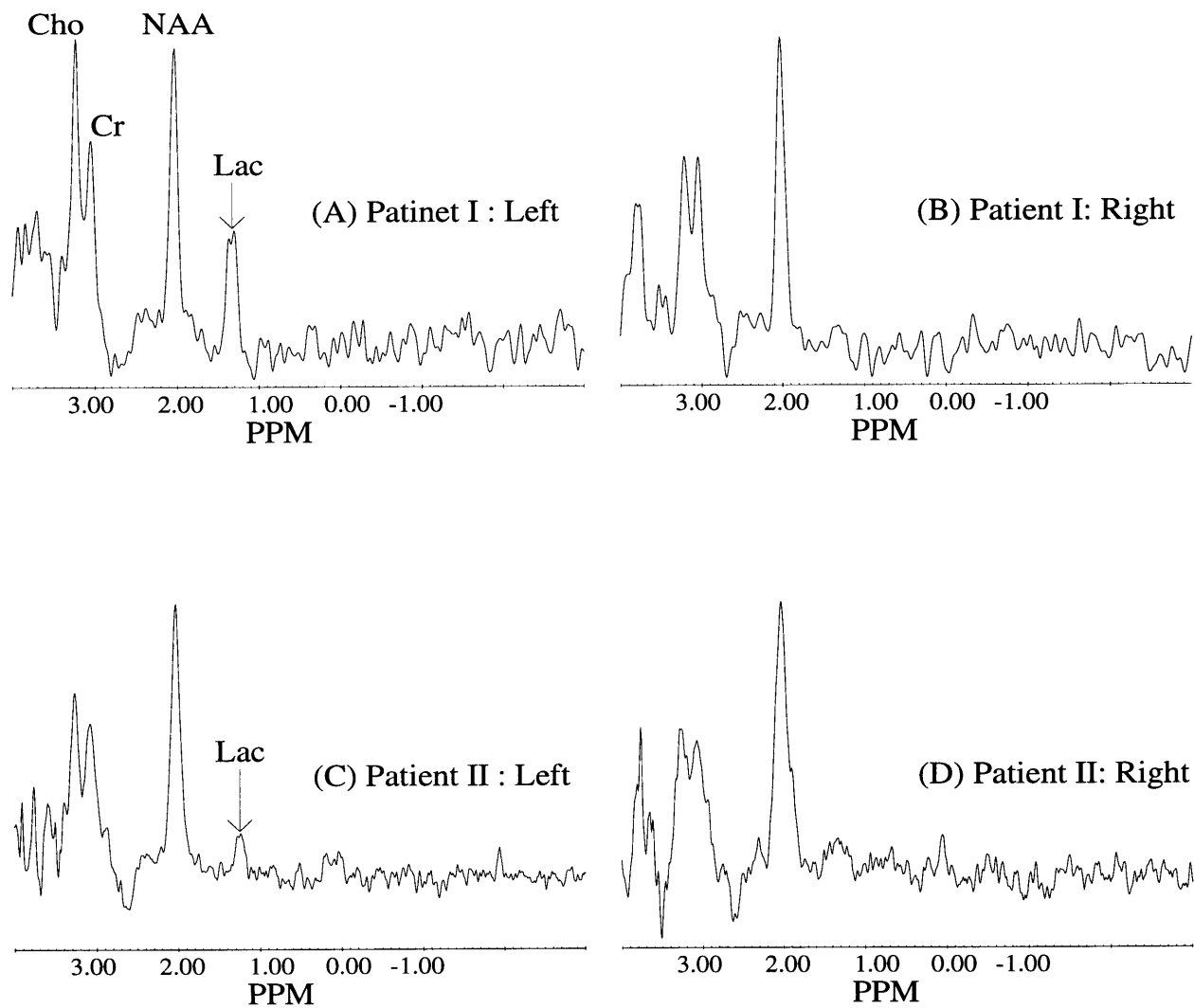


Figure 3-3. Asymmetric lactate level in the striatal spectra. (A) and (B) are from PD patient I and (C) and (D) are from PD patient II. Note the left striatum has higher lactate than the right side.

Lactate/NAA (%)	High (>10%)	Low (<10%)
age (yrs)	60±10	58±12 ^{NS}
Duration of PD (yrs)	7.9±1.2	8.2±0.9 ^{NS}
DOPA dose (mg/day)	510±65	500±89 ^{NS}
Hoehn-Yahr stage	1.9±0.2	1.8±0.1 ^{NS}

Table 3-3 Correlations of the PD lactate to NAA ratios with clinical parameters. NS: not significant (unpaired t test, 2-tailed)

	Lactate/NAA (%)		P (small v.s. big)	age
	small side	big side		
PD n=20	8.17±0.50	17.85±1.17	< 0.001	61±10
Control n=9	6.11±0.29	10.85±0.85	< 0.02	56±5
P (PD vs Control)	> 0.17	< 0.05		> 0.4

Table 3-4 Metabolite levels from both striata of the same subject. When the metabolite levels were grouped as to small versus big lactate levels (relative to NAA), both the PD and control groups showed asymmetric lactate amounts in the striata. The ‘small’ group showed no significant difference between PD and control groups. However, the ‘big’ group showed significant elevation of lactate in the PD group.

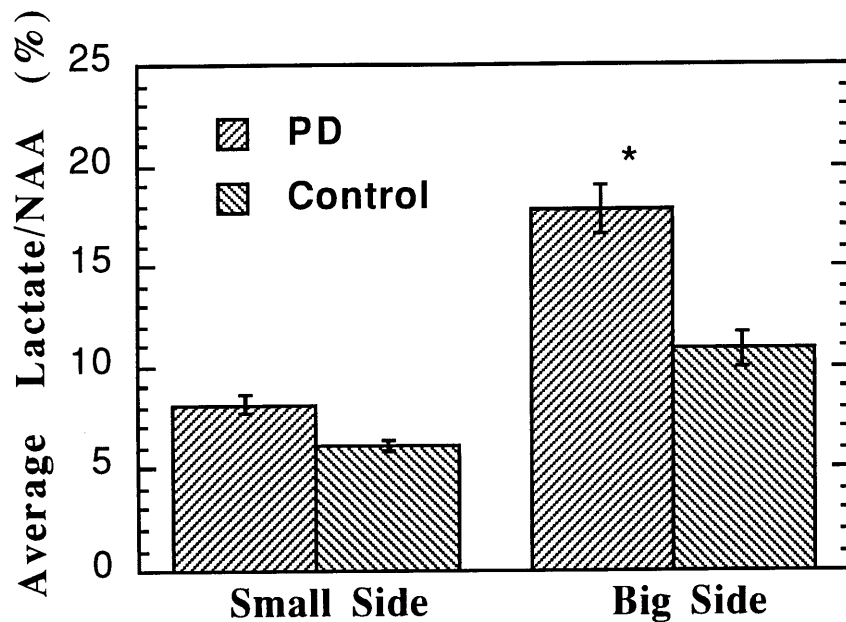


Figure 3-4 Lactate/NAA ratio comparison when the spectra from both striata are broken into small versus big lactate side. The lactate level is significantly higher on the 'Big' side in the PD but not the control group (* $p < 0.045$).

Aspartate Elevation

Although there was no other $^1\text{H-MRS}$ detectable cerebral metabolite beside lactate showing a significant change in the PD group (Table 3-2), some of the PD spectra however showed some suspicious modulation at around 2.8 ppm. This modulation may result from elevated aspartate. Figure 3-5 shows some of these spectra. For those spectra with narrow linewidths, a peak could be roughly distinguished. However, for most of the cases, the linewidths were not narrow enough to resolve the 2.8 ppm peak from the creatine peak (3.0 ppm) resulting in an asymmetric shoulder on the creatine peak. This adds to the difficulty of accurate quantification of both the creatine peak and the aspartate peak. This aspartate peak,

however, could potentially be better resolved from the creatine peak and hence quantified more accurately at higher magnetic fields such as 3T or 4T. The finding of this suspicious aspartate peak reveals that PD may involve more complicated neurological modulations which may provide valuable information worth pursuing to more precisely establish the etiology of PD and also to verify more completely the pathological changes in PD.

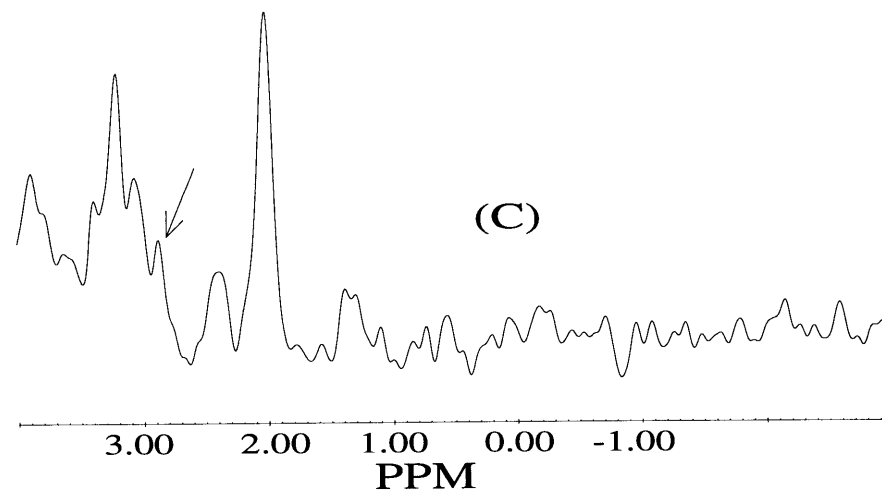
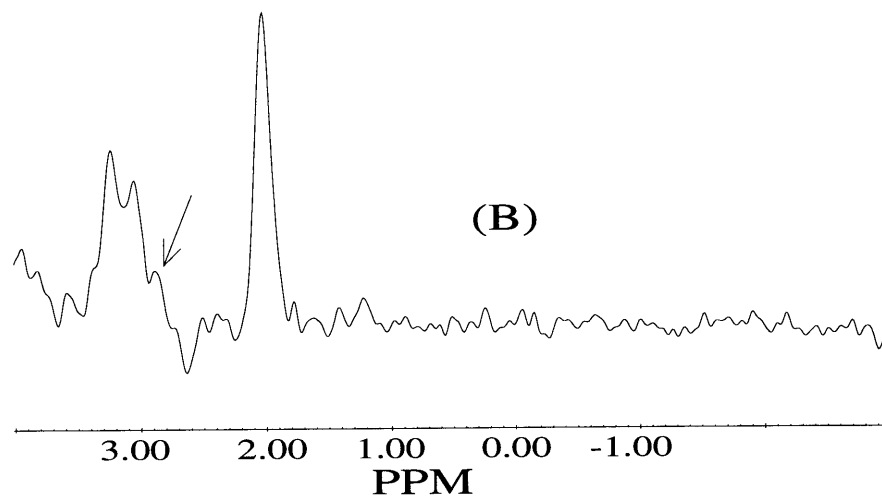
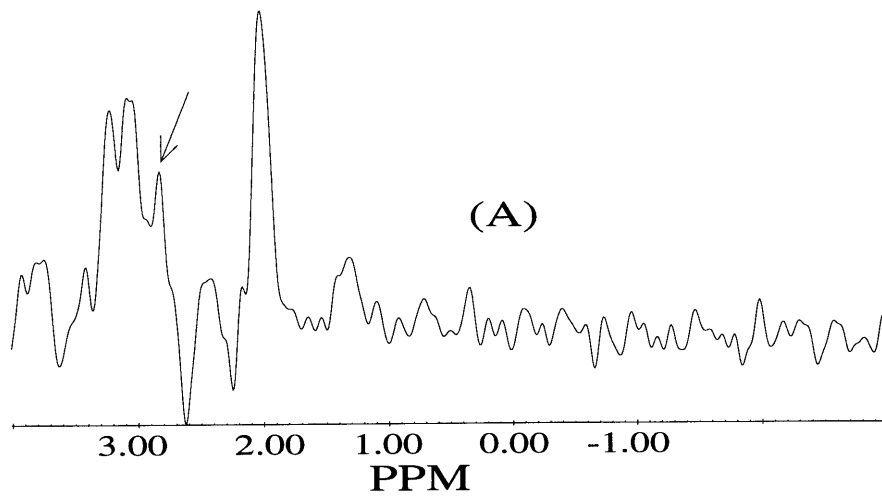


Figure 3-5. A peak at around 2.8 ppm may represent an elevation in aspartate [indicated by arrows]. These 3 striatal spectra are from 3 PD patients (A, B, C).

Discussion

Morphology and SNR considerations:

Defects in mitochondrial phosphorylation have been reported in various movement disorders, such as Huntington's disease (HD) and Parkinson's disease (PD). In PD patients, deficiencies in complex I have been found in platelets [28], skeletal muscle [29,30], and brain [31,32]. Our ¹H-MRS study has supported the hypothesis of a possible mitochondrial respiration deficiency in striatum by showing significant elevation of the striatal lactate level in PD patients. However, Holshouser et. al. [33] did not find significant elevation in the striatal lactate in their multicenter ¹H-MRS studies on PD patients. However, we believe we have reasonable criticism of their results. The Holshouser et. al. multicenter studies claimed to use a voxel size of 8 ml to cover the striatum with less than 10 to 20 % non-gray matter contamination. Morphological study of brain structures reveals that the total volume of a normal adult striatum (whole brain) is about 17 ± 2.48 ml [34], or about 8 ml in one hemisphere. However, the shape of the striatum is complicated and extends over [3cm, 3cm, 3.5cm] in the [AP, ML, DV] directions [35]. In other words, the 7 to 10 ml of striatal volume is nonevenly distributed over a big volume of approximately 30 ml. The cubic voxel of 8 ml Holshouser et. al. reported to use in their ¹H-MRS studies thus can not possibly cover less than 10 to 20 % of white matter. Our ¹H-MRS study used much smaller voxel in size ($\approx 4 \pm 0.4$ ml) to cover most of the body of caudate nucleus, putaman, and part of globus pallidus only. This small voxel can still not avoid the contamination of white matter such as internal capsule, by our

estimation the contamination is about 30 %. The neuronal physiological demand and consumption of energy is essentially restricted to gray matter only and any elevation in lactate level is expected be located in gray matter. With the consideration of voxel contamination, the ^1H -MRS detectable lactate amount is to be reduced by the degree of the contamination of white matter, e.g., a 30% contamination of white matter in the spectral voxel may bring the ratio Lactate to NAA of 20% (pure grey matter) down to 14% (whole voxel). The other notable problem is the issue of signal to noise ratio (SNR). In theory, any measurable quantity has to have SNR bigger than 1. In most of the spectral analysis, only the SNR of NAA has been estimated since NAA is in general the most prominent component in the ^1H -MR spectra. For a given SNR of NAA, there is a minimum detectable lactate to NAA ratio which is:

$$\frac{\text{Lactate}}{\text{NAA}}_{\min} (\%) = \frac{100}{\text{SNR}_{\text{NAA}}} \quad (3-1)$$

In other words, for spectrum with given SNR of NAA (SNR_{NAA}), the lactate to NAA ratio is only reliable when the value is bigger than the values obtained from equation 3-1. Although Holshouser et. al. used a lactate sensitive echo time ($\text{TE} = 136\text{ms}$) which should yield nice negative doublet peaks of lactate at 1.33 ppm, the criteria they used to screen the spectra were not strict enough to detect the minimum lactate level smaller than 33% of NAA (one of the criteria for them to screen the spectra is $\text{SNR} > 3$). In our ^1H -MRS study, we used much stricter and flexible criteria to screen the spectral data for the lactate level. Figure 3-6 shows a scatter plot of (Lactate/NAA) to SNR_{NAA} with the solid line indicating the theoretically minimum detectable

(lactate/NAA) as a function of SNR_{NAA} . This SNR-(Lac/NAA) line separates the spectral data into 2 distributions: any data point falling into the area to the right side of the solid line is reliable, while any data point falling into the left side of this line is problematic. We further classified the area to the left side of the theoretical line to 2 subsets with the SNR_{NAA} of 12.5 as the boundary line (≈ 1 standard deviation below the mean SNR_{NAA} in normal control group)—the vertical dashed line in Figure 3-6: area A for $SNR > 12.5$ and area B for $SNR < 12.5$. A signal to noise ratio of NAA of 12.5 (one standard deviation above the mean of SNR_{NAA}) will yield the theoretically minimum detectable Lac/NAA of 8.5%. Therefore, it would be safe to float those data points in area A (indicated as ∇ in Figure 3-6) to the values right below the SNR-Lac/NAA line (indicated as \diamond in Figure 3-6). However, any data point in area B has too much uncertainty in the lactate level and has to be dropped off from this study (indicated as \times in Figure 3-6). With the confidence of our spectral quality, we can be sure now that our detection of the lactate elevation in the PD group is reliable at least with respect to SNR.

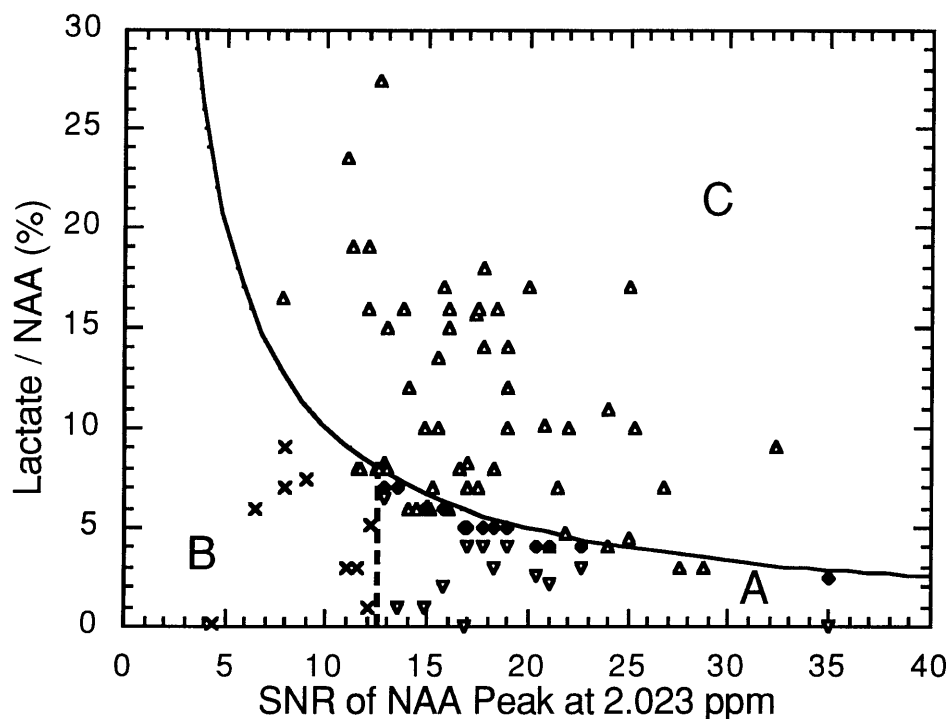


Figure 3-6 Distribution of Lactate to NAA ratio versus signal to noise ratio of NAA. The solid line indicates the theoretically minimum detectable Lactate to NAA ratio as a function of the SNR of NAA. Any data point to the right of the solid line (area C) is reliable. The dashed line indicates 1 standard deviation below the mean SNR_{NAA} in normal control group. Any data point in area B will be discarded (with symbol x) and any point in area A will be floated to the value right below the theoretical line (float from symbol ∇ to symbol \diamond).

Therapeutic Implication:

If the mitochondrial respiration deficiency hypothesis is true, the finding of elevation in PD lactate level may provide some therapeutic strategies to slow progression of PD, such as boosting the mitochondrial function using metabolic cofactors. In Huntington's disease, Koroshetz et al [36] has administrated several mitochondrial

respiration boosters such as co-enzyme Q (Q10) to those HD patients with elevated basal striatal/occipital lactate levels. The post-medication ¹H-MRS examinations in those HD patients showed significant drop in the previously elevated lactate levels. Although striatum may only be one of the downstream structures in the neurodegenerative process in PD, an energy boost may help to decrease the rate of degeneration in the striatum and thus stop the worsen of the movement disorder which PD patients may suffer.

Asymmetric Lactate levels :

The asymmetric lactate data brings up some interesting questions about how the elderly human brain functions. In most of the PD patients, the high lactate side happened to be the left striatum. Similar findings have been reported by Jenkins et. al. in ¹H-MRS studies of Huntington's disease (HD)[36], although the age distribution in HD patients was much lower than the PD patients. A hypothesis can be proposed that the left and right striata in the human brain may possess different degrees of vulnerability when the striata encounter certain energetic stress. In other words, the vulnerability of the striatum may correlate with the working/firing frequency that the striatum has performed over its life time. Since most people are left hemisphere dominant and the left hemisphere has long been hypothesized to govern the mental computation and language. The left striatum thus has been hypothesized to have a heavier working load than the right striatum. The higher neuronal firing rate in the left striatum may lead to greater vulnerability with energy stress or activation and this may be the cause of the asymmetric lactate levels in the two striata.

Conclusions

The *in vivo* chemical/ metabolite study of the human brain using ¹H-MRS has provided valuable information to evaluate the neuronal status in various neurological diseases. Here we used this technique to explore the possibility that prolonged energy stress may lead to mitochondrial impairment and cause dysfunction in the striata of the PD patients. The finding from this ¹H-MRS study may help provide clues to the etiology of Parkinson's disease and may help researchers to design more advanced and sophisticated experiments for a better understanding of the normal striatal function as well as the dysfunction in the PD patients. Such designs may include the monitoring of the dynamics of the lactate levels or regional cerebral blood flow (rCBF) and volume (rCBV) changes in the striatum during physiological challenges such as the performance of certain motor tasks. However, unlike in HD, PD may not represent a single disease process and may be involved in multiple modulation of the neurotransmission system as well. The results from our ¹H-MRS study provide information about possible energy defects in PD, but many other hypotheses and techniques need to be studied before the etiology of PD is understood.

References

-
- 1 A. H. Rajput, Frequency and cause of Parkinson's disease, *Can. J. Neurol. Sci.*, **19(1 suppl)**:103-107 (1992)
 - 2 J. Parkinson, An essay on the shaking palsy, London (1817)
 - 3 B. R. Bloem, I. Irwin, O. J. S. Buruma, J. Haan, R. A. C. Roos, J. W. Tetrud, J. W. Langston, The MPTP model: versatile contributions to

-
- the treatment of idiopathic Parkinson's disease, *J. Neurol. Sci.*, **97**:273-293 (1990)
- 4 P. Chan, L. E. DeLanney, I. Irwin, J. W. Lanston, D. Di Monte, Rapid ATP Loss caused by 1-methyl-4phenyl-1,2,3,6-tetrahydropyridine in mouse brain., *J. Neurochem*, **57**:348-351 (1991)
 - 5 B. Janetzky, S. Hauck, M. B. H. Youdim, et al., Unaltered aconitase activity, but decreased complex I activity in substantia nigra pars compacta of patients with Parkinson's disease. *Neurosci.*, **169**:126-128 (1994)
 - 6 V. M. Mann, J. M. Cooper, D. Kridge, et al., Brain skeletal muscle and platelet homogenate mitochondrial function in Parkinson's disease, *Brain*, **115**:333-342 (1992)
 - 7 A. H. V. Schapira, Evidence for mitochondrial dysfunction in Parkinson's disease -- a critical appraisal., *Movement Disorders*, **9**:125-138 (1994)
 - 8 P. Lestienne, P. Riederer, K. Jenninger, Mitochondrial DNA in postmortem brain from patients with Parkinson's disease, *J. Neurochem*, **56**:1819 (1991)
 - 9 A. H. V. Schapira, V. M. Mann, J. M. Cooper, et. al., Anatomic and disease specificity of NADH CoQ reductase (complex I) deficiency in Parkinson's disease. *Ann. Neurol.*, **30**:563-571 (1990)
 - 10 L. Stryer, Biochemistry, Chapter 15-16, pp. 349-375, Freeman press, New York, (1988)
 - 11 H. Tallan, S. Moore, W. Stein, N-acetyl-L-aspartic acid in brain, *J. Bio. Chem.*, **219**:257-264 (1956)
 - 12 J. Nadler, J. Cooper, N-acetyl-L-aspartic acid, content of human neural tumours and bovine peripheral nervous tissues., *J. Neurochem.*, **14**:551-554 (1972)

-
- 13 M. L. Simmons, C. G. Frondoza, J. T. Coyle, Immunocytochemical localization of N-acetyl-aspartate with monoclonal antibodies, *Neurosci.*, **45(1)**:37-45 (1991)
 - 14 A. S. R. Guimaraes, Quantitative ¹H NMR chemical shift imaging of neuronal content, Ph.D. Dissertation, Massachusetts Institute of Technology, MA, 1994
 - 15 K. L. Behar, J. A. den Hollander, M. E. Stomski, T. Ogino, R. G. Shulman, O. A. D. Petroff, J. W. Prichard, High resolution ¹H nuclear magnetic resonance study of cerebral hypoxia *in vivo*, *Proc. Natl. Acad. Sci. USA*, **80**:4945-4948 (1983)
 - 16 C. Arus, Y. Chang, M. Barany, Proton nuclear magnetic resonance spectra of excised rat brain: assignment of resonances. *Physiol Chem. Phys. Med. NMR*, **17**:23-33 (1985)
 - 17 E. Brouillet, B. G. Jenkins, B. T. Hyman, R. J. Ferrante, N. W. Kowall, R. Srivastava, D. S. Roy, B. R. Rosen, M. F. Beal, Age-dependent vulnerability of the striatum to mitochondrial toxin 3-nitropropionic acid, *J. Neurochem.* **60(1)**:356-359 (1993)
 - 18 B. G. Jenkins, W. Koroshetz, M. F. Beal, B. R. Rosen, Evidence for a n energy metabolism defect in Huntington's disease using localized proton spectroscopy, *Neurology*, **43**:2689-2695 (1993)
 - 19 A. Carlsson, The occurrence, distribution and physiological role of catecholamines in the nervous system, *Pharmacol. Rev.*, **11**:490-493 (1959)
 - 20 O. Hornykiewicz, Metabolism of brain dopamine in juman parkinsonism: Neurochemical and clinical aspects. In E. Costa, L. J. Cote, and M. D. Yahr (eds.), *Biochemistry and Pharmacology of the Basal Ganglia*, New York, Raven Press, pp. 171-185 (1966)
 - 21 Bernheimer et al., 1973, *J. Neurol Sci* **20**, 415-455; Lloyed et al., *Exp. Ther.* **195**:453-464 (1975)

-
- 22 T. E. Robinson, E. Castaneda, I. Q. Whishaw, Compensatory changes in striatal dopamine neurons following recovery from injury induced by 6-OHDA or methamphetamine: a review of evidence from microdialysis studies, *Can. J Psychol.*, **44(2)**:253-275 (1990)
- 23 Y. Mizuno, K. Suzuki, S. Ohno, Postmortem changes in mitochondrial respiratory enzymes in brain and a preliminary observation in Parkinson's disease, *J. Neurol. Sci.*, **96**:49-57 (1990)
- 24 Y. Mizuno, S. Ohta, M. Tanaka, S. Takamiya, K. Suzuki, T. Sato, Deficiencies in complex I subunits of the respiratory chain in Parkinson's disease. *Biochem. Biophys. Res. Commun.*, **163**:1450-1455 (1990)
- 25 A. S. Jun, M. D. Brown, D. C. Wallace, A mitochondrial DNA mutation at nucleotide pair 14459 of the NADH dehydrogenase subunit 6 gene associate with maternally inherited Leber hereditary optic neuropathy and dystonia, *Proc. Natl. Acad. Sci. USA*, **91**:6206-6210 (1994)
- 26 J. M. Shoffner, M. D. Brown, A. Torroni, M. T. Lott, M. F. Cabell, S. S. Mirra, M. F. Beal, C. C. Yang, M. Gearing, R. Salvo, et. al., Mitochondrial DNA mutation associated with Alzheimer's and Parkinson's disease., *Genomics*, **17**:171-184 (1993)
- 27 BG Jenkins, HD Rosas, YI Chen, BR Rosen, T Makabe, R Myers, M Macdonald, MF Beal, WJ Koroshetz, 1H NMR spectroscopy studies of Huntington's disease: striateal asymmetries and correlations with CAG repeat number, *Neurology*, in press (1997)
- 28 W. D. Parker, Jr., S. J. Boyson, J. K. Parks, Abnormalities of the electron transport chain in idiopathic Parkinson's disease, *Ann. Neurol.* , **26**:719-723 (1989)

-
- 29 L. A. Bindoff, M. Birch-Machin, N. E. F. Cartledge, W. D. Parker, Jr., D. M. Turnbull, Mitochondrial function in Parkinson's disease, [letter & comment] *Lancet*, **2**:49 (1989)
- 30 J. M. Shoffner, R. L. Watts, J. L. Juncos, A. Torroni, D. C. Wallace, Mitochondrial oxidative phosphorylation defects in Parkinson's disease, *Ann. Neurol.*, **30**:332-339 (1991)
- 31 A. H. V. Schapira, J. M. Cooper, D. Dexter, J. B. Clark, P. Jenner, C. D. Marsden, Mitochondrial complex I deficiency in Parkinson's disease, *J. Neurochem*, **54**:823-827 (1990)
- 32 A. H. V. Schapira, V. M. Mann, J. M. Cooper, D. Dexter, S. E. Daniel, P. Jenner, J. B. Clark, C. D. Marsden, Anatomic and disease specificity of HADH CoQ1 reductase (Complex I) deficiency in Parkinson's disease., *J. Neurochem*, **55**: 2142-2145 (1990)
- 33 B. A. Holsouse, M. Komu, H. E. Moller, J. Zijlmans, H. Kolem, D. B. Hinshaw Jr., P. Sonninen, P. Vermathen, A. Heerschap, H. Masur, U. K. Rinne, A. De Coster, J. M. Tosk, Localized Proton NMR Spectroscopy in the Striatum of Patients with Idiopathic Parkinson's Disease: A Multicenter Pilot Study, *MRM*, **33**:589-594 (1995)
- 34 E. H. Aylward, J. Brandt, A. M. Codori, R. S. Mangus, P. E. Barta, G. J. Harris, Reduced Basal Ganglia Volume Associated with the gene for Huntington's Disease in Asymptomatic at-risk Persons, *Neurol.*, **44**:823-828 (1994)
- 35 J. Talairach, P. Tourmoux, Co-Planar Stereotaxic Atlas of the Human Brain, Thieme Medical Publishers, Inc, New York, (1988)
- 36 HD 1H spectra papaer, Koroshetz, *Ann Neurol*, in press, 1997

Chapter 4 An Animal Model of Parkinson's Disease using 6-hydroxydopamine Lesions in Rats --- Anatomical and Metabolite Magnetic Resonance Imaging Studies

Introduction and background

Dysfunction of the nigrostriatal dopaminergic system has been long recognized to be involved in idiopathic Parkinson's disease. Postmortem histological studies in PD brains have found significant loss of the pigmented dopaminergic neurons in the substantia nigra pars compacta (SNc) with little apparent atrophy in the striatum (str) [1,2,3,4,5]. The SNc is the primary dopamine source of the dopaminergic neurotransmission system. Dopamine is synthesized in the pigmented dopaminergic cells in SNc and transported to the striatum through the medial forebrain bundle (MFB), the

nigrostriatal dopaminergic pathway [6,7]. Thus, anterograde degeneration from the SNc to the neostriatum is a distinct possibility. 6-hydroxydopamine (6-OHDA), a well known dopaminergic neurotoxin, has been widely used in animal models to mimic the dopaminergic depletion of Parkinson's diseaseⁱ [8,9]. Injection of 6-OHDA into the medial forebrain bundle can selectively destroy the dopaminergic neurons without interruption of many of the functions of other neurotransmitters and thus is able to ablate the dopaminergic innervation from the SNc to striatum [8]. When the 6-OHDA lesion is performed unilaterally, only the ipsilateral striatum suffers the abnormality in dopaminergic stimulation while the contralateral striatum remains intact and is essentially normal. This unilateral abnormality makes it possible to inspect the survivability of the dopaminergic terminals in the ipsilateral striatum by using behavioral tests without sacrificing the animals (pharmacological stimulation) and to have an internal comparison between the 2 striata (intact versus ipsilaterally lesioned striata) in the same rat as well as make external comparisons among individual rats. The well established behavioral test using pharmacological stimulation of amphetamine (5 mg/kg, s.c.) provides a method to estimate the degree of the dopaminergic loss quantitatively in the striatum unilateral to the 6-OHDA lesioning (see appendix). The 6-OHDA animal model provides the opportunity to investigate the connections

ⁱ Six-hydroxydopamine is an analogue of dopamine with high affinity for the catecholamine uptake systems. It can be administered either via the cerebrospinal fluid or directly into brain parenchyma and the neurotoxin will be transported into catecholaminergic neurons. Pretreatment of animals with desipramine (DMI) blocks the uptake of 6-OHDA into norepinephrine containing terminals and constrains the neurotoxin to the dopamine-containing terminals [1,6,17,18,19].

between : 1. the hypothesis that the neuronal loss in SNc is induced by a possible energy impairment in the mitochondria [10,11,12,13], and 2. the fact that the striatal dysfunction in PD is caused by the insufficient dopaminergic supply from SNc [1,14,19]. We thus propose using unilaterally 6-OHDA lesioned animals to investigate the possible association between the dopaminergic innervation and the global striatal physiology. In this chapter, we will to examine the possible global physiological and neurological abnormalities in striata, such as the changes in the macro cellular water properties using T_2 and diffusion weighted images, the major brain metabolite levels using spectroscopic imaging (chemical shift images, CSI) of NAA and lactate, and the hemodynamic properties (rCBF and rCBV) by using bolus injection of Gd-DTPA [15,16]. In the next chapter, we will propose to examine a possible abnormality in neuronal activity—the coupling between the dopamine-receptor activity and the regional hemodynamics in response to pharmacological stimulation.

Methods

Animals :

Sprague-Dawley rats were used for all studies. Control animals were studied as well as 6-OHDA lesioned ones. To make lesions in the MFB, rats were first anesthetized with ketamine (50 mg/kg ketamine, 5mg/kg xylazine, 2.5mg/kg acepromazine). Desipramine (20 mg/kg, i.p.) was injected intraperitoneally (i.p.) 30 minutes prior to the 6-OHDA infusion to restrict the effect of 6-OHDA to the dopaminergic neurons[17,18,19, also see footnote i in page 98]. The animals were then placed in a stereotaxic device and received

unilateral injection of 6-OHDA into the medial forebrain bundle (Coordinates: [AP, ML, DV] = [-4.5,+1.2,-7.6], 8 $\mu\text{g}/2\mu\text{l}$, iced and stabilized with ascorbic acid [6,17]). After the intracranial surgery, animals were transferred back to the animal facility and allowed to recover for at least 3 weeksⁱⁱ [20,21]. Behavior was assayed by rotational testing to screen out those rats with less than 90% dopaminergic neuronal loss in striatum [22]. For this, 5 mg/kg amphetamine was given subcutaneously (s.c.) and the animal was placed in a computerized rotameter (San Diego Instruments, CA) to record the number of turns ipsilateral or contralateral to the lesioned side for 90 minutes in 10 minute intervals (see appendix). The criterion for inclusion in the study was > 600 net ipsilateral turns per 90 min. intervals. This has been shown to correlate with >90% loss of nigrostriatal dopaminergic innervation [23].

MR Studies:

The MR studies were performed on a 4.7 T GE Omega CSI imaging system. All of the 6-OHDA lesioned animals were anesthetized with a halothane/N₂O/O₂ mixture (1% halothane in volume) and imaged using a 35 mm birdcage coil. All animals were temperature regulated using a circulating water blanket at 38°C over the whole study period.

ⁱⁱ Although the 6-OHDA can produce acute insults in the dopaminergic neurons, the supersensitivity (upregulation) in the postsynaptic striatal neurons does not begin to appear until one to two weeks after the lesions. Therefore, the behavioral tests can only be used to screen out the improperly lesioned animals at least 3 weeks after the 6-OHDA lesions.

Anatomical Images:

Both conventional spin-echo T_2 -weighted sequences and diffusion-weighted sequences were used to screen for possible abnormalities such as edema or intracellular swelling. The parameters used were:

1) **T_2 -weighted images** — TR/TE 3s/80ms, 2 average, 8 slices, 2.2mm slice thickness and 2.3mm slice separation with in plane resolution of 0.195mm x 0.390mm.

2) **Diffusion-weighted images** — TR/TE 2.2s/53ms, 2 average, 4 slices with 2.2mm slice thickness and 2.3mm slice separation, in plane resolution 0.195mm x 0.390mm, diffusion gradients were $[G_x, G_y, G_z] = [4, 4, 0]$ gauss/cm, equivalent b value $\approx 500 \text{ s/cm}^2$ ($\delta=12.5\text{ms}$, $\Delta = 20.5\text{ms}$).

3) **Hemodynamic Measurement** — In order to study the hemodynamic properties of the lesioned striatum, measurements of rCBV and rCBF were made using bolus injections of 0.2mmol/kg Gd(DTPA) (Magnevist, Schering AG, Berlin) [15,16] and rapid gradient echo imaging with 1.28 s/image temporal resolution (TR/TE 20/7ms; Ernst Angle RF).

Chemical Shift of metabolite Images :

The metabolite images were acquired by using a spin-echo chemical shift sequence (TR/TE = 2s/272ms). This CSI sequence uses a binomial 180° RF pulse with null point at 4.7 ppm to suppress the water signal [24,25] and with the maximum RF power set at 2.023 ppm (the methyl group of NAA). Lipid suppression was done by using short-TI inversion recovery (STIR) technique with varied inversion time (TI) [26]. The initial TI value was optimized according

to individual animal to minimize the lipid signal at the $K_y = 0$ line. The inversion recovery waiting time (T_i) was then stepped through the (K_x, K_y) domain (phase encodings) with $600\mu\text{s}$ increment. Three dimensional chemical shift images $[f, x, y]$ were obtained through x and y phase encodings with in plane resolution $\approx 2.18\text{mm} \times 2.18\text{mm}$ (fov 35mm with 16×16 x/y phase encodings) and the spectral resolution $\approx 7.18\text{Hz}$ (spectral width of 4000Hz with 512 points digitization). The raw data (t, K_x, K_y) were zero filled to 32 by 32 matrix in the K_x and K_y domain, individual spectral line was modulated by a low pass sine filter and then 3D Fourier transform is applied to reconstruct the 3D chemical shift images $[f, x, y]$. The metabolite images (NAA and lactate) were reconstructed by adding together the spectral lines containing the desired metabolite peak and viewed along the frequency axes (a $[x, y]$ image). To avoid the possible spatial distortion of the spectral lines due to field inhomogeneities across the imaging field (i.e., a shift in the spectral axis $[f]$ at different spatial coordinate $[x, y]$ due to field inhomogeneities ΔB_0), a homemade program is applied to trace the spectral location of the metabolite peaks through the spatial domain to correct for this distortion (i.e., correct the shift in the spectral frequency axis). The NAA image was reconstructed from the methyl group signal centered at 2.023 ppm and the lactate image was reconstructed from the spectral peak centered at 1.33 ppm by assuming the planes corresponding to the linewidth of the peak analyzed.

Data Analysis—

The anatomical images (T_2 or diffusion weighted images) were overlaid onto the metabolite (CSI) and hemodynamic (rCBV, rCBF) images to segment the outer contour of the hemispheres and the striata. The abnormality indices, I_{abn} , were then determined as:

$$I_{abn} = (SI_{ips\ str} - SI_{cont\ str}) / SI_{cont\ str} \times 100 \quad (4-1)$$

The abnormality indices I_{abn} from each animal were then pooled together to investigate the statistical differences between the control and ipsilateral striata (paired student t test).

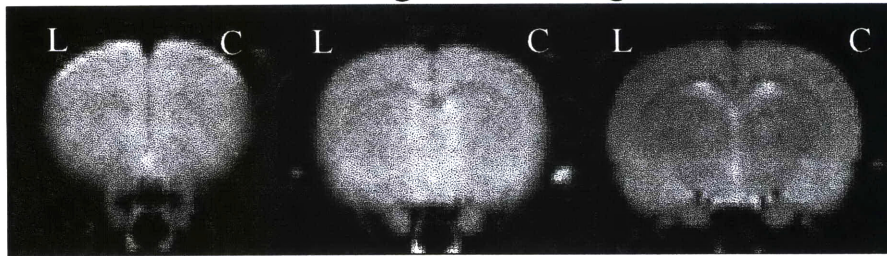
Results:

Water images:

There was no obvious abnormality on either the T_2 or diffusion weighted images of the 6-OHDA lesioned animals (Figure 4-1). This indicates that the loss of the dopaminergic innervation in the striatum may just lead to functional impairment but not to a global morphological modification. This indicates that although there is a certain degree of abnormality in the dopaminergic supply to the striatal area, there are no gross tissue abnormalities. In contrast to this normalcy, other neurotoxins, such as malonate or MPP⁺ induced striatal lesions, show very early striatal lesions that are detectable using diffusion weighted images and the mature lesions are not likely to be missed on T_2 weighted images [27]. The hemodynamic maps (rCBF and rCBV, figure 4-2) from the bolus injection of Gd-DTPA showed no significant differences in the resting states between the two hemispheres (and striata), either. The resting rCBV was

slightly higher in the lesioned striatum but this was not significant ($\approx 5 \pm 27\%$, $p > 0.85$) and the rCBF was about equal in both striata ($\approx -1 \pm 11\%$, $p > 0.4$). This suggests that there may not be much change in the resting state of regional hemodynamics or any significant change in vascularization due to the 6-OHDA lesions in the medial forebrain bundle. The stable resting rCBV and rCBF status are important and essential in the investigation of the neuronal coupling between the pharmacological stimulation and the hemodynamic response, which we will discuss further in the next chapter (chapter 5).

T2 Weighted Images



ADC Images

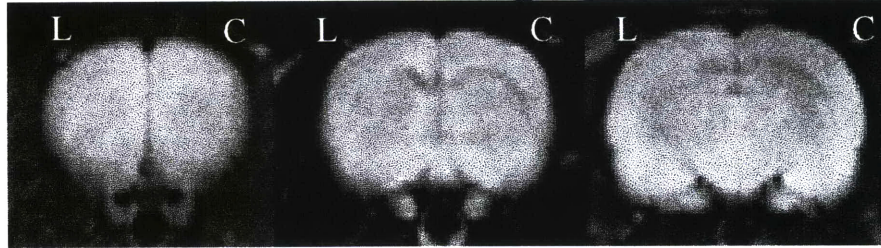


Figure 4-1. T2 and ADC weighted image of rat with unilateral lesioning in the medial forebrain bundle. There is no global abnormality in the hemisphere ipsilateral to the lesioning.
L: Lesioned side, C: Control side.

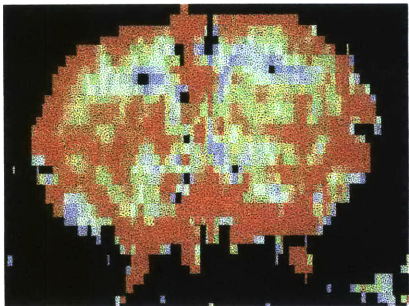
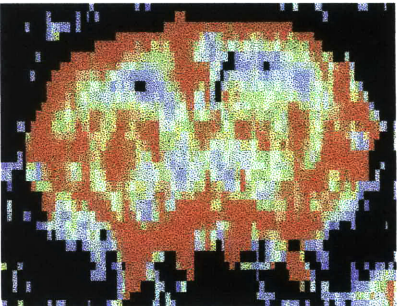
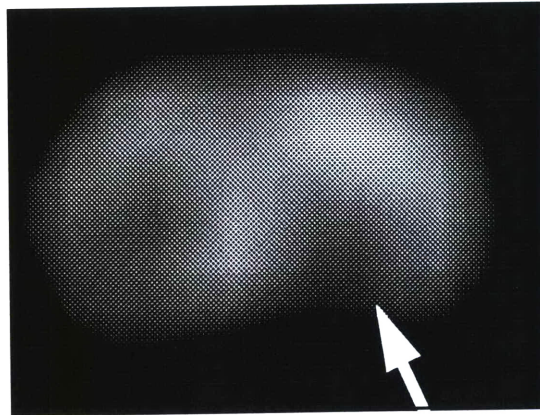
	CBV	CBF
	 Control side 6-OHDA lesion	 Control side 6-OHDA lesion
Control side / Lesioned side	1.05 ± 0.27	0.99 ± 0.11
Significant level	$p > 0.85$	$p > 0.45$

Figure 4-2. Bolus injection of Gd-DTPA shows normal baseline state in hemodynamic properties (CBV and CBF, n = 9).

2) Metabolite images:

The metabolite images, on the other hand, provide different information. There was no apparent increase of the lactate level in either striatum, ipsilateral or contralateral to the MFB lesion. The neuronal marker N-acetylaspartate (NAA), which is abundant in healthy neurons, however, showed a decrease in the ipsilateral striatum (figure 4-3; average = $9.61 \pm 0.01\%$, $p < 0.0003$; range between 5 to 21 % signal decrease compared to the control striatum). Curiously, this signal depletion in the ipsilateral striata extends to the medial bottom part of the brain. Since the slice thickness for the metabolite images is 7 mm, and thus we lose the spatial resolution in the antero-posterior axis, the signal loss of this tail (marked with a white arrow in figure 4-3) is suspected to be the track of the medial forebrain bundle. Similar NAA signal loss and lactate elevation along this tail have been found in the MPP⁺ lesions via intrastriatal injection (unpublished data from B. G. Jenkins). MPP⁺ injected intrastriatally will follow the reuptake pathway of the endogenous dopamine and be shunted to the substantia nigra via the medial forebrain bundle.

NAA Image



Control
side

6-OHDA
lesion

Figure 4-3. NAA image on a 6-OHDA lesioned rat. There is significant NAA signal loss in the striatum ipsilateral to the 6-OHDA lesioning. Note the signal loss extending to the medial-ventral part of the brain may indicate the tract of the medial forebrain bundle.

Discussion:

Although we detected no apparent global changes in the T_2 and diffusion weighted images, several investigators have demonstrated global histological changes following 6-OHDA lesioning. Immunohistochemical staining with tyrosin-hydroxylase showed that the afferent dopaminergic terminals ipsilateral to the 6-OHDA lesion were reduced 90% compared to the normal control striatum. However, a large dopaminergic projection deficit to the striatum could lead to many other alterations in the biochemical balance of the striatal cells. Such alterations include: supersensitivity, i.e. upregulation of the postsynaptic dopaminergic receptors (D1 and D2), and higher turnover rates in acetylcholine (ACh), serotonin (5-HT), and the remaining DA. Zhou et. al. [28] demonstrated that following lesioning of the SNc via 6-OHDA, the dopaminergic neurons are diminished in the striatal area while the serotonin (5-HT) fibers showed increased sprouting. Normally, the 5-HT fibers innervate the striatum sparsely and the globus pallidus densely with a sharp delineation between the two. The interruption of the dopaminergic innervation induced the sprouting of 5-HT fibers into the dopaminergic territories, and the delineation of 5-HT fibers between the striatum and globus pallidus became vague. Current evidence also indicates that 6-OHDA lesions may trigger trophic signals or remove an inhibition for the growth of 5-HT neurons which may initiate the sprouting of 5-HT in the nigra as well as in the striatum [28,29]. Although the role and the mechanism of the remodulation and rebalance of various neurotransmitter systems after the striatal dopaminergic denervation is not clear, it may play an important

role in maintaining the integrity of the striatal function after lesioning of the nigrostriatal pathway.

Although the NAA depletion in the ipsilateral strata is highly significant compared to the control striata in our study, literature has not reported significant neuronal loss in the striata of 6-OHDA lesioned animals [30] or from postmortem histology of idiopathic PD brains. This raises the question that the NAA loss in our metabolite study is caused by the degeneration of those dopaminergic terminals, or that there are some other factors which may lead to the NAA signal loss. That the NAA signal in the striatum ipsilateral to the 6-OHDA lesion is less than 15% depleted compared to the normal contralateral striatum may appear surprising since immunohistological studies with tyrosine hydroxylase staining in the normal brains show a relatively high population of the TH-positive cell clusters covering the striatal slices (6-OHDA kills cells that stain positive for tyrosine hydroxylase). However, since more than 90% of the striatal neurons are gabaergic instead of dopaminergic and the overlap of Nissl-stain and TH-stain show that the high TH-positive cells are clustered at the areas with low Nissel-stain density [31,32,33]. In other words, the striatal cell organization is heterogeneous and the average volume density does not reflect real local neuron density (neuron counts). The dopaminergic neurons, which seems to be diffuse and widely covering the striatal section in the TH-stain, may not be the major fraction of the total striatal neuron population. In this sense, the 9.6% NAA in the ipsilateral striatum depletion from the chemical shift images may just reflect the net neuronal loss after accounting for the degeneration of the dopaminergic cells, the resprouting of the 5-HT fibers which might

be expected to increase NAA, and the real neuronal population. Or, since NAA is higher in neurons with long axonal projections such as the SNc neurons, the NAA loss may just represent the loss of the SNc Dopaminergic terminals[34].

The other possible factor leading to the NAA signal depletion is an increase in susceptibility mismatch, which may be induced by extra iron accumulation in the ipsilateral SNc and striatum. As we discussed in chapter 1, one hypothesis about the etiology of Parkinsonism is that iron deposition in the SNc may lead to or accelerate the death of the dopaminergic neurons [5,35,36,37]. Oestreicher et. al. also showed that 6-OHDA lesions in the medial forebrain bundle lead to higher iron contents in SNc[38]. Since iron is paramagnetic and may introduce an extra susceptibility factor into the R_2^* relaxation rate of NAA, it may lead to the NAA signal depletion if there is extra iron in the ipsilateral striatum. This extra ΔR_2^* term may not play an important role in the water images (T_2 and diffusion weighted images) due to the much shorter T_2 of water. We have performed water R_2^* measurements in one of our 6-OHDA lesioned animals and found no significant changes in R_2^* .

For the energy impairment marker lactate, there was no significant difference between striata in our 6-OHDA lesioned animals (both are in the baseline levels). However, as we could only examine the 6-OHDA lesioned animals at a minimum of 3 days after the medial forebrain bundle lesioning, any lactate generated during cell death would likely have been washed out by the time we performed the chemical shift images. Jenkins et. al. [27] has shown the general lactate time courses involved in striatal excitotoxicity. The lactate

level started to build up steadily while the energy impairment occurred with intracranial injection of the neuronal toxins malonate or MPP⁺. Then the lactate level reached a maximum value and started to decline to the baseline level over the course of approximately 1 ~ 24 hours. The 6-OHDA lesioning of the medial forebrain bundle is likely to be similar to these models and hence by the time we were able to acquire the metabolite images, we may have missed the peak of lactate and only detected the post-impairment stage with no lactate left. However, the ¹H-MRS with PD patients showed elevation of striatal lactate level. Since the disease progress in PD is a slower process, we may have the chance to monitor the lactate level over a much longer time period than in the animal model with acute lesioning. The lactate level shown in PD patients may indicate the slow energy impairment process instead of the near completion of cell death.

Conclusions:

The 6-OHDA lesions in the medial forebrain bundle interrupt the dopaminergic supply from the SNc to striatum and can mimic some of the symptoms of Parkinsonism in rats. However, the 6-OHDA lesions induce an acute abnormality in the dopaminergic supply to the striatal area in contrast to the chronic slow degenerative process in idiopathic Parkinsonism. The ¹H MRS studies in the idiopathic PD patients (chapter 3) showed elevated striatal lactate levels while the 6-OHDA animal model showed no significant elevation. The cause of this difference may be the result of a progressive degenerative process of PD versus the acute insult of the 6-OHDA model. Nonetheless, neither the PD patients nor the 6-OHDA animals showed

brain atrophy or anatomical abnormalities compared to normal controls. This suggests that the abnormalities of Parkinsonism may not be induced by a massive striatal neuronal abnormality but may just be caused by the malfunction of the minor neuronal population, the dopaminergic terminals in the striatum. To explore these issues more deeply, we have to investigate the coupling between the dopaminergic receptor system and the regional cerebral hemodynamic responses. In the next chapter (chapter 5), we will use the 6-OHDA model again to investigate the neuronal activity-regional hemodynamic coupling by the pharmacological stimulation induced by the dopaminergic agonist d-amphetamine and the dopaminergic reuptake blocker CFT.

Appendix -- Behavioral Rotational Test

After unilateral 6-OHDA lesioning in the medial forebrain bundle, the insufficient dopamine supply to the ipsilateral striatum will induce supersensitivity, an increase in the number of postsynaptic dopamine receptors. The degree of dopamine-receptor coupling in each striatum will be proportional (though not necessarily linearly) to the number of dopaminergic receptors on the postsynaptic side. Since each hemispheric motor cortex circuit of the brain controls the motion on the contralateral side of the body, the animals will turn ipsilaterally to the 6-OHDA lesioning with the stimulation of D-amphetamine (a dopamine releaser and reuptake blocker [39]) due to the loss of dopaminergic innervation in this striatum. More than 600 ipsilateral turns in 90 minutes indicates more than 90% loss of the dopaminergic innervation in the striatum ipsilateral to the 6-OHDA lesioning. While more than 900 ipsilateral turns in 90 minutes

indicates more than 95% innervation loss. On the other hand, if injected with apomorphine, the dopamine agonist, due to the supersensitivity built up in the striatum ipsilateral to the 6-OHDA lesioning, the animal will turn contralateral to the lesion. According to the literature [40,41,42], the ipsilateral SNc of an animal with a partial lesion of the medial forebrain bundle will synthesize more dopamine than the normal level to compensate for the insufficiency in dopamine transport from SNc to striatum. Therefore, the dopamine level in the ipsilateral striatum may not show any abnormality until the loss of the dopaminergic neuronal terminals in the striatum is greater than 85%. This contention has been tested experimentally [see fig 3 in ref. 40].

Reference:

- 1 O. Hornykiewicz, S. J. Kish, Biochemical pathophysiology of Parkinson's disease, *Advances in Neurology*, (M. Yahr and K. Bergman) **45**:19-34, Raven Press (1987).
- 2 M. L. DeLong, Primate models of movement disorders of basal ganglia origin, *TINS*, **13**(7):281-285(1990)
- 3 J. W. Mink, W. T. Thach, Basal ganglia intrinsic circuits and their role in behavior, *Current opinion in Neurobiology*, **3**: 950-957 (1993)
- 4 J. Fearnley, A. Lees, Aging and Parkinson's disease: substantia nigra regional selectivity, *Brain*, **114**:2283-2301 (1991)
- 5 E. Hirsch, A. Graybiel, Y. Agid, Melanized dopaminergic neurons are differentially susceptible to degeneration in Parkinson's disease, *Nature*, **334**:345-348 (1988)
- 6 M. J. Zigmond, E. D. Abercrombie, T. W. Berger, A. A. Grace, E M. Stricker, Compensations after lesions of central dopaminergic

-
- neurons; some clinical and basic implications, *TINS*, **13(7)**:290-296 (1990)
- 7 K. Fuxe, L. F. Agnati, M. Kalla, M. Goldstein, K. Andersson, A. Harfstrand, Dopaminergic systems in the brain and pituitary, *Basic and Clinical Aspects of Neuroscience*, Springer-Sandoz Advanced Texts, Berlin, 11-25(1985)
 - 8 U. Ungerstedt, Use of intracerebral injections of 6-hydroxydopamine as a tool for morphological and functional studies of central catecholamine neurons. In 6-hydroxydopamine and catecholamine neurons. Edited by T. Malmfors and H. Thoenen., North-Holland Publishing Co., Amsterdam, London, pp. 315-332
 - 9 J. H. Thakar, M. N. Hassan, Effects of 6-hydroxydopamine on oxidative phosphorylation of mitochondria from rat striatum, cortex, and liver, *Can. J. Physiol. Pharmacol.*, **66**:376-379 (1988)
 - 10 Y. Mizuno, S. Ikebe, N. Hattori, Y. Nakagawa-Hattori, H. Mochizuki, M. Tanaka, T. Ozawa, Role of mitochondria in the etiology and pathogenesis of Parkinson's disease, *Biochimica et biophysica Acta*, **1271(1)**:265-274 (1995)
 - 11 A. C. Bowlin and M. F. Beal, Bioenergetic and oxidative stress in neurodegenerative disease, *Life Sciences*, **56(14)**, 1151-1171, (1995)
 - 12 K. F. Tipton T. P. Singer, Advances in our understanding of the mechanisms of the neurotoxicity of MPTP and related compounds, *J Neurochem.*, **61(4)**:1191-1206 (1993)
 - 13 M. F. Beal, Does impairment of energy metabolism result in excitotoxic neuronal death in neurodegenerative illnesses? *Ann Neurol.* **31(2)**:119-30, (1992)
 - 14 M. J. Zigmond, E. M. Stricker, International Review of Neurobiology **31**:1-79, Academic Press, (1972)
 - 15 A. Villringer, B. R. Rosen, J. W. Belliveau, J. L. Acerman, R. B. Lauffer, R. B. Buxton, Y. S. Chao, V. J. Wedeen, T. J. Brady, Dynamic imaging

-
- with lanthanidechelates in normal brain: contrast due to magnetic susceptibility effects, *Magn. Reson. Med.*, **6(2)** 164-174 (1988)
- 16 L. M. Hamberg, R. Macfarlane, E. Tasdemiroglu, P. Boccalini, B. G. Hunter, J. W. Belliveau, M. A. Moskowitz, B. R. Rosen, Measurement of cerebrovascular changes in cats after transient ischemia using dynamic magnetic resonance imaging, *Stroke*, **24(3)**, 444-450 (1993)
- 17 S. I. Bellin, S. K. Landas, A. K. Johnson, Selective catecholamine depletion of structures along the ventral lamina terminalis: effects on experimentally-induced drinking and pressor responses., *Brain research*, **456(1)**: 9-16 (1988)
- 18 S. Lopez-Sanudo, E. Arilla, Desmethylimipramine pretreatment prevents 6-hydroxydopamine induced somatostatin receptor reduction in the rat hippocampus., *Regul Pept*, **41(3)**:227-236, (1992)
- 19 M. J. Zigmond, T. G. Hastings, E. D. Abercrombie, Neurochemical Responses to 6-hydroxydopamine and L-dopa therapy: Implications for Parkinson's disease, *Ann. N Y, Acad. Sci.*, **648**:71-85 (1992)
- 20 D. A. Staunton, B. B. Groves, P. M. Groves, P. B. Molinoff, *Brain Research*, **211**:315-327 (1981)
- 21 U. Ungerstedt, *Acta Physiol. Scand.*, **361(suppl.)**:69-93 (1971)
- 22 J. L. Hudson, C. G. Van Horne, I. Stromberg, S Brock, J. Clayton, J. Masserano, B. J. Hoffer, G. A. Gerhardt, Correlation of apomorphine- and amphetamine-induced turning with nigrostriatal dopamine content in unilateral 6-hydroxydopamine lesioned rats, *Brain Research*, **626**, 167-74 (1993)
- 23 D. A. Perese, J. Ulman, J. Viola, S. E. Ewing, K. S. Bankiewicz, A 6-hydroxydopamine-induced selective Parkinsonian rat model, *Brain Research*, **494**, 285-293 (1989)
- 24 A. A. De Graaf, W. M. Bovee, N. E. Deutz, R. A. Chamuleau, In vivo ¹H NMR procedure to determine several rat cerebral metabolite

-
- levels simultaneously, undisturbed by water and lipid signals, *Magn. Reson. Imagin*, **6(3)**:255-261 (1988)
- 25 D. Bourgeois, C. Remy, Y. Lefur, P. Devoulon, A. L. Benabid, M. Decops, Proton spectroscopic imaging: a tool for studying intracerebral tumor models in rat, *Magn. Reson. Med.*, **21(1)**:10-20 (1991)
- 26 B. G. Jenkins, E. Storey, M. F. Beal, B. R. Rosen, Chemical shift imaging of focal neurochemical lesions in rat brains, proceeding Society of Magn. Reson. Med., 10th meeting at San Francisco, (1): 437 (1991)
- 27 B. G. Jenkins, E. Brouillet, Y. I. Chen, E. Storey, J. B. Schulz, P. Kirschner, M. F. Beal, B. R. Rosen, Non-Invasive Neurochemical Analysis of Focal Excitotoxic Lesions in Models of Neurodegenerative Illness Using Spectroscopic Imaging, *J Cereb. Blood Flow Metab.*, **16**:450-461 (1996).
- 28 F. C. Zhou, S. Bledsoe, J. Murphy, Serotonergic sprouting is induced by dopamine-lesion in substantia nigra of adult rat brain, *Brain Research*, **556(1)**:108-16, (1991)
- 29 Y. Yoshimoto, Q. Lin, T. J. Collier, D. M. Frim, X. O. Breakefield, M. C. Bohn, Astrocytes retrovirally transduced with BDNF elicit behavioural improvement in a rat model of Parkinson's disease, *Brain Research*, **691(1-2)**: 25-36, (1995)
- 30 S. Mraovitch, Y. Calando, B. Onteniente, M. Peschanski, J. Seylaz, Cerebrovascular and metabolic uncoupling in the caudate-putamen following unilateral lesion of the mesencephalic dopaminergic neurons in the rat, *Neuroscience letter*, **157**:140-144 (1993)
- 31 A. M. Graybiel, Correspondence between the dopamine islands and striosomes of the mammalian striatum, *Neuroscience*, **13**:1157-1187 (1984)

-
- 32 H. Newman-Gage, A. M. Graybiel, Expression of calcium/calmodulin-dependent protein kinase in relation to dopamine islands and synaptic maturation in the cat striatum, *J Neurosci*, **8(9)**: 3360-3375, (1988)
- 33 S. Halpain, J. A. Girault, P. Greengard, Activation of NMDA receptors induces dephosphorylation of DARPP-32 in rat striatal slices, *Nature* **343**:369-372 (1990)
- 34 M Rango, D Spagnoli; G Tomei, F Bamonti; G Scarlato, L Zetta, Central nervous system trans-synaptic effects of acute axonal injury: a 1H magnetic resonance spectroscopy study, *Magn. Reson. Med*, **33(5)**: 595-600(1995)
- 35 P. Riederer, E. Sofic, W. Rausch, B Schmidt, G. Reynolds, K. Jellinger, M. Youdim, Transition metals, ferritin, glutathione, and ascorbic acid in Parkinsonian brain, *J. Neurochem*, **52**:515-520 (1989)
- 36 K. Earle, Studies on Parkinson's disease including x-ray fluorescent spectroscopy of formalin fixed brain tissue, *J. Neuropathol. Exp. Neurol.*, **27**:1-14 (1968)
- 37 E. Sofic, P. Riederer, H. Heinsen, H. Beckmann, G. Reynolds, G. Hebenstreit, M. Youdim, Increased iron III and total iron content in postmortem substantia nigra in Parkinsonian brain, *J. Neural Transm.*, **74**:199-205 (1988)
- 38 E. Oestreicher, G. J. Sengstock, P. Reiderer, C. W. Olanow, A. J. Dunn, G. W. Arendash, Degeneration of nigrostriatal dopaminergic neurons increases iron within the substantia nigra: a histochemical and neurochemical study, *Brain Research*, **660**:8-18 (1994)
- 39 B. Giros, M. Jaber, S.R. Jones, R. M. Wightman, M.G. Caron, Hyperlocomotion and indifference to cocaine and amphetamine in mice lacking the dopamine transporter, *Nature* **379**: 606-612 (1996)

-
- 40 T. E. Robinson, Whishaw I. Q., Normalization of extracellular dopamine in striatum following recovery from a partial unilateral 6-OHDA lesion of the substantia nigra: a microdialysis study in freely moving rats, *Brain Research*, **450(1-2)**:209-224, (1988)
- 41 W. Q. Zhang, H. A. Tilson, K. P. Nanry, P. M. Hudson, J. S. Hon, M. K. Stachowiak, Increased dopamine release from striata of rats after unilateral nigrostriatal bundle damage, *Brain Research*, **461(2)**:335-342, (1988)
- 42 E. D. Abercrombie, A. E. Bonatz, M. J. Zigmond, Effects of L-dopa on extracellular dopamine in striatum of normal and 6-hydroxydopamine-treated rats, *Brain Research*, **525(1)**:36-44 (1990)

Chapter 5 Pharmacological MRI (*ph* MRI)

Introduction

Detection of specific neurotransmitter activity non-invasively and longitudinally could be of great assistance for understanding brain pathology and subsequent therapy of many disease processes. For instance, the destruction of the nigral dopaminergic innervation of the striatum in Parkinson's disease and subsequent therapy using fetal cell transplantation would be greatly aided by a means of following progression of the graft. Studies of receptor binding can be performed *in vivo* using positron emission tomography (PET) imaging, or can be performed post mortem using autoradiography. These techniques allow one to use receptor agonists or antagonists to directly map out the receptor density of these binding sites in the brain and also allow for investigation of the drug induced neuronal

metabolic changes such as changes in regional cerebral blood flow (rCBF) or regional glucose utilization (CMR_{glu}) induced by stimulation of drugs such as d-amphetamine [1,2,3,4,5]. However PET is compromised in its ability to evaluate humans longitudinally due to the radioactivity involved in the *in vivo* studies. The technique of functional magnetic resonance using either BOLD or T_1 -based techniques has led to a revolution in brain mapping. These techniques are based upon the coupling between neuronal activity, metabolism and hemodynamics leading to changes in MR signal intensity sensitive to these parameters [6,7,8]. The technique has been labeled as functional MRI or fMRI and has been widely applied to task initiated brain functional studies. In addition to neuronal activity induced by task activation, stimulation of neurons using pharmacological ligands is also possible. The use of fMRI to perform such experiments is tempting due to its non-invasive repeatable nature. However, due to the large doses necessary to obtain a response measurable by MR techniques, compared to autoradiography or PET, it is necessary to ascertain that the measured response is due to activation of the neurotransmitter system in question. There are a number of issues which arise in this context which are relevant to understanding the coupling between neurotransmitter binding and the hemodynamic response. The issue of whether the potential fMRI response is due to direct neurotransmitter binding or indirect effects (such as a change in pCO_2) needs to be investigated. One approach to solving this problem would be delineation of the correlations between the hemodynamics, the receptor binding, neurotransmitter release and

behavior. Several useful techniques exist for studying these events including PET imaging [9,10] and microdialysis [11].

We have chosen to study the dopamine system to examine the utility of fMRI for investigation of neurotransmitter activation for a number of reasons. The dopamine system, unlike the glutamatergic, for instance, shows great regional specificity with high receptor density in the frontal cortex and basal ganglia. In addition, very reproducible animal models of dopaminergic binding and ablation exist. These models are of great interest in studying neurodegeneration (Parkinson's disease) as well as, for instance, drug abuse (cocaine addiction). The ability to selectively and unilaterally denervate the dopaminergic system using 6-hydroxydopamine (6-OHDA) also allows for a controlled experiment to measure the efficacy of whether or not the phMRI response is due directly to dopamine. There is a large body of autoradiographic data on the response of both rCBF and glucose utilization rates to dopaminergic ligands such as d-amphetamine, as well as a wealth of behavioral and autoradiographic data on the 6-OHDA model [12,13]. We have utilized two different dopaminergic ligands. D-amphetamine is a dopamine release compound which appears to work by increasing the dopamine concentration in the synapse by release of dopamine from the transporter receptor [14]. CFT (2 β -carbomethoxy-3 β -(4-fluoropheny) tropane, or ¹¹C-WIN 35,428 compound) is a dopamine transporter antagonist whose effects are much like cocaine, only more specific [15,16]. We demonstrate here that the fMRI response to pharmacological stimulation (hereafter dubbed phMRI) shows a tight coupling to the regional distribution of dopamine transporters

using PET and to the release of dopamine as studied using microdialysis.

Methods

Animal preparation—

Unilateral medial forebrain bundle lesions with 6-OHDA were processed and tested as mentioned in the animal preparation session in chapter 4. The successfully lesioned animals (n = 18) and normal control rats (n = 5) were scheduled for both PET and MRI studies. Six dopaminergic fetal cell transplanted rats were included in this study, too, to validate the tight correlation between the pHMRI responses and the dopaminergic neuronal activities. The success of the graft can be assessed by behavioral testing using the amphetamine rotational test described in the last chapter (see appendix in chapter 4). Unfortunately, due to the tremendously long preparation time for the 6-OHDA lesioning plus the fetal cell transplantation, no baseline studies (MR or PET) could be done in the graft recipients before the neuronal transplantation.

MR Measurements—

All MR measurements were performed on a 4.7T GE Omega CSI imager (Fremont, CA). Animals were imaged using a 35mm birdcage coil under halothane/N₂O/O₂ anesthesia (1.5% halothane). All animals were temperature regulated using a circulating water blanket at 38°C and were monitored for arterial oxygen saturation using a Nonin pulse oximeter (Minneapolis, MN) during imaging. The immobility of the animal during the drug stimulation and the homogeneous signal intensity of the gradient echo images over the

whole brain tissue were two critical conditions for the success of the phMRI studies. To attain these goals, the animal heads were shaved and wrapped with either dental hydroplastic gel or water-soluble bathroom adhesive caulk to immobilize the head and to reduce the susceptibility differences created by the tissue-air interface. The rats were imaged using conventional gradient recalled echo images acquired repeatedly from the striatal area (TR/TE 400ms/15ms, Ernst angle RF, 3 or 5 slices with slice thickness 1.5mm). At least 15 stable base line image sets were acquired before the pharmacological stimulation. Three mg/kg D-amphetamine or 0.75mg/kg 2 β -carbomethoxy-3 β -(4-fluoropheny) tropane (CFT, or WIN 35,428 compound, RBI, Cambridge, MA) were then given intravenously while the images were being acquired, the imaging was continued for 90 to 180 minutes post injection. In addition to the blood oxygenation saturation monitoring, an arterial line from the femoral artery was connected to a cardiac monitoring device (706 patient monitor, Ivy Biomedical System Inc.) in the nonlesion control group. The mean blood pressure and heart rate were recorded every 3 minutes and the arterial blood gases (pO₂, PCO₂, and pH) were sampled in 15 minute intervals. However not all animals, especially for the rats with 6-OHDA lesions and the group with grafts, could have blood sample or blood pressure monitored during MR scanning due to the impossibility of performing the necessary survival studies with the surgery required to insert the femoral arterial line.

In addition to the MR study, another control population of animals was studied on bench tops under similar physical conditions as the in-magnet studies (using 1.5% halothane anesthesia, body

temperature regulated, blood oxygenation monitored, etc). Measurements of blood gases (pO_2 , pCO_2 , and pH), heart rate and blood pressure were obtained the same fashion as the in-magnet studies over two-three hour time periods including baseline and post pharmacological stimulations (3mg/kg amphetamine i.v. or 0.75mg/kg CFT i.v.).

PET Measurements—

The same animals studied by phMRI were also scanned using positron emission tomography (PET). Anesthetized animals were placed on an imaging table. The head was secured in a customized Plexiglas head holder equipped with ear and mouth bars designed to ensure reproducible head positioning in PET. Imaging studies of dopamine transporters were performed using carbon-11 labeled CFT as a tracer. For PET imaging 0.8-1.2 mCi of the labeled compound (specific activity 800-1600 mCi/mmol) was administered into the tail vein. Serial dynamic imaging was acquired over the rat brain for 60-90 min using 4.5 mm steps and counts were block averaged for between 15-60s intervals depending upon how far along the 20 min half life ^{11}C decay curve the measurement occurred. PET Imaging was performed using a home-built high resolution single ring tomograph, PCR-I described earlier [17]. The resolution of PCR-I for a point source at the center is 4.5 mm and the sensitivity is 46,000 Hz for a source of 20 cm in diameter with a concentration of 1 mc/cc. The overall efficiency is 64% of the theoretical maximum for a plane thickness corresponding to the 2 cm high crystals. The plane thickness of 4.5 mm used in this study was obtained by the use of cylindrical collimators which limit the effective height of the crystals.

Imaging data were corrected for uniformity, attenuation, decay and acquisition time. Images were reconstructed using a ramp filter with a cut off value of 1.0 and convolution back projection.

Microdialysis --

The extracellular dopamine concentration from the dorsal lateral striatum was accessed by using microdialysis. For amphetamine stimulation, we used the existing data of dopamine release from literature [11,18,19]. For CFT stimulation, home made glass dialysate probes were implanted into the dorsal lateral striatum in the normal control rats. The dialysates were collected in 20 minute time blocks. The same CFT protocol as in the fMRI study was followed in the microdialysis study (40 minutes baseline and 90 minutes post CFT injection.) HPLC was used to analyze the dopamine concentration in the dialysis. Unfortunately, because of the invasiveness of this procedure, we can not perform microdialysis longitudinally and we used a different set of control animals than the fMRI study.

Data Analysis—

The activation maps of the phMRI data sets were generated using Komolgorov-Smirnov statistics and overlaid on the gradient echo images. Two approaches were utilized to define the activation. Areas of activation as defined by the statistical maps were calculated using automated segmentation of the maps at a predefined threshold of $p < 0.01$ (determined by requiring at least four activated pixels to be significant). The percent signal changes were also measured in these areas as well. In order to determine specificity, the anatomic structures were segmented using a rat brain atlas [20]. The fraction

of each structure activated, as determined from the statistical maps was then calculated. The differences between the ipsilateral and contralateral hemispheres were then measured using both the percent signal change and the areas as

$$\frac{\text{Contralateral} - \text{Ipsilateral}}{\text{Contralateral}}$$

These numbers were then compared with the PET data by averaging together the three 1.5 mm MRI slices to obtain the same slice thickness as in the PET studies.

For analysis of the PET data, since there is very little specific dopaminergic binding occurred in the cerebellum, the signal changes in cerebellum are assumed to represent non-specific binding and hence can be used to normalize the signal responses in other brain areas such as striatum. Regions of interest (ROI) including left and right striatum and cerebellum were drawn and the percent activity of the injected dose was calculated. Binding ratios of ^{11}C -CFT into the dopamine transporter were calculated according the following formula:

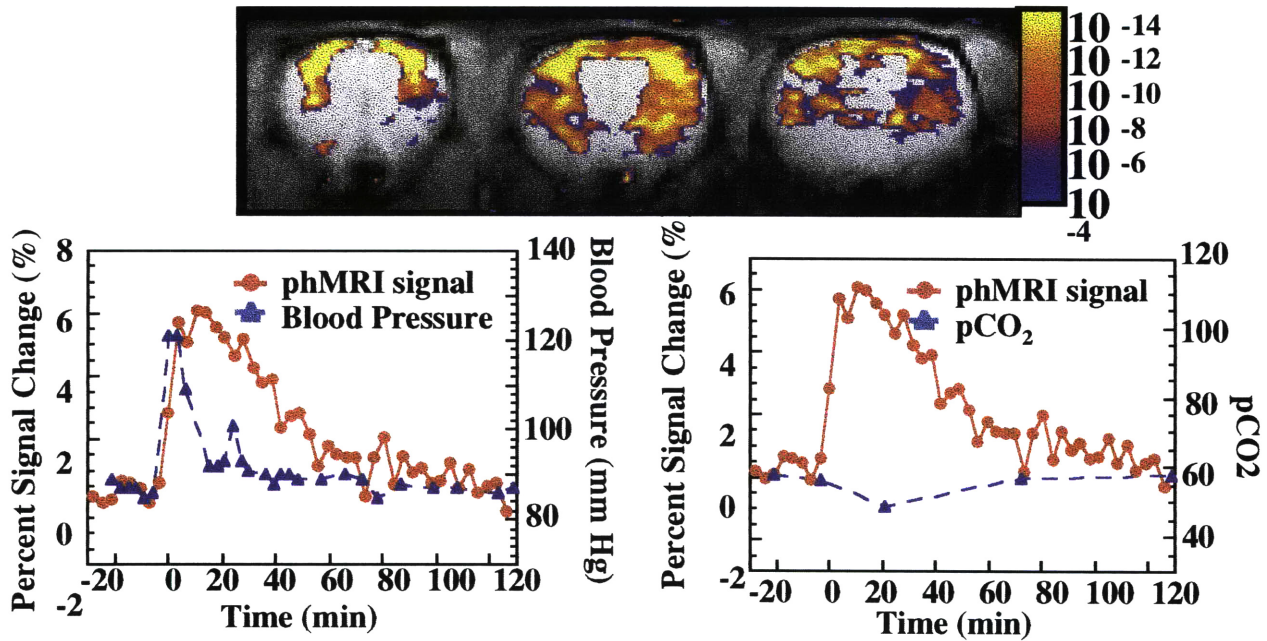
$$\text{Binding ratio} = \frac{\left(\frac{\text{Percent Activity}}{\# \text{ of Pixel}}\right)_{str} - \left(\frac{\text{Percent Activity}}{\# \text{ of Pixel}}\right)_{cerebellum}}{\left(\frac{\text{Percent Activity}}{\# \text{ of Pixel}}\right)_{cerebellum}}$$

The values of the binding ratios were averaged between 55 and 65 min (so as not to include the initial activity due largely to flow) and compared to the values of hemodynamic indices from MR studies as well as to rotational behavior using the amphetamine stimulation described above.

Results

The injection of either amphetamine or CFT caused an increase in signal intensity using BOLD imaging that was regionally localized to areas of the brain that are high in dopaminergic receptor density as shown in Fig. 5-1. These areas include cingulate and frontal cortex (but not parietal cortex) and striatum. Initially, we used higher doses of amphetamine which led to non-specific increases in all areas of the brain as also reported by Silva et al. using 20 mg/kg amphetamine [21]. The dose of 3mg/kg i.v. of amphetamine produces an pHMRI response which is similar to that produced by 0.75 mg/kg of CFT. The regional specificity of brain activation was measured by automated segmentation analysis of the statistical maps generated by analysis of the time courses and measuring the fraction of the anatomic structure activated. These results are shown in Fig. 5-2. It is clear that the frontal cortex and the striatum are the areas which show the largest activation, in keeping with their large dopaminergic innervation. Parietal cortex which is relatively low in dopamine innervation has relatively low fMRI response. The reason why the parietal cortex activation is not zero may be due to the partial volume averaging of our relatively thick slice (1.5 mm). Figure 5-3 illustrates the parietal cortex in the mid-striatal slice is overlapped with the striatal area in the more posterior slice. The overlap is 10% in the parietal area.

(A) D-Amphetamine: 3mg/kg i.v.



(B) CFT: 0.75 mg/kg i.v.

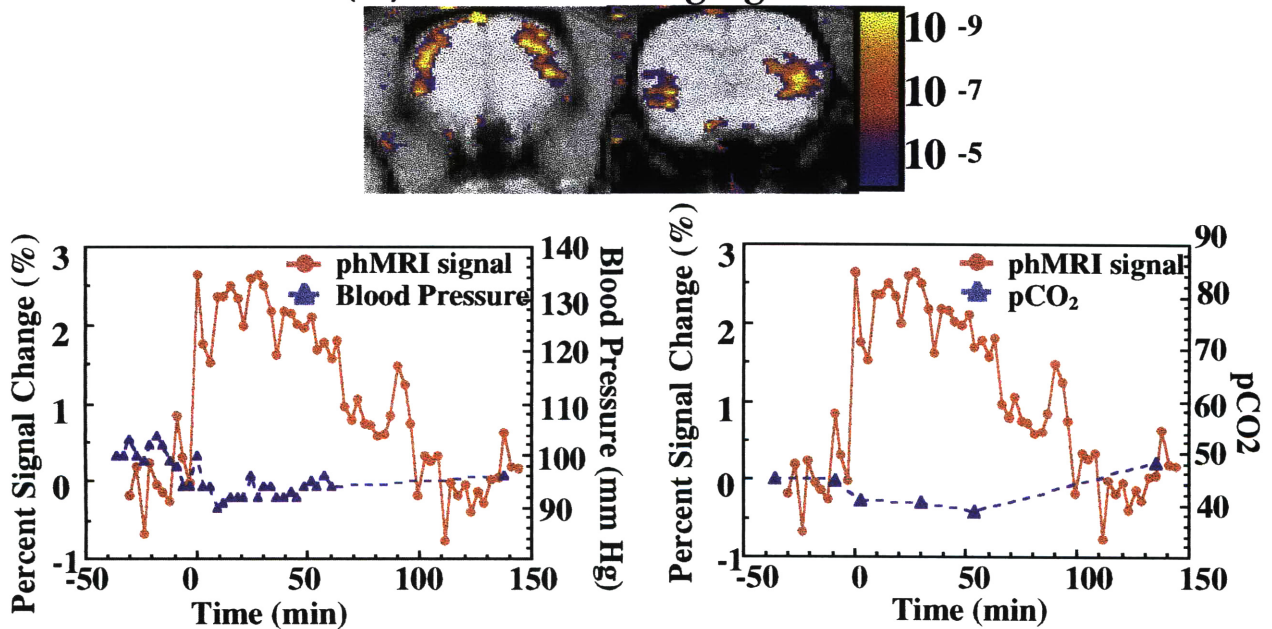


Figure 5-1 Statistical maps of increased BOLD signal change in normal control rats after injection with (A) 3 mg/kg amphetamine or (B) 0.75 mg/kg CFT. Changes in blood pressure and pCO₂ as measured in the magnet are shown with the percent signal changes. Note the BOLD signal change is delineated from blood pressure and pCO₂ changes.

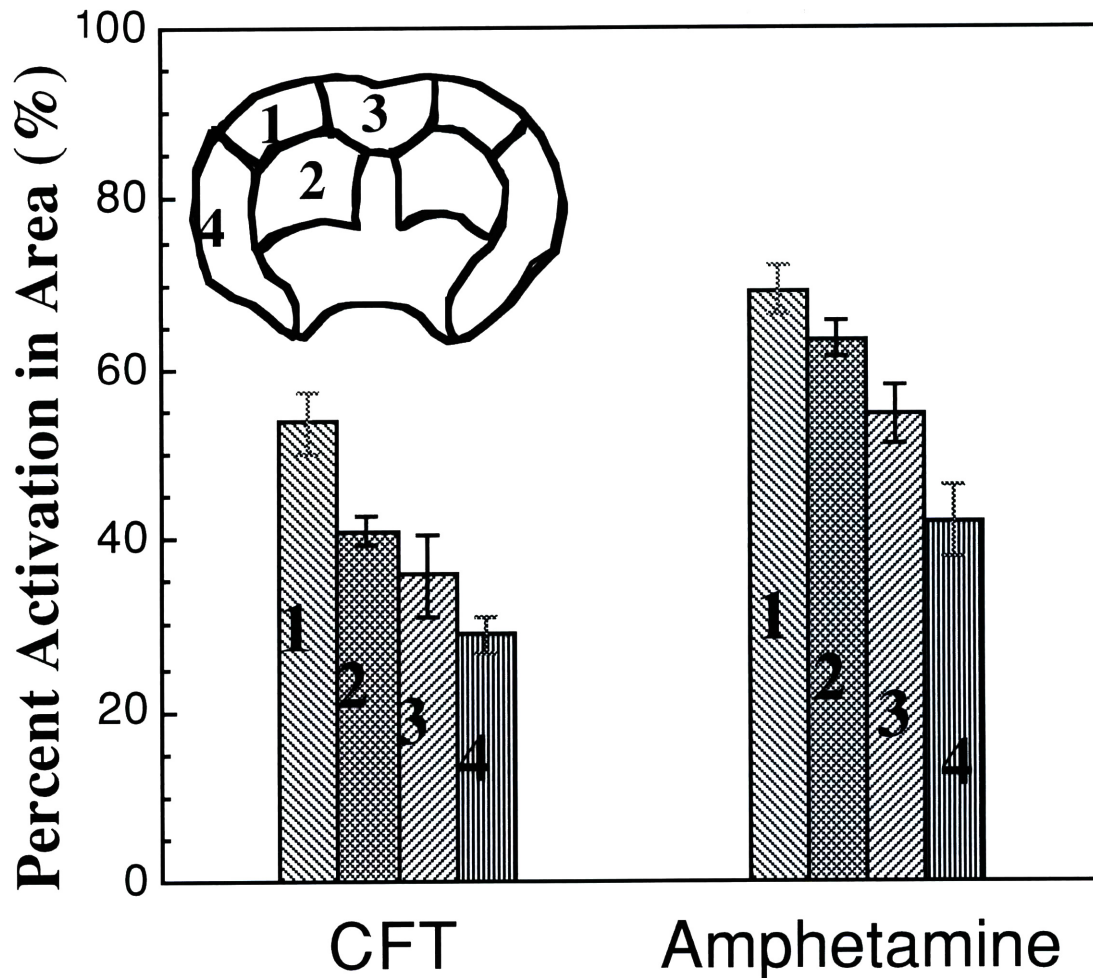
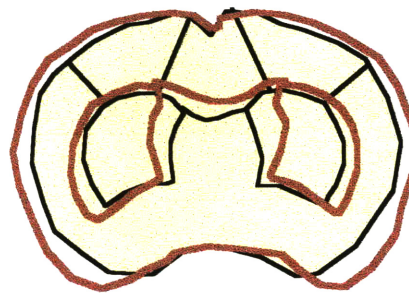
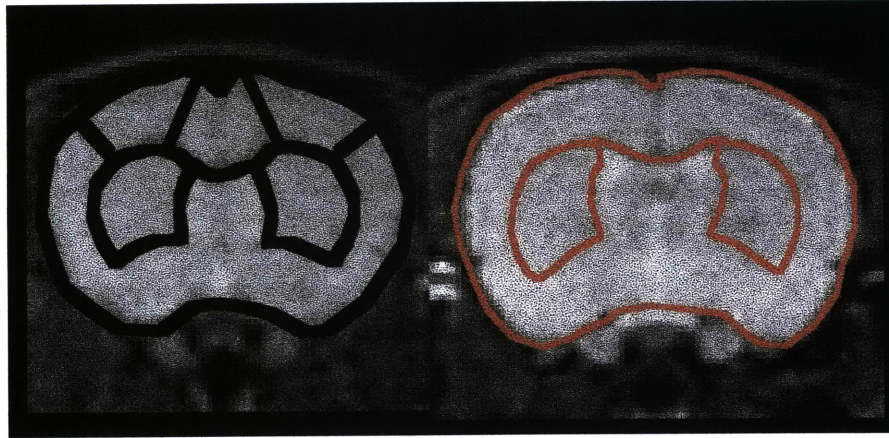


Figure 5-2 Bar graph showing the fraction of anatomic area activated by either amphetamine (n = 18) or CFT (n= 12). Segmentation was performed as described in text. A schematic of the areas segmented is shown. 1. frontal cortex, 2. striatum, 3. cingulate cortex, 4. parietal cortex.



10% of the parietal cortex
is overlapped with the striatum
from the more posterior slice

Fig. 5-3 Partial volume averaging in the parietal cortex. Yellow area with black line indicates the contour of the slice from the mid-striatum. Red line indicates the contour from the more posterior slice. The slice thickness in this study is 1.5 mm with 0 mm gape between slices.

Analysis of the time courses show that the response of the phMRI is transient, peaking at about 40 min and decreasing back to the baseline in about 70-90 min. This time course has the potential to reveal much about the nature of the effect. We thus performed a number of experiments. Shown in figure 5-4 are the effects of amphetamine and CFT on blood gases and blood pressure. It is clear that the time courses for these changes do not parallel those of the phMRI response as seen in figure 5-1. The effect is clearly not due to increased $p\text{CO}_2$ or the transient spike seen in the blood pressure curves.

In order to show that the time course of fMRI signal changes parallels the time course for release of dopamine in the dorsal-lateral striatum, we block averaged the fMRI time courses with time bins corresponding to the microdialysis data points. As shown in figure 5-5, the fMRI time course is virtually superimposable with the release of dopamine measured by microdialysis (Fig. 5-5 A) and is well correlated to the percent change in extracellular dopamine concentration (Fig. 5-5 B).

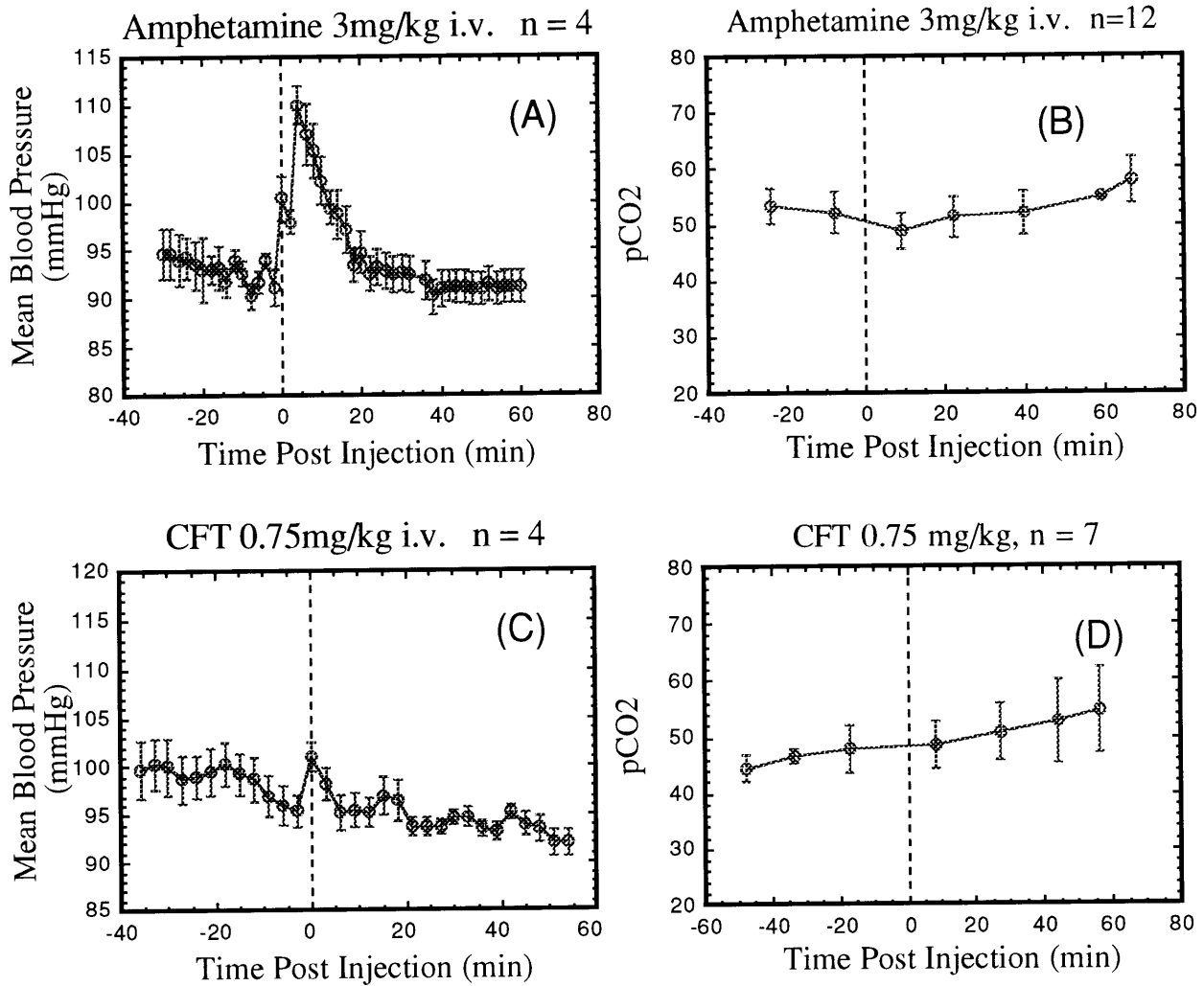


Figure 5-4 Changes in blood pressure and pCO2 for all the animals pooled for amphetamines and CFT.

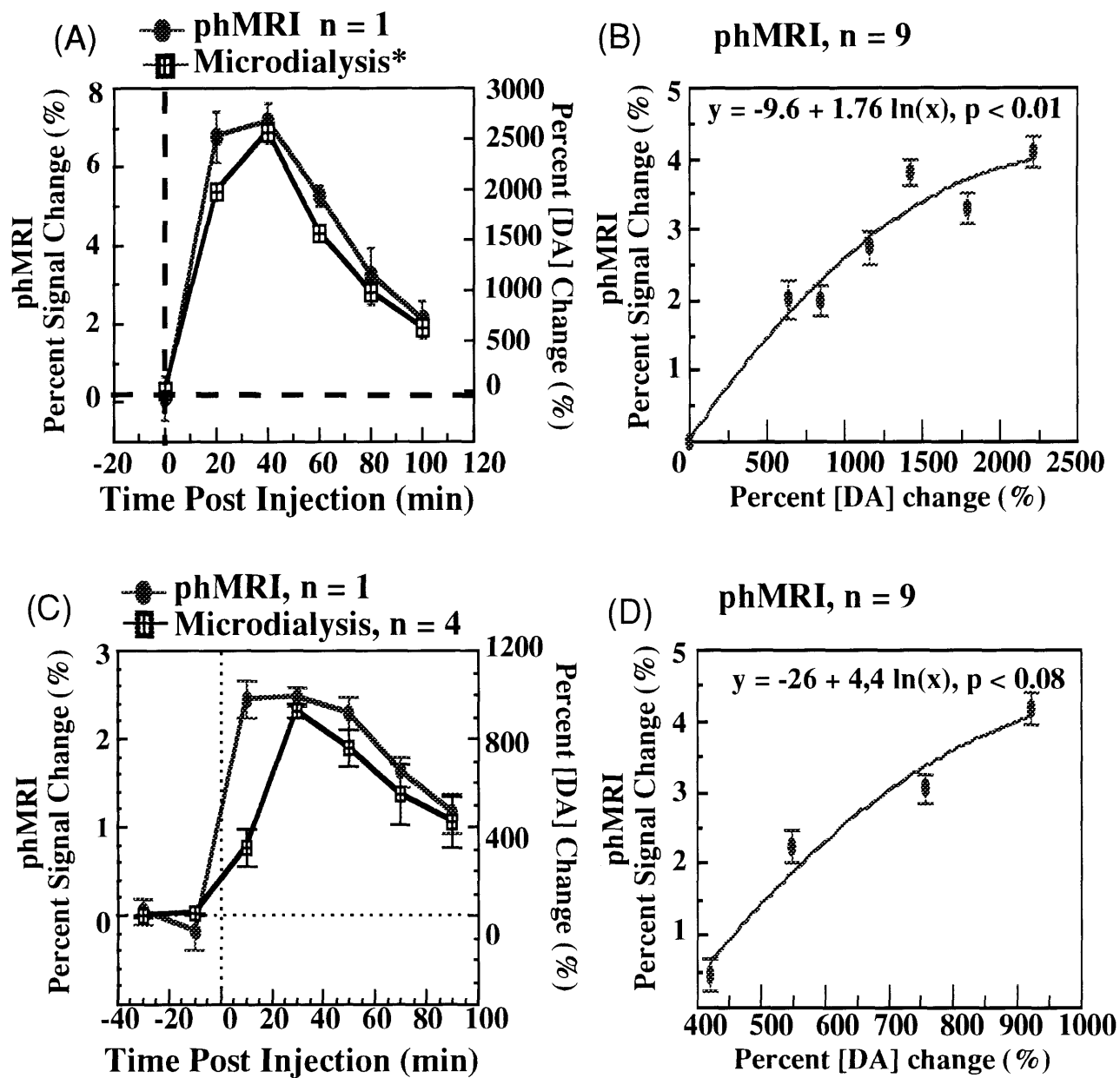
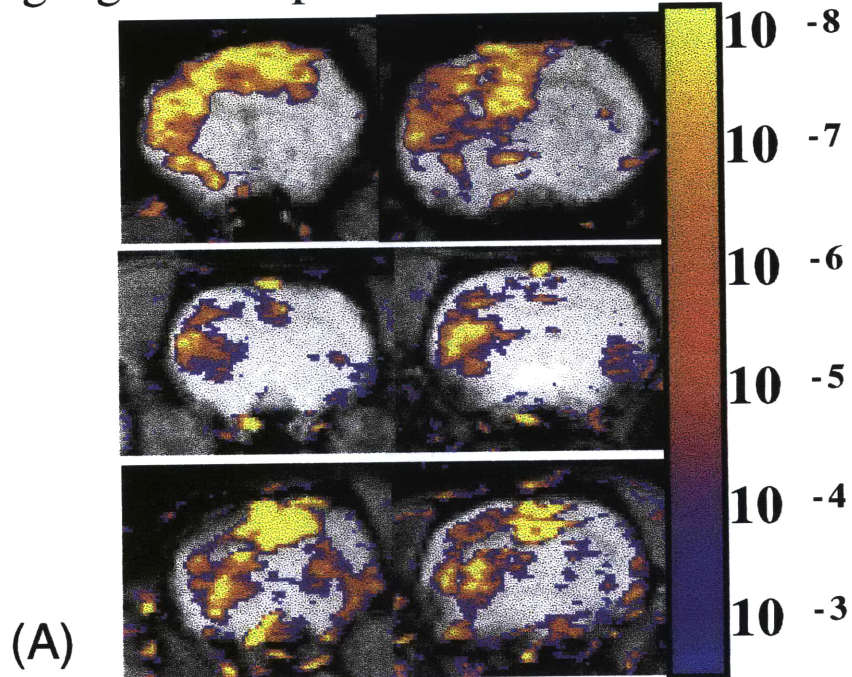


Figure 5-5 phMRI time points are block averaged with time bins corresponding to the microdialysis data points. (A) amphetamine (C) CFT stimulation. (B) and (D) show the correlation between the percent phMRI signal changes versus percent increase in dopamine release.

Destruction of the dopaminergic input to the frontal cortex and striatum should lead to an ablation of the phMRI response. This is shown in Fig. 5-6 using both amphetamine and CFT. Responses typical of the greatest, average and least differences between the ipsilateral and contralateral sides are shown in this figure in order to get an indication of the reproducibility and range of responses measured. Two time courses of the signal changes seen in the animals shown in Fig. 5-6 are presented in Fig. 5-7 for amphetamine and CFT. It is apparent that the response is much decreased on the ipsilateral side. To prove this was not due to an artifact, such as loss of regional blood flow or hemodynamics, we measured these latter parameters (rCBV and rCBF) using bolus injections of Gd(DTPA) [22, 23]. There was no statistically significant difference in the resting rCBV or rCBF between the two hemispheres indicating that the decreased phMRI response is not due to a decrease in the pre-stimulus values of these parameters on the ipsilateral side as shown in the previous chapter. These data are presented, along with rCBV and rCBF images in Fig. 5-8. In order to compare the phMRI response to behavioral changes, we time binned the fMRI time courses to correspond to the behavioral data (figure 5-9 A). The fMRI signal changes in the striata ipsilateral to the lesioning parallel the time courses of the rotational behavior in these animals. Figure 5-9 B also shows that the time course for the behavioral data of the unilaterally lesioned rats also correlates well with the extracellular dopamine concentration.

3 mg/kg D-amphetamine i.v. injection



0.75 mg/kg CFT i.v. injection

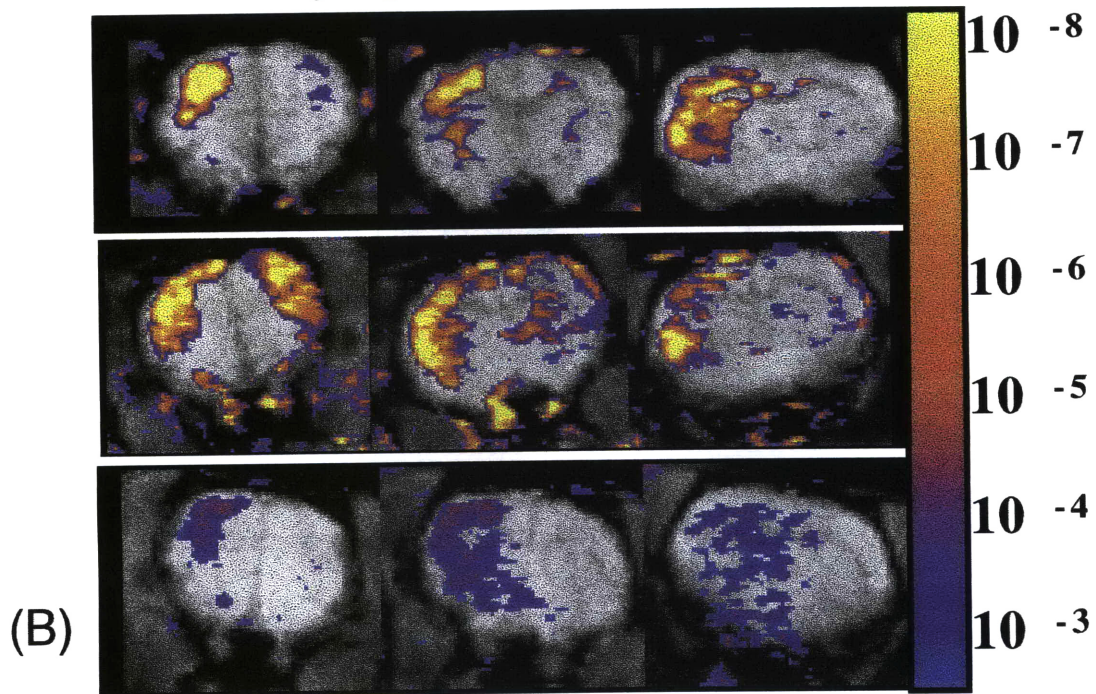


Figure 5-6 pHMRI responses of the unilaterally lesioned rats with stimulation of (A) amphetamine (B) CFT. Shown here are rats with good to bad pHMRI responses (top to bottom).

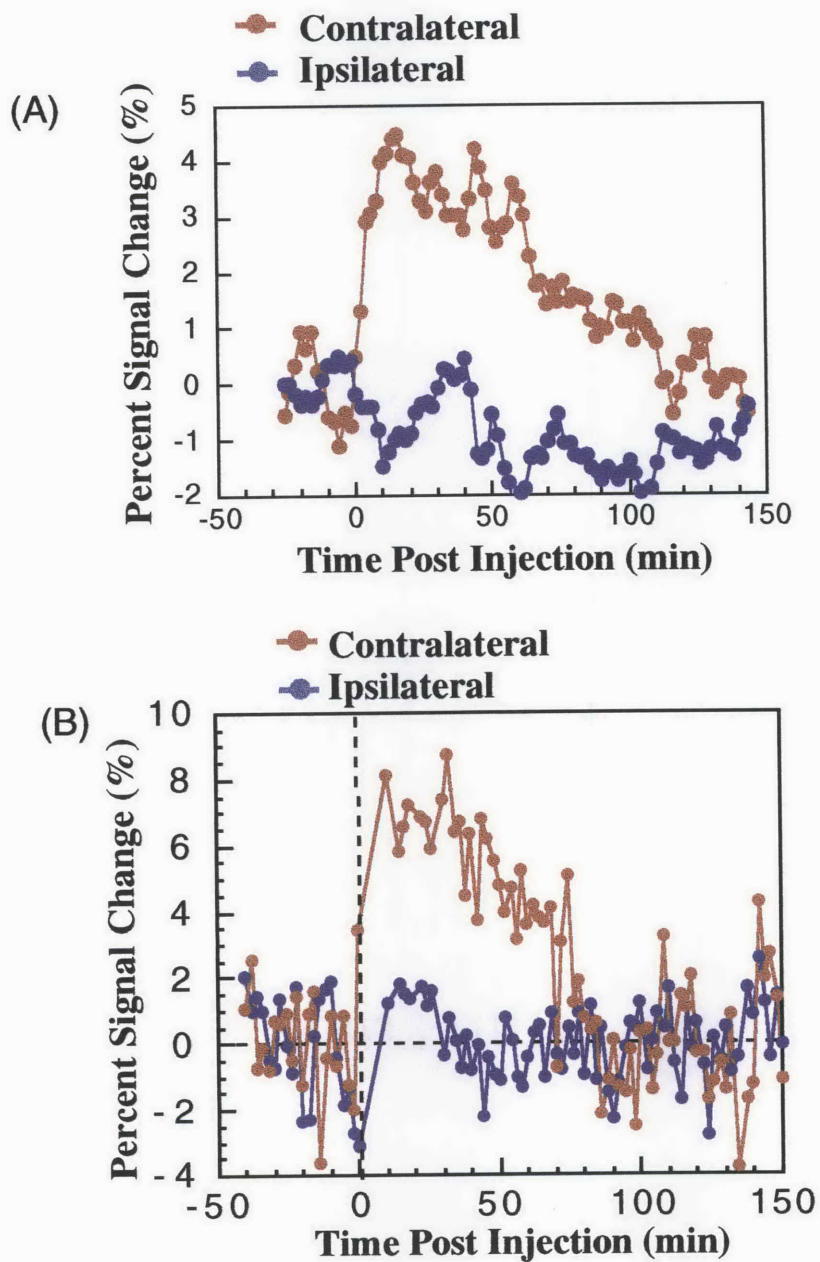
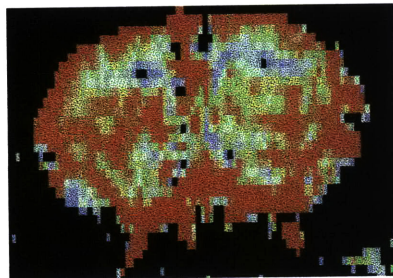


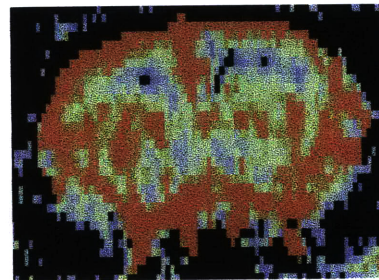
Figure 5-7 Time courses in the ipsilateral and contralateral striata in one of the 6-OHDA lesioned animals. (A) amphetamine 3mg/kg (B) CFT 0.75 mg/kg

CBV



Control Lesion

CBF



Control Lesion

Lesioned striatum / Control Striatum (<i>n</i> = 9)	
CBV = 1.05 ± 0.27 p = 0.88	CBF = 0.99 ± 0.11 p = 0.47

Figure 5-8 Maps of rCBV and rCBF generated using bolus injection of Gd(DTPA) in the resting state (no amphetamine or CFT) in 6-OHDA lesioned animals. Note there is no significant differences between the lesioned and control sides indicating that 6-OHDA does not cause destruction of the vascular bed. See chapter 4.

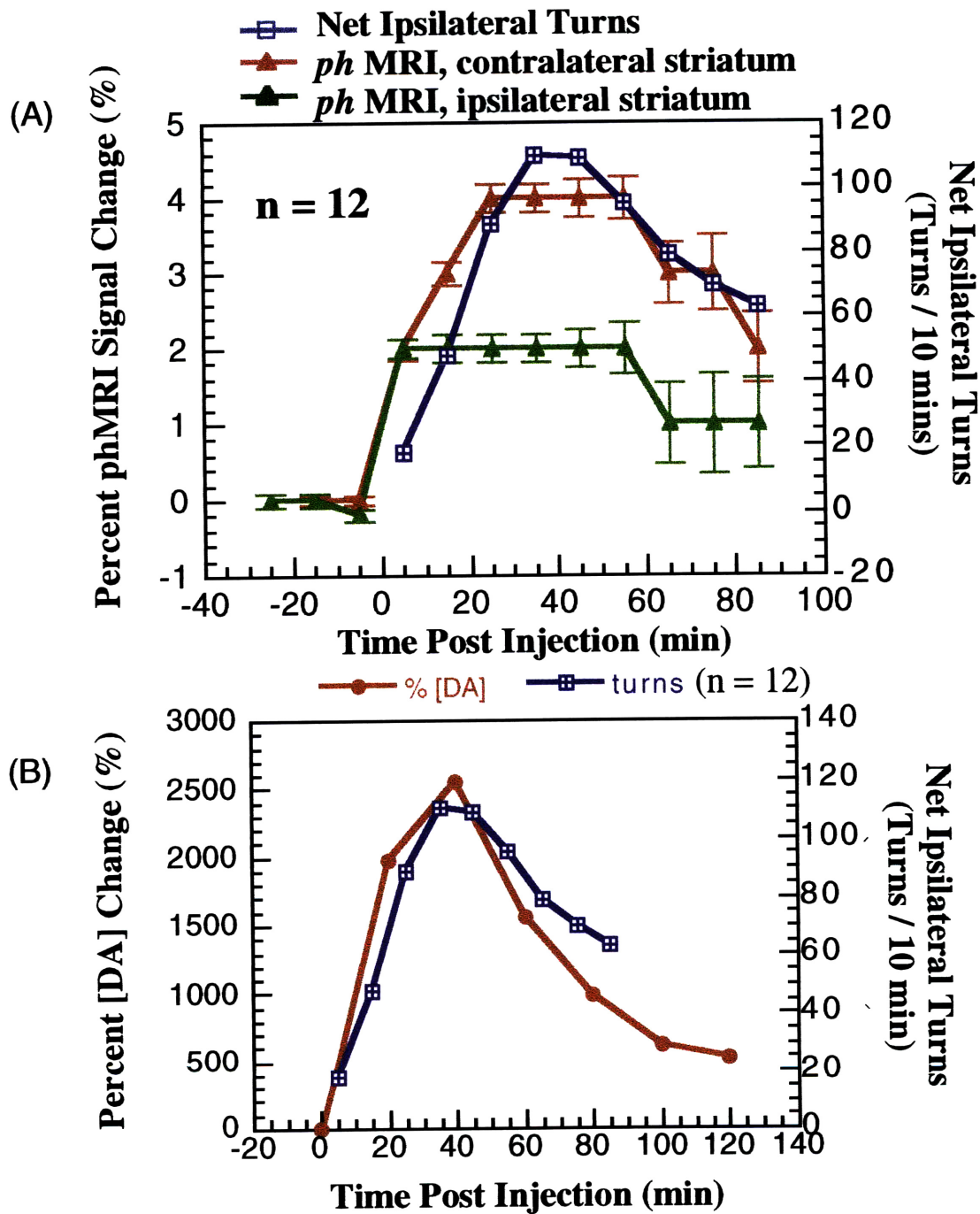


Figure 5-9 (A) phMRI response to amphetamine stimulation in a unilaterally lesioned rat (with time bins corresponding to the behavioral data points): the contralateral striatal time courses parallels to the behavioral data. (B) Correlation between dopamine release and behavioral data post amphetamine stimulation.

In order to investigate the relationship between the dopamine transporter receptor and the pHMRI we decided to run PET experiments on the same animals studied using the pHMRI techniques above. The comparison between the PET results and the pHMRI results was, in general, very consistent. In the lesioned animals a loss of ^{11}C -CFT uptake is noted in the ipsilateral striatum, compared to the unlesioned, control animals (Fig. 5-10). The pHMRI results faithfully reproduce this finding as is also seen in Fig. 5-8. The average change in the parameter describing the percent difference between the ipsilateral and contralateral striatum (contralateral -ipsilateral)/contralateral) was $39 \pm 4\%$ for PET and the decrease in pHMRI response to amphetamine or CFT stimulus was $39 \pm 16\%$ (n=12; p < .001) and $42 \pm 18\%$ (n=18; p < 0.001) respectively when measured as change in areas (figure 5-11). However, there is a large decrease in this asymmetry post transplantation [PET = $20.90 \pm 8.64\%$ (n=9; p >0.25), fMRI with CFT = $15.76 \pm 3.66\%$ (n=9; p >0.35)]. Obviously because the grafts are much smaller than the total striatum, we may not get return of full symmetry even though there was a full behavioral recovery for all transplanted animals. The good correlation with the PET images clearly indicates that the decreased binding of both CFT and amphetamine to the dopamine transporter is well reflected by the metabolic response as shown by pHMRI. Although the rats were screened by rotational data to correspond to those with greater than 95% loss of dopaminergic nigro-striatal innervation, there were clear differences in the number of rotations between animals. Thus, we looked to see if the behavioral data had any correlation with the imaging data. We compared loss of CFT binding in the ipsilateral striatum using PET or

metabolic response using phMRI as $[(\text{Contralateral} - \text{Ipsilateral})]/\text{Contralateral}$) The correlation between the PET, the phMRI and the behavioral data (rotation) is shown in Fig. 5-12. It is clear that there is a weak, but significant, correlation between the rotation and the PET. There was a strong correlation between the CFT and rotation, but none with amphetamine.

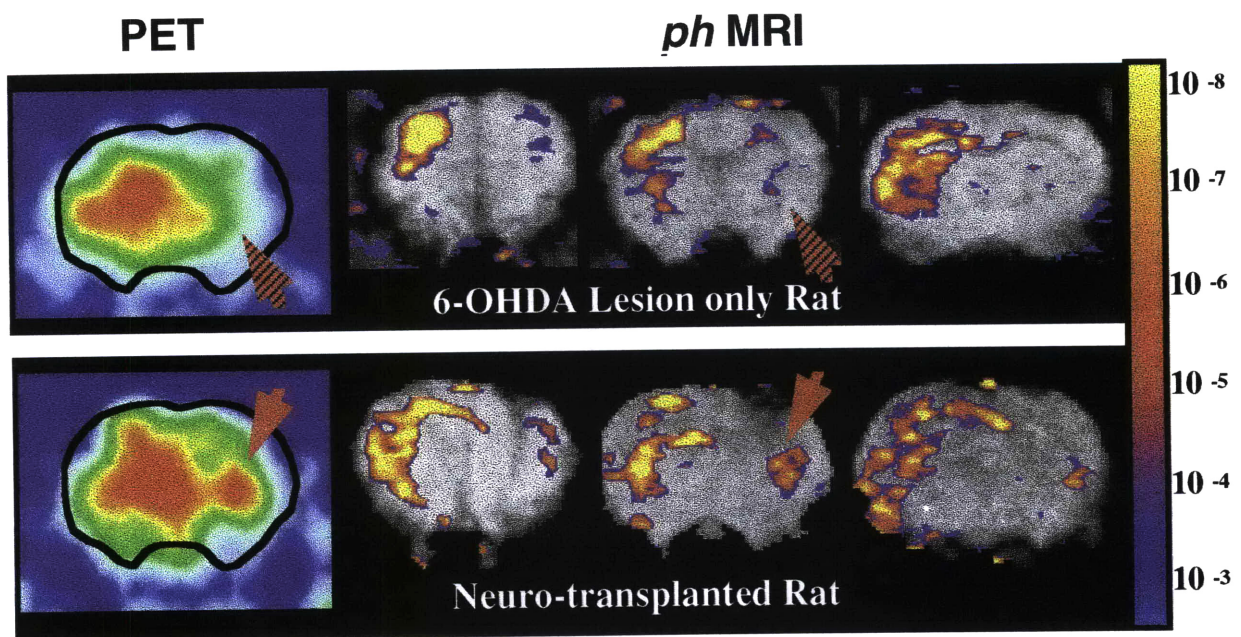


Figure 5-10 PET images and the corresponding phMRI images from a 6-OHDA lesioned and a neuronal transplanted animal. PET images come from a slice centered on the striatum. There is good correspondence between the PET images of CFT uptake and the phMRI images of the metabolic response, with the exception of the cortical regions.

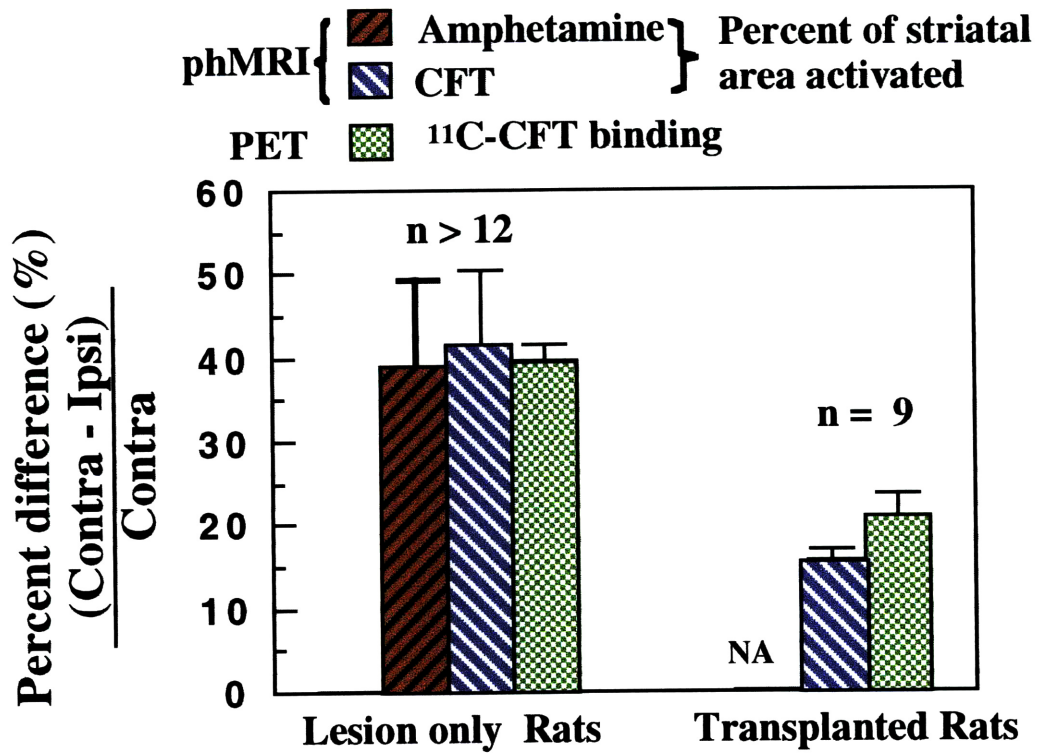


Figure 5-11 There is big asymmetric response in the two striata in the lesioned only rats. The asymmetry is greatly reduced in the neuron transplanted rats.

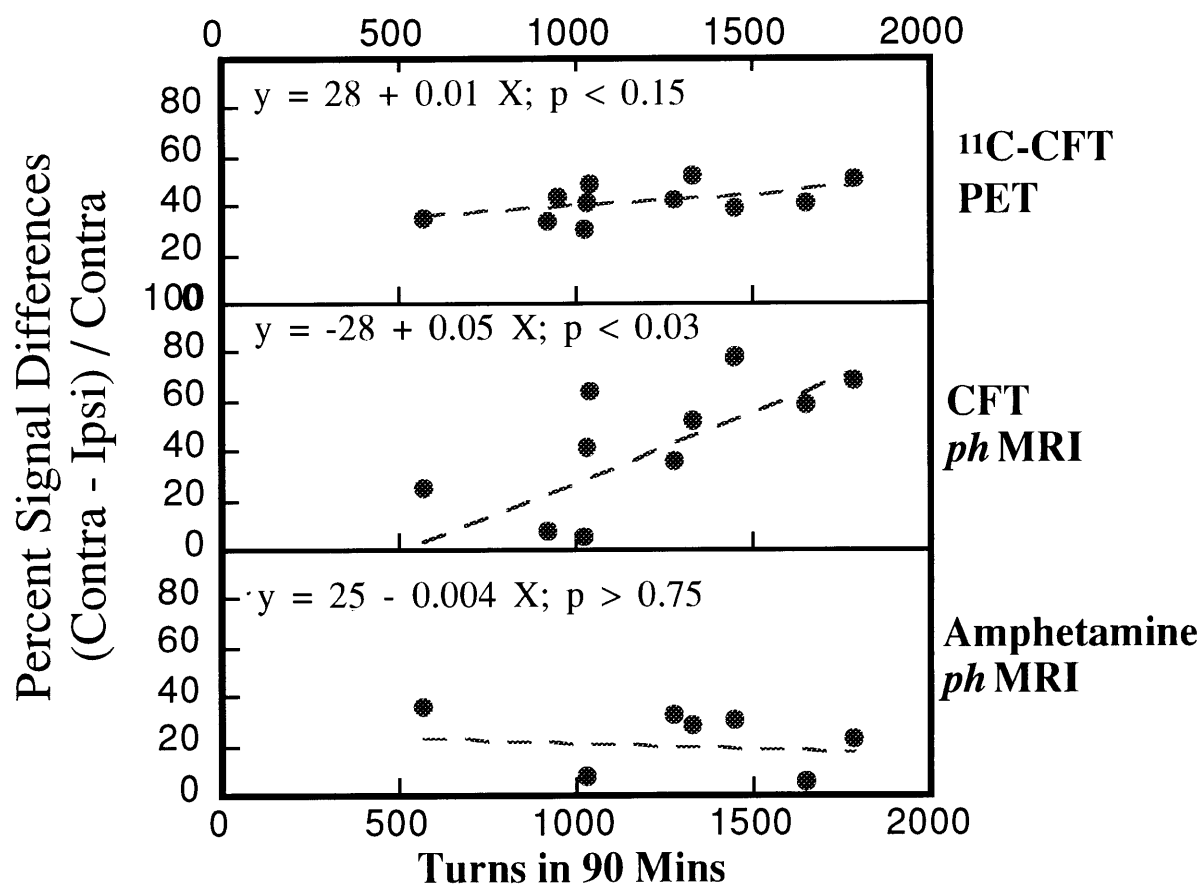


Figure 5-12 Correlations between the PET and the phMRI and the behavioral data.

Discussion:

We have demonstrated that the techniques commonly employed for fMRI studies of brain function during task activation are also appropriate for examination of the effects of neurotransmitter receptor stimulation. We utilized a well characterized model of dopamine denervation to show that the metabolic response resulting from stimulation of the dopamine system is well circumscribed to those areas of the brain containing large dopamine innervation and that the response is ablated when the nigro-striatal dopamine connections are denervated. There are a number of issues which need to be addressed before studies of this nature become routine both for the dopamine system in particular; and other neurotransmitter systems in general. The fact that we are observing a metabolic response to neurotransmitter binding rather than the binding itself, as in PET, creates some problems. One problem is that the large doses necessary to see an effect may lead to non-specific effects. This problem is especially acute in the dopamine system because of the possibility of stimulating other monoamine systems in the brain using a compound like amphetamine [1,2,3,4]. Another problem is understanding the coupling between the changes in the hemodynamics with the changes in dopamine concentrations. If the metabolic response is only coupled by very indirect means to the neurotransmitter release then the phMRI technique is not as useful as if there is a direct correlation.

Our results shed light on these problems. First, the spatial specificity we observed in our phMRI results with high fMRI responses in those brain areas with high dopaminergic innervation and the nice

correlation between fMRI and microdialysis data indicate that the fMRI effect is primarily due to dopamine and not other monoamine systems which would lead to more non-specific cortical activity. This is indeed what we observed with higher doses of amphetamine and has also been seen in autoradiographic studies of CBF [1,2,3,4]. Secondly, we showed that the time course for the signal changes are not reflective of simple physiological changes like hypercapnia, further indicating that the response is due to a metabolic response to neurotransmitter binding. Denervation of the dopaminergic input to the striatum using the well known model of 6-OHDA also showed that the response was due to dopamine as the change in signal intensity was nearly ablated on the ipsilateral side for both amphetamine and CFT. Measurements of resting rCBV and rCBF using bolus injection of Gd(DTPA) showed this was not due to impairment of vascularization or hemodynamics on the lesioned side. The dopaminergic denervation in the ipsilateral striatum was also demonstrated using PET imaging of ^{11}C -labeled CFT, thus lending more credence to the origins of the phMRI signal differences in the ipsilateral and contralateral striatum. The mean values of the percent differences $((\text{Contralateral} - \text{Ipsilateral})/\text{Contralateral})$ for both the PET binding and phMRI percent signal changes were identical. While it is not clear at this time how to turn PET binding measurements into blood flow changes, nonetheless the tight coupling between loss of CFT binding as measured by PET and loss of BOLD signal change using the 6-OHDA model indicates that the coupling between these two parameters may be quantitative.

In this regards it would be instructive to evaluate other pulse sequences to examine rCBF using T_1 -type techniques [7,21,24] as well

as BOLD. If there are dissociations between flow, oxygen consumption and glucose utilization these should show up as differences in these two signal responses. We initially tried using IR and GE sequences in these experiments in an interleaved mode for amphetamine stimulation, but came to the conclusion that the statistical power was not sufficient given the relatively low SNR of the images. Use of EPI techniques would alleviate this problem, but our current implementation of EPI involves a tradeoff of spatial resolution for temporal resolution (1 mm vs. 0.25 mm in plane resolution) which makes it difficult to adequately segment structures such as the cingulate and the accumbens in the small rat brain.

The time course noted for the phMRI signal changes are quite similar to those seen using microdialysis measurements [11,18,19]. In particular, the peak time for dopamine release measured using similar doses of amphetamine corresponds exactly to the peak of the phMRI response at about 40 minutes. This implies that the phMRI response is due to the release of dopamine in the striatum.

The sum of these facts, and the loss of phMRI response after 6-OHDA lesioning, strongly suggests that the metabolic response is due primarily to the release of dopamine in the striatum. In this regards it is instructive to compare the behavioral and PET data to the phMRI. As shown in Figs. 5-9, 5-11 and 5-12 there was a good correlation between the PET, rotation and CFT phMRI results. This was somewhat surprising as, according to the literature, rotations of greater than 600turns/90mins should reflect greater than 95% dopamine cell loss in the striatum [12,25]. Since all our rats were screened to manifest this behavior, the amphetamine results we

obtained (i.e. no correlation with behavior) were what we expected. The fact that we observe correlations of behavior with PET and phMRI using CFT implies that the some dopamine transporter may still be present in spite of the supposed loss of the pre-synaptic terminals. There is some precedent for this in the microdialysis literature, as when one measures extracellular dopamine levels versus percent dopamine neuronal depletion, there is a good deal of scatter - even for animals with nearly complete lesioning (see Fig. 3 in ref. 19). This same inter-animal variability has also been seen in behavioral/histological studies [25]. This finding has also been observed in PET studies of CFT binding in an MPTP model of Parkinsonism in primates where CFT uptake is sometimes still seen, even after lesioning (Brownell et al., unpublished).

The sensitivity manifested by the phMRI technique may make it a useful tool for pre-screening of Parkinson's disease in the earlier stages. Since symptoms of PD do not seem to occur until roughly 80% of the dopaminergic innervation of the striatum is destroyed, there is the possibility of being sensitive to changes that are on this order. This technique may also prove useful for evaluation of other dopamine ligands such as D1 and D2 agonists and antagonists. The ability of MRI to be used longitudinally and repeatedly may enable one to study up and down-regulation of the dopamine receptors over time. This could be of great interest in phenomena such as drug abuse. In addition, the possibility of examination of other neurotransmitter systems is quite feasible and will prove to be a fruitful area for future investigations.

Conclusions:

We show here that use of the dopamine transporter agonist CFT and the dopamine release agonist, amphetamine, cause a hemodynamic response to dopaminergic stimulation which has the following features: 1) The response is regionally specific to those areas of the brain with highest dopaminergic density; 2) The time course follows the time course for release of dopamine in the striatum via microdialysis; 3) The response is selectively ablated via unilateral lesioning of the nigral-striatal tract using 6-OHDA; 4) The response is well correlated with in vivo PET and histologic measures of dopaminergic transporter binding as measured using ^{11}C -CFT; and 5) the response is restored in those same animals using neural transplantation of fetal mesencephalon cells into the striatum.

References:

-
- 1 C. Carlsson, M. Hagerdal, B. K. Siesjo, Influence of amphetamine sulfate on cerebral blood flow and metabolism, *Acta Physiol. Scand.*, **94**:128-129 (1975).
 - 2 M. McCulloch, A. M. Harper, Cerebral circulatory and metabolism changes following amphetamine administration, *Brain Research*, **121**:196-199 (1977).
 - 3 L. R. Wechsler, H. E. Savaki, L. Sokoloff, Effects of d- and l-amphetamine on local cerebral glucose utilization in the conscious rat, *J. Neurochem.*, **32**:15-22 (1979).
 - 4 K. E. Russo, W. Hall, O. Z. Chi, A. K. Sinha, H. R. Weiss, Effect of amphetamine on cerebral blood flow and capillary perfusion, *Brain Research*, **542**:43-48 (1991)

-
- 5 J. M. Trugman, C. L. James, D1 dopamine agonist and antagonist effects on regional cerebral glucose utilization in rats with intact dopaminergic innervation, *Brain Research*, **607**: 270-274 (1993)
 - 6 J. W. Belliger, D. N. Kennedy, R. C. McKinstry, B. R. Buchbinder, R. M. Weisskoff, M. S. Cohen, J. M. Vevea, T. J. Brady, B. R. Rosen, Functional mapping of the human visual cortex by magnetic resonance imaging, *Science*, **254**: 716-719 (1991)
 - 7 K. K. Kwong, J. W. Belliger, D. A. Chester, I. E. Coldberg, R. M. Weisskoff, B. P. Poncelet, D. N. Kennedy, B. E. Hoppel, M. S. Cohen, R. Turner, H. M. Cheng, T. J. Brady, B. R. Rosen, Dynamic magnetic resonance imaging of human brain activity during primary sensory stimulation. *Proc. Natl. Acad. Sci.*, **89**:5675-5679 (1992).
 - 8 S. Ogawa, D. W. Tank, R. Menon, J. M. Ellermann, S-G. Kim, H. Merkle, K. Ugurbil, Intrinsic signal changes accompanying sensory stimulation: functional brain mapping with magnetic resonance imaging, *Proc. Natl. Acad. Sci.*, **89**: 5951-5955 (1992)
 - 9 C. J. Aine, A conceptual overview and critique of functional neuroimaging techniques in humans: I. MRI/fMRI and PET, *Crit Rev. Neurobiol.*, **9(2-3)** : 229-309 (1995).
 - 10 A. P. Wolf, J. S. Fowler, Positron emission tomography: biomedical research and clinical application, *Neuroimag. Clin. N. Am.*, **5(1)** : 87-101 (1995).
 - 11 G. W. Arbuthnott, I. S. Fairbrother, S. P. Butcher, Dopamine release and metabolism in the rat striatum: an analysis by in vivo brain microdialysis, *Pharmacol. Ther.*, **48(3)** : 281-93 (1990)
 - 12 D. A. Perese, J. Ulman, J. Viola, S. E. Ewing, K. S. Bankiewicz, A 6-hydroxydopamine-induced selective parkinsonian rat model, *Brain Research*, **494**: 285-293 (1989)
 - 13 M. J. Zigmond, E. D. Abercrombie, T. W. Berger, A. A. Grace, E. M. Stricker, Compensations after lesions of central dopaminergic

-
- neurons: some clinical and basic implications, *TINC*, **13(7)** : 290-296 (1990)
- 14 B. Giros, M. Jaber, S.R. Jones, R. M. Wightman, M.G. Caron, Hyperlocomotion and indifference to cocaine and amphetamine in mice lacking the dopamine transporter, *Nature* ,**379**: 606-612 (1996)
 - 15 B. K. Madras, M. A. Fahey, J. Bergman, D. R. Canfield, R. D. Spealman, Effects of cocaine and related drugs in nonhuman primates. I. [3H] Cocaine binding sites in caudate-putamen, *J. Pharmacol. Exp. Ther.* ,**251(1)** : 131-141 (1989)
 - 16 B. K. Madras, J. Bergman, M. A. Fahey, J. L. Neumeyer, J. K. Saha, R. A. Milius, Cocaine receptors labeled by [3H]2b-carbomethoxy-3b-(4-fluorophenyl)tropane, *Mol. Pharmacol.*, **36**: 518-524 (1989)
 - 17 G. L. Brownell, C. A. Burnham, C. W. Sterns, D. A. Chesler, A-L. Brownell, M. R. Palmer, Developments in high-resolution positron emission tomography at MGH, *Internatl. J. Imag. System and Technology*, **1**: 207-217 (1989)
 - 18 D. Kuczenski and D. Segal, Concomitant characterization of behavioral and striatal neurotransmitter response to amphetamine using in vivo microdialysis, *J. Neurosci.*, **9**: 2051-2065 (1989).
 - 19 T.E. Robinson, E. Castaneda, I.Q. Whishaw, Compensatory changes in striatal dopamine neurons following recovery from injury induced by 6-OHDA or methamphetamine: A review of evidence from microdialysis studies, *Can. J. Psychol.*, **44**: 253-275 (1990).
 - 20 G. Paxinos, C. Watson, The rat brain in stereotaxic coordinates, Academic Press, San Diego, CA, (1986)
 - 21 A. D. Silva, W. Zhang, D. S. Williams, A. P. Koretsky, Multislice MRI of rat brain during amphetamine stimulation using arterial spin labeling, *Magn. Reson. Med.*, **33**: 209-214 (1995)

-
- 22 A. Villringer, B. R. Rosen, J. W. Belliveau, J. L. Acerman, R. B. Lauffer, R. B. Buxton, Y. S. Chao, V. J. Wedeen, T. J. Brady, Dynamic imaging with lanthanidechelates in normal brain: contrast due to magnetic susceptibility effects, *Magn. Reson. Med.*, **6(2)** : 164-174 (1988)
- 23 L.M. Hamberg, R. Macfarlane, E. Tasdemiroglu, P. Boccalini, B. G. Hunter, J. W. Belliveau, M. A. Moskowitz, B. R. Rosen, Measurement of cerebrovascular changes in cats after transient ischemia using dynamic magnetic resonance imaging, *Stroke*, **24(3)** : 444-450 (1993)
- 24 J.A. Detre, J.S. Leigh, D.S. Williams, A.P. Koretsky, Perfusion Imaging, *Magn Reson. Med.*, **23**: 37-45 (1992).
- 25 L.S. Carman, F.H. Gage, C.W. Shults, Partial lesion of the substantia nigra: relation between extent of lesion and rotational behavior. *Brain Research*, **553**: 275-283 (1991).

Chapter 6 Thesis Summary and Future Work

The primary objectives of this thesis were to investigate and verify neurodegenerative processes. We focused primarily on Parkinson's disease (PD) to evaluate the possible neurochemical modulation and the neuronal responses caused by disturbance of the dopaminergic system in the movement disorder of PD.

Although the Parkinsonian symptoms have been well documented and described since the 19th century, the etiology of PD is still unclear. Human evidence includes drug abusers who received MPTP and subsequently developed signs and symptoms resembling idiopathic PD[1]. Further studies showed that MPP⁺, the metabolite of MPTP, can block the enzymatic activity of complex I in the electron transport chain. This human evidence suggests that PD may

be associated with dysfunction of mitochondrial respiration in the basal ganglia [2,3]. Blockade of the electron transport chain may lead to cessation of the TCA cycle, which in turn leads to accumulation of lactic acid [4]. This provides us an opportunity to monitor the lactate levels in the PD brains by using ¹H-MRS. The lactate level in the resting state of a normal brain is nearly undetectable using ¹H-MRS and any extra accumulation of cerebral lactate in the resting state may indicate an abnormality in energy respiration. In this thesis we tried to measure the cerebral metabolites in PD brains and normal age-matched subjects by using ¹H-MRS.

Although the energy impairment theory may provide valuable information regarding neuronal degeneration, the question of how this neuronal degenerative process is associated with movement disorders is yet to be answered. In order to understand the mechanism involved in basal ganglia function better, one has to investigate the neurotransmitter system as well. Postmortem studies of PD brain show neuronal loss in the substantia nigra pars compacta (SNc) [5,6]. Functionally, the neuronal loss in the SNc will lead to alterations in the striatal dopaminergic innervation. However, data from both PD patients and animal models of PD show that the Parkinsonian symptoms will not start to show up until there is about 80% to 90% loss of the dopaminergic innervation in the striatum [5,6,7]. To mimic the abnormal dopaminergic innervation in the striatum, we used a well studied animal model with injection of 6-hydroxydopamine (6-OHDA) to selectively and unilaterally deplete the striatal dopaminergic innervation [8,9]. This animal model allows us to investigate 1) the possible striatal metabolite changes after the

dopaminergic denervation, and 2) to assess the regional dopaminergic activity in brain. The striatal metabolites can be assessed using ^1H -MRS technique. In this thesis, we chose to use 3D-chemical shift imaging technique (3D-CSI) which allowed us not only assess the cerebral metabolite information but also the spatial distribution of those metabolites over the whole brain. The regional dopaminergic activity can be assessed using functional MRI (fMRI) with the stimulation of specific dopaminergic ligands. We dubbed this technique as pharmacological MRI or phMRI.

The main goals of this thesis are 1) to accurately evaluate the cerebral metabolite levels using ^1H -MRS, and 2) to validate the possibility of using fMRI to assess the neurotransmitter activity. In order to evaluate the cerebral metabolite level accurately, we investigated in this thesis the conditions that may alter the accuracy of spectral analysis. We used computer simulations to synthesize ^1H -MR spectra under various magnetic field strengths and homogeneities. We also evaluated the possible errors involved in both relaxation times and absolute concentration measurements. Only accurate spectral analysis allows us to have a reasonable comparison in the cerebral metabolite changes between the normal and disease states.

Technical Concerns in using ^1H -MRS to explore the striatal metabolites

The utilization of ^1H -MRS to quantify the metabolic concentration in the striatum involves several technical difficulties, such as spectral

overlap, low signal to noise ratios (SNR) and relaxation rate measurements. We used computer simulations to demonstrate how each factor alters the estimation of the relaxation times and the absolute metabolite concentrations. We found that it would be difficult to obtain accurate relaxation times T_1 and T_2 because of spectral overlap, macromolecular contamination [10,11] and J-coupling. The T_2 measurement is usually achieved by multi-echo spin echo experiments and the signal intensity will be a mono-exponential decay as function of TE. With spectral overlap, the signal decay is no longer a mono-exponential. When the overlap involves J-coupling, the decay curve oscillates in a sinusoidal fashion which makes the T_2 relaxation time measurement even more complicated. Our computer simulations showed that the T_2 error could be as high as over 100% and the error does not depend on the number of TE points chose in the measurement and there are no magic TE values one can use to minimize this error.

When propagating the relaxation time error into the estimation of the metabolite concentration, we found that the T_1 error of NAA is more critical than the T_1 errors of water. The percent error in the NAA concentration caused by the T_1 error of NAA is between 45% to 65% as a function of TEs. The error essentially comes from the saturation factor and the longer the T_1 value is ($T1_{NAA} > T1_{water}$), the greater error will be in the concentration measurement ($[NAA] Error_{T1NAA} > [NAA] Error_{T1water}$). This T_1 error factor could be minimized by using a longer TR value. When TR is longer than 3 sec, the concentration error due to T_1 error can be ignored. However, none of the concentration errors propagated from the T_2 errors of

water or NAA can be neglected. The T_2 errors can make the error of the NAA concentration as high as over 100%. Therefore, the accuracy of T_2 measurement is much more important than the accuracy of T_1 measurement in estimating the absolute metabolite concentration.

Although our computer simulated spectra showed great similarity to the *in vivo* and the phantom spectra, our simulation was only based upon the assumption of weak J-coupling and lack of macromolecular components. Future work would add in these two factors to the computer simulations. It is also important to investigate the J-coupling effects under the influence of different pulse sequences.

In conclusion, absolute metabolite concentration measurements may have been a great objective but are not practically reliable. We believe that the relative concentration measurements [12] may provide more useful and reasonable comparisons for quantitative analysis, especially for inter-laboratory comparisons.

¹H-MRS in PD patients and animal model of PD

The hypothesis that disruption of the electron transport chain in the basal ganglia may be responsible for the movement disorder in PD was assessed by monitoring the lactic acid level. We chose to examine the striatal lactate level in both PD patients and age-matched normal controls using a spatially localized ¹H-PRESS sequence. We also examined the lactate level in an animal model of PD (6-OHDA lesioning) using a 3D-CSI technique.

In the human study, we found that the striatal lactate level in PD patients was elevated 59% compared to normal controls ($p < 0.0004$).

No other major ^1H -MRS detectable striatal metabolite showed significant differences between the PD and the normal control groups. We also found a significant lactate asymmetry in the two striata for both PD patients and normal controls ($p < 0.02$). Just comparing the lactate levels on the largest side, the PD patients showed a significant increase in the lactate level compared to the normal controls (64.51% increase, $p < 0.05$). Interestingly, most of the subjects (PD and normal controls) have a higher lactate level in the left striatum. Since most of the people are left hemisphere dominant, and the left hemisphere has long been hypothesized to govern the mental computation, language, and motor tasks. The left striatum thus has been hypothesized to have a heavier working load than the right striatum. The higher neuronal firing incident rate in the left striatum may lead to higher vulnerability with energy insults and this may be the cause of the asymmetric lactate levels in the two striata

However, for the 6-OHDA lesioned animals, we did not find significant lactate elevation in the striatum ipsilateral to the lesioning. This may be due to the fact that the acute 6-OHDA lesioning causes cell death too rapidly (i.e. within 24 hours), and lactate may only be elevated during the first few days post-lesioning. Since we only studied these animals at least three weeks after lesioning, we may not have seen lactate for this reason. In contrast, the neurodegeneration in PD patients is a much slower progressive process which allows us to monitor the dynamic changes in the lactate level in a much wider time window. However, the neuronal marker N-acetylaspartate (NAA) showed a significant decrease in the

striatum ipsilateral to the 6-OHDA lesioning (9.61%, $p < 0.0003$; range 5~21%). Although histological studies of postmortem PD brain did not find any significant cell loss in the striatum. The mismatch between the animal NAA loss and the human histological finding may represent the rebalance of the degeneration of the dopamine terminals and the resprouting of the serotonin (5-HT) fibers [13,14]. In other words, the NAA loss may just reflect the net neuronal population (cell bodies) in the striatum after the 6-OHDA assault. The other possibility is a susceptibility mismatch due to the extra iron deposition in the ipsilateral striatum. It has been found that PD patients and 6-OHDA lesioned animals have relatively high iron deposits in their brain [15,16]. Iron is paramagnetic and can induce ΔR_2^* changes and alter the signal intensity of NAA. This extra ΔR_2^* term may not play an important role in the water images (T_2 and diffusion weighted images) due to the much shorter T_2^* of water than NAA.

Overall, ^1H -MRS provides reliable access to the *in vivo* cerebral metabolites. Although our studies showed elevated lactate levels in PD patients, which did not correlate with age, disease severity, DOPA dose administered or the duration of PD, there are still other possible clinical variables which may influence the lactate levels. Most of the PD patients were continuously taking medication to reduce the movement disorder. Whether or not these medications can alter the brain metabolism and how long it would be for the neuronal metabolism to return to the baseline level after withdrawal of the medication is unclear. Although we would like to examine naive

patients without any interference of the drug medication, it is very difficult practically for ethical reasons, due to the possible uncomfortable and disabling side effects patients may suffer during the medication off period. Finally we can ask if there are any clinical applications of this technique. Can we use $^1\text{H-MRS}$ as a diagnostic tool for early detection of Parkinson's disease? Can it be an important clinical tool to investigate possible therapeutic interventions? Since PD is a disease associated with aging, and many elderly persons may suffer neuronal problems due to natural aging and Alzheimer's disease, it is possible that the detection of a small lactate elevation may be associated with other neuronal conditions rather than PD. It is known that PD symptoms don't show up unless more than 80% of the dopaminergic innervation in the striatum is lost [5,6,7]. Thus, the high lactate level in PD patients may only indicate the near completion of the neuronal degenerative process but not be present as an early symptomatic sign. However, it may be of use to measure lactate for aid in the evaluation of possible therapies by estimating the lactate levels pre- and post- medication; using perhaps electron transport chain cofactors such as CoQ10. Furthermore, the lactate level may provide a way to help to understand the striatal function in PD patients. Under certain physiological challenges, PD brains may have greater difficulty in providing enough energy to perform tasks, and thus the lactate level during neuronal stimulation may be different than normal subjects. This hypothesis remains to be investigated for future studies. For instance, Scholz et. al. [17] has shown several motor tasks which will activate basal ganglia in fMRI studies in the normal controls. One can

monitor lactate level before, during, and after the motor tasks in both PD patients and normal controls. In other words, one can combine motor tasks and functional spectroscopy to evaluate the response of the basal ganglia under possible energetic stress postulated to occur in PD.

Validation of using pharmacological MRI (phMRI) to assess the dopaminergic neuronal activity

PD is the neurodegenerative disease associated with dysfunction in energy respiration and dopaminergic innervation in the striatum [5,6,7]. To better understand the dopaminergic functions in PD, we used functional MRI with pharmacological stimulation to probe the dopaminergic system (phMRI). Unlike positron emission tomography (PET) or autoradiography, this phMRI technique provides a possibility to examine the same animals longitudinally (better temporal resolution). The phMRI technique also provides better spatial resolution when compared to PET. In this thesis, we used D-amphetamine [18] and CFT [19,20] as our specific probes. Both ligands can increase the synaptic dopamine concentration transiently.

In order to validate that the phMRI response to the stimulation of D-amphetamine or CFT is truly linked to the dopaminergic system, we have to answer two questions:

- 1) Can we detect the metabolic response to direct neurotransmitter stimulation by using fMRI?
- 2) Is this fMRI response specific to a neurotransmitter system?

To answer these questions, we designed experiments which showed 1) the BOLD signal changes differed from the blood pCO₂ and global blood pressure changes, 2) phMRI responses are regionally specific to those brain areas with highest dopaminergic innervation, 3) the phMRI responses correlated well with the ¹¹C-CFT binding maps obtained via PET, 4) the phMRI time courses correlated with the extracellular dopamine release assessed by microdialysis.

Further to verify that the phMRI responses were truly linked to the dopaminergic system, we tested this technique on 3 groups of animals—normal control rats, unilaterally dopaminergic denervated rats, and dopamine fetal cell transplanted rats. We demonstrated that the phMRI responses were symmetric in the normal control rats, unilaterally ablated in the dopaminergically denervated striatum, and later restored at the graft site in the dopamine fetal cell transplanted rats.

Although the results from our phMRI experiments strongly suggest that the phMRI responses are linked to the dopaminergic system, we are still not clear what caused the BOLD or rCBV changes. Does amphetamine or CFT modulate mainly the D1 or D2 receptor system [21,22]? Do the positive BOLD signal changes represent excitatory or inhibitory neuronal activity? Is the effect mainly on the presynaptic side or the postsynaptic side? Can the modulation of the dopaminergic system induce alterations in other neurotransmitter systems such as serotonin [23,24], GABA [25], or glutamate [25, 26] as well? Is this phMRI response associated with any alteration in the gene expression such as c-fos [27,28]? Are there any clinical

application of this techniques? To continue investigating these question, we may need to modulate the fMRI signals by combining various agonists and/or antagonists. Pre- or post-treatment of D1/D2 agonists or antagonists with the amphetamine or CFT stimulation in phMRI experiments may help us to monitor to these two major dopamine receptor systems. We can also monitor the phMRI response to pure D1 or D2 agonists/antagonists stimulation to see whether or not we can obtain similar phMRI response as in the amphetamine/CFT cases. This can help us to understand the phMRI signal changes corresponding to excitatory or inhibitory neuronal activity. One of the advantages of using this pure D1/D2 stimulation protocol is that we can again correlate the spatial distribution of the phMRI responses to the binding maps obtained via PET [29]. The gene responses to stimulation in the dopaminergic system has been a popular topic recently. Scientists have been trying to investigate various mRNA responses to drug stimulation such as cocaine and amphetamine. The c-fos gene has been drawing a lot of attention due to its instant response to cocaine or amphetamine[30,31]. Histological studies showed that c-fos expression increases in the dorsal lateral striatum after the D-amphetamine stimulation [32], which reflects the spatial distribution of the phMRI response quite well. Whether or not the phMRI response is due to the increase in c-fos expression or simply reflects the dopaminergic innervation needs further investigation. Antisense oligonucleotides have been found to eliminate the c-fos expression [33] and one can possibly combine the phMRI amphetamine study with the intrastriatal injection of antisense oligonucleotides to reveal the role of c-fos in the phMRI

signal changes. Although all of our 6-OHDA lesioned animals passed the behavioral test for at least 90% dopaminergic denervation in the striatum unilaterally, the difference of the phMRI responses in the two striata (when calculated as percent striatum activated), however, is only about 40% instead of 90%. Castaneda et. al. [34] showed great variance in the release of dopamine under the condition of over 90% loss of the striatal dopamine terminals (figure 3 in ref. 7). Our phMRI measurement may reflect the real quantity of dopamine released instead of the number of intact dopaminergic terminals in the striatum. If we can build the linkage between the phMRI response and the dopaminergic function quantitatively, the phMRI technique may help 1) to detect the early loss of dopaminergic innervation in the elderly brain before any clinical indication of PD symptoms, 2) to determine the successful sprouting rate of the transplanted fetal cells over time when neuronal transplantation is performed on PD patients.

Conclusions

The data presented in this thesis demonstrate the ability of magnetic resonance techniques to explore various aspects of the neurodegenerative process. We have demonstrated the ability of ¹H-MRS to investigate the striatal metabolite state in the PD brain. We have found that the lactate levels in PD patients support the hypothesis of energy impairment. We also demonstrated the ability of phMRI to assess neuronal activity. This phMRI technique may not only help to explore the etiology of PD but also to assess the functions of various neurotransmitter systems in both normal and

disease states. We believe the techniques presented in this thesis have great potential to furnish information that could possibly monitor treatment strategies and improve the care of patients suffering from neurodegenerative diseases.

References

- 1 BR Bloem, I Irwin, OJS Buruma, J Haan, RAC Roos, JW Tetrad, JW Langston, The MPTP model: versatile contributions to the treatment of idiopathic Parkinson's disease, *J. Neurol. Sci.*, **97**: 273-293 (1990)
- 2 KF Tipton and TP Singer, Advances in our understanding of the mechanisms of the neurotoxicity of MPTP and related compounds, *J Neurochemistry*, 61(4): 1191-1206 (1993)
- 3 I Kanazawa, Short review on monoamine oxidase and its inhibitors, *Eur. Neurol.*, 34(suppl. 3): 36-39 (1994)
- 4 Vyas et. al., Study of the neurotoxicity of MPTP: inhibition of NADH-linked substrate oxidation by its metabolite MPP+, *J. Neurochem.*, 46: 1501-1507 (1986)
- 5 Bernheimer et. al., *J. Neurol. Sci.* 20: 415-455 (1973)
- 6 Lloyed et. al., *Exp. Ther.* 195: 453-464 (1975)
- 7 TE Robinson, E. Castaneda, IO Wishaw, Compensatory changes in striatal dopamine neurons following recovery from injury induced by 6-OHDA or methamphetamine: a review of evidence from microdialysis studies, *Can. J. Psychol.*, 44(2): 253-75 (1990)
- 8 U Ungerstedt, Use of intracerebral injections of 6-hydroxydopamine as a tool for morphological and functional studies of central catecholamine neurons. In 6-hydroxydopamine and catecholamine

-
- neurons. Edited by T. Malmfors and H. Thoenen., North-Holland Publishing Co., Amsterdam, London, pp. 315-332
- 9 JH Thakar, MN Hassan, Effects of 6-hydroxydopamine on oxidative phosphorylation of mitochondria from rat striatum, cortex, and liver, *Can. J. Physiol. Pharmacol.*, 66: 376-379 (1988)
 - 10 KL Behar, DF Rothman, DD Spencer, OA Petroff, Analysis of macromolecule resonances in ¹H NMR spectra of human brain, *Magn. Reson. Med.*, 32(3): 294-302 (1994)
 - 11 KL Behar and T Ogino, Characterization of macromolecule resonances in the ¹H NMR spectrum of rat brain, *Magn. Reson. Med.*, 30(1): 38-44 (1993)
 - 12 BG Jenkins, E Brouillet, YI Chen, E Storey, JB Schulz, P Kirschner, MF Beal, BR Rosen, Non-invasive neurochemical analysis of focal excitotoxic lesions in models of neurodegenerative illness using spectroscopic imaging, *J. Cereb. Blood Flow Metab.*, 16:450-462 (1996)
 - 13 FC Zhou, S. Bledsoe, J Murphy, Serotonergic sprouting is induced by dopamine-lesion in substantia nigra of adult rat brain, *Brain Research*, 556(1): 108-116 (1991)
 - 14 Y Yoshimoto, Q Lin, TJ Collier, DM Frim, XO Breakefield, MC Bohn, Astrocytes retrovirally transduced with BDNF elicit behavioral improvement in a rat model of Parkinson's disease, *Brain Research*, 691(1-2): 25-36 (1995)
 - 15 M Youdim et. al., The possible role of iron in etiopathology of Parkinson's disease, *Mov. Disord.*, 8: 1-14 (1993)

-
- 16 P Riederer, M Youdim et. al., Transition metals, ferritin, glutathione and ascorbic acid in Parkinsonian brain, *J. Neurochem.*, 52:515-520 (1989)
 - 17 Scholz VH, BG Jenkins, JR Keltner, YI Chen, KK Kwong, BR Rosen, Comparison of different motor tasks for fMRI studies of the basal ganglia: reproducibility, specificity and artifacts, *Proc. Intl. Soc. Magn. Res. Med.*, p. 446 (1996)
 - 18 B. Giros, M Jaber, SR Jones, RM Wightman, MG Caron, Hyperlocomotion and indifference to cocaine and amphetamine in mice lacking the dopamine transporter, *Nature*, 379: 606-612 (1996)
 - 19 MK Madras, MA Fahey, J Bergman, DR Canfield, RD Spealman, Effects of cocaine and related drugs in nonhuman primates. I.[³H] Cocaine binding sites in caudate-putamen. *J. Pharmacol. Exp. Ther.*, 251(1): 131-141 (1989)
 - 20 BK Madras, J Bergman, MA Fahey, JL Neumeyer, JK Saha, RA Milius, Cocaine receptors labeled by [³H]2b-carbomethoxy-3b-(4-fluorophenyl)tropane, *Mol. Pharmacol.*, 36: 518-524 (1989)
 - 21 CB Tyler, MP Galloway, Acute administration of amphetamine: differential regulation of dopamine synthesis in dopamine projection fields, *J. Pharmacol. Exp. Ther.*, 261(2): 567-573 (1992)
 - 22 T Hamamura, K Akiyama, K Akimoto, K Kashihara, K Okumura, H. Ujike, S Otsuki, Co-administration of either a selective D1 or D2 dopamine antagonist with methamphetamine prevents methamphetamine-induced behavioral sensitization and neurochemical changes, studied by in vivo intracerebral dialysis, *Brain Res.*, 546(1): 40-46 (1991)

-
- 23 L Hernandez, F Lee, BG Hoebel, *Brain Res. Bull.*, 19(6): 623-628 (1987)
- 24 MM Iravani, ZL Kruk, Real-time measurement of stimulated 5-hydroxytryptamine release in rat substantia nigra pars reticulata brain slices, *Synapse*, 25(1): 93-102 (1997)
- 25 N Linderfors, Dopaminergic regulation of glutamic acid decarboxylase mRNA expression and GABA release in the striatum: a review. *Prog. Neuropsychophar. Biol. Psych.*, 17(6): 887-903 (1993)
- 26 I Exposito, F Mora, S Oaknin, Dopamine-glutamic acid interaction in the anterior hypothalamus: modulatory effect of melatonin, *Neuroreport*, 6(4): 661-665 (1995)
- 27 AM Snyder-Keller, Striatal c-fos induction by drugs and stress in neonatally dopamine-depleted rats given nigral transplants: importance of NMDA activation and relevance to sensitization phenomena, *Exp. Neurol.*, 113(2): 155-165 (1991)
- 28 B Johansson, K Lindstrom, BB Fredholm, Differences in the regional and cellular localization of c-fos messenger RNA induced by amphetamine, cocaine and caffeine in the rat, *Neuroscience*, 59(4): 837-849 (1995)
- 29 G Sedvall, PET imaging of dopamine receptors in human basal ganglia: relevance to mental illness. *Trends Neurosci.*, 13(7): 302-8 (1990)
- 30 TV Nguyen, BE Kosofsky, R Birnbaum, BM Cohen, SE Hyman, Differential expression of c-fos and zif268 in rat striatum after haloperidol, clozapine, and amphetamine, *Proc. Natl. Acad. Sci.*, 89(10): 4270-4 (1992)

-
- 31 AJ Cole, RV Bhat, C Patt, PF Worley, JM Baraban, D1 dopamine receptor activation of multiple transcription factor genes in rat striatum, *J Neurochem.*, **58** (4): 1420-6 (1992)
- 32 SM Lillrank, BK Lipska, SE Bachus, GK Wood, DR Weinberge, Amphetamine-induced c-fos mRNA expression is altered in rats with neonatal ventral hippocampal damage. *Synapse*, **23**(4): 292-301 (1996)
- 33 BJ Chiasson, MI Hooper, PR Murphy, HA Robertson HA, Antisense oligonucleotide eliminates in vivo expression of c-fos in mammalian brain, *Eur J Pharmacol.*, 227 (4): 451-3 (1992)
- 34 E Castaneca, IO Whishaw, TE Robinson, Changes in extracellular dopamine concentrations measure by in vivo intracerebral dialysis after dopamine depletion, *Society for Neuroscience Abstract*, **15**: 559 (1989)